Turbulence structures in isolated pool-riffle units

by

Hamed Dashtpeyma

A thesis

presented to the University of Waterloo

in fulfillment of the

thesis requirement for the degree of

Doctoral philosophy

in

Civil and Environmental Engineering

Waterloo, Ontario, Canada, 2019

AUTHOR'S DECLARATION

This thesis consists of material all of which I authored or co-authored: see Statement of Contributions included in the thesis. This is a true copy of the thesis, including any required final revisions, as accepted by my examiners.

I understand that my thesis may be made electronically available to the public.

Statement of Contributions

I would like to acknowledge the contributions made towards this thesis by my supervisor Dr. Bruce MacVicar. All the results were generated by myself, and I prepared the final document under the supervision of Dr. MacVicar. I have done 90% of conceptual design, writing and editing, and Dr. MacVicar has done the rest. Chapter 3 is based on a manuscript that has been submitted to the Journal of Geophysical Research: Earth Surface.

Examining Committee Membership

The following served on the Examining Committee for this thesis. The decision of the Examining Committee is by majority vote.

External Examiner:

Dr. Ana Maria da Silva

Professor

Supervisor:

Dr. Bruce MacVicar

Associate Professor

Internal Member:

Dr. Don Burn

Professor

Internal-external Member:

Dr. Marek Stastna

Professor

Internal-external Member:

Dr. Mike Stone

Professor

Abstract

The macroscale morphology of a river has significant effects on sediment transport, flow pattern, bed stability, and ecosystem function. Pools and riffles, which are respectively the deeper and shallower parts of the bed, are a common morphology that is formed naturally in many rivers and also used as an analog in stream restoration. However, the formation and maintenance mechanisms of these structures remain unclear. Most of the previous studies on pool-riffle maintenance and shaping mechanisms did not consider the effects of riffle height, stream width variations, and constrictions on stream flow patterns and turbulence. These studies also did not comprehensively investigate different responses of sediments to turbulence.

The contributions of this thesis can be summarized as 1) identifying and characterizing turbulent structures in idealized pool-riffle units based on transient turbulence modelling; 2) studying the effect of pool-riffle geometrical parameters on turbulent structures, and 3) studying the influence of turbulent structures on sediment transport.

Riffle pools are defined by their undulating bed, and for this reason the simplest geometry of the bedforms we investigated were bed rises in straight channels similar to broad crested weirs. Other investigated geometries considered the additional effects of local constrictions in width and the overall width of the channel.

The research is a combined numerical and experimental study of turbulent structures and sediment transport in idealized pool-riffle units. Large eddy simulation was used to capture detailed information on flow characteristics. The numerical simulations were then validated using previously reported results and the experimental part of this study. The Q-criterion was used to detect turbulent flow structures in simulation

results. For the experiment on sediment transport, a visual qualitative scoring method was designed to assess sediment entrainment. Velocity profiles were acquired in the lab using an acoustic Doppler profiling velocimeter (Vectrino II) to validate the simulation results.

In the results, four types of vortical structures that largely control the flow pattern were identified, namely, (1) ramp rollers, (2) corner eddies, (3) surface turbulent structures, and (4) axial tails. Ramp rollers are shaped on downsloping ramps, corner eddies are formed at the corners of pool heads, surface turbulence structures are shaped at the free-surface of pool-head, and all the generated vortices in the pool-head get stretched and form axial tails vortices.

Pool-riffle geometry (riffle height, width size, and width constriction) and hydraulic characteristics (sub or supercritical flow types in riffles) exert a strong control over the size and strength of vortical structures as described below:

- Higher riffles create stronger ramp rollers and corner eddies.
- If the riffle height creates critical or supercritical flow in the riffle, surface undulation hydraulic jump will create strong surface turbulent structures.
- Wider channels provide more space for the shaping of corner eddies and ramp rollers.
- Width constrictions amplify corner eddies and ramp rollers and create horseshoe vortices in the upstream at convective accelerating flow zone.
- Even in subcritical flow condition, strong corner eddies can be transported to the free surface and shape boiling structures in the form of surface turbulence.

These structures are generated as a result of flow deceleration and are large structures generated away from the boundary and so are not thought to be dependant on surface roughness. To help unite the observations of the interaction between the main flow and turbulent structures, the ‘vortex-resistance hypothesis’ is

proposed. The hypothesis is based on the idea of eddy viscosity, which models the effects of turbulence as increased viscosity that exerts a force on the main flow. Using this concept, vortical structures increase the effective viscosity, which in turn increases the resistance of highly turbulent regions to the flow and thus steers a high velocity core of fluid through the pool.

Interaction and combination of the aforementioned four vortices types are shown to create three different types of flow through the pool, which are called 'skimming,' 'rifting,' and 'plunging' flow. Building upon the 'vortex-resistance hypothesis,' if surface turbulences are stronger than the ramp rollers, they combine with corner eddies and direct the incoming flow to plunge into the pool. If ramp rollers are strong and the surface turbulence is relatively weak, the ramp rollers push the incoming flow to skim the free-surface. If they both have similar strength, the flow has a high velocity core in the middle of the flow depth resulting into a rifting flow. These results help to explain the variety of flow patterns that have been identified in the previous field and laboratory experiments and highlight that the hydrodynamics of pools and riffles may be entirely different depending on local geometry, flow stage and the Froude number.

Vortical structures increase the pulsation and mean shear stress if they are close to the bed. Based on observations of sediment entrainment and deposition, it appears that a zone with local low shear stresses at the end of the downsloping ramp can trap the large particles before they enter the pool. The particles that pass the trap point will be washed away from the pool head due to strong turbulence in that region. The vortical structures become weaker as they travel downstream; therefore, the bed mean and shear stress pulsation decrease as well. Moreover, the transported particles are likely to be deposited respectively by their size further downstream, with only the smallest particles being transported through to the next riffle.

The research presented in this thesis offers a new look into the hydraulics and the variability of hydraulics in pool-riffle units. The variety of turbulent structures and flow regimes in the pool has the

potential to unite a wide set of seemingly contradictory observations and hypotheses that have propagated through the literature on this subject. The research also has important implications for design that should lead to better rehabilitation and maintenance strategies for natural or restored streams. The original scope of work should be extended to include more realistic natural shapes for the bedforms with lateral asymmetry and meandering, but the richness of behaviours and similarities with more complex forms of these structures necessitated a deeper examination of these relatively simple forms before extending the results to real systems.

Acknowledgements

We acknowledge that we live and work on the traditional territory of the Attawandaron (Neutral), Anishinaabeg and Haudenosaunee peoples. The University of Waterloo is situated on the Haldimand Tract, the land promised to the Six Nations that includes ten kilometers on each side of the Grand River.

I would like to express my sincere appreciation to my advisor Prof. Bruce MacVicar. I have been amazingly fortunate to have an advisor who gave me the freedom to explore on my own. A distinguished supervisor whose academic advice, encouragement, and unconditional support helped me step forward throughout my PhD. I appreciate all his contributions of time, inspiring suggestions, and funding to make my PhD experience productive and stimulating.

Table of Contents

List of Figures

List of Tables

Chapter 1: Introduction

1.1 Motivation

One of the most common topographical elements of rivers are pool-riffle units. The deeper parts of undulations in the bed are called pools, whereas the shallower parts are riffles. Pool-riffle sequences can be shaped naturally, but are also made artificially. Pools and riffles are essential elements in river restoration projects. As reported by Bernhardt et al. (2005) the most imperative objectives of restoration projects are to 1) improve water quality 2) improve fish habitats and aquatic lives 3) control sediment transport rate and stream energy. “Prior to July 2004, 37099 restoration projects were documented in National River Restoration Science (NRRSS) “ in the United States alone, a number thought to be underestimated due to underreporting of projects to NRRSS for various reasons. Between 1990 and 2004, they estimated that 15 billion dollars had been spent on restoration projects. Among the projects, only 10% of them were assessed by NRRSS (Bernhardt et al., 2005). Despite these reporting problems, a high failure rate of restoration projects is reported by researchers, which is caused by the irrational design of channel geometry; therefore, there is a need for better understanding of river elements, river mechanics, and hydrodynamics in natural streams (Bernhardt and Palmer 2007; Miller and Kochel 2009; Wohl et al. 2005).

1.2 Research gap

Many researchers have focused on the hydraulic characteristics of pool-riffle sequences using numerical analyzes, experimental investigations, and field work studies, but many of the existing studies have limitations. Many researchers noted that the turbulent structures are the most influential sources of shear stress in pools (Roy et al. 2004). Moreover, bed shear stress can maintain the form of pool-riffle units by cleaning the pools and storing large particles in the riffles. The most significant part of the pool-riffle unit in terms of turbulence generation is the area of convective decelerating flow (CDF) in the ramp at the head of pools (MacVicar and Rennie 2012). This turbulence is thought to be important in sediment transport mechanism (Celik et al. 2013) and pool-riffle maintenance (Thompson 2006) but most of the researches in this field have limitations in assessing bed shear stress and turbulent structures for the reason that most of the experimental analysis cannot instantaneously measure velocity domain in near-wall regions. Existing numerical studies also did not consider turbulent structures accurately because of their predominant use of steady-state methods, which cannot model dynamic structures in pool-riffle units. Transient numerical analysis is particularly suited to illustrate the complex mechanisms of flow such as vortex generation and dissipation, turbulent structures, and instantaneous bed shear stress (Keylock et al. 2012). Also, a better understanding of hydrodynamic in pool-riffle units helps to unify the controversial hypothesis in pool-riffle formation, which are based on field observations. However, the key problem in numerical simulations is that sediment transport and scouring cannot be modelled directly and without using empirical approximations; therefore, there is a need to establish a linking between numerical hydrodynamics results and experimental sediment transport studies.

1.3 Approach

This study is using advanced numerical methods to continue a series of flume experiments, which was done by MacVicar and Obach (2015). They used a reductionist approach by representing the complex

geometry of pool-riffle units as a two-dimensional bedform in an open channel flume with smooth vertical walls. In addition, they stated that this unnatural and artificial geometry was chosen to allow them to isolate the effects of longitudinal vertical contraction and expansion from different geometrical characteristics. Another benefit of modelling pool-riffle units as a two-dimensional bedform is that it can contribute to the current design methods in restoration projects suggested by Newbury (2013), which is based on fundamental hydraulic principles and constructing simple two-dimensional riffles along the width of the channel. This thesis was designed to investigate the effects of two major geometrical factors (riffle height and width variation) on the formation of flow pattern and turbulent structures.

This approach has some limitations; for instance, the effects of alternate bars, bed roughness, side slopes, and meandering on flow pattern and turbulent structures in pool-riffle units are not investigated. Sediment transport mechanisms are not completely investigated, and it is limited to entrainment of non-cohesive particles without considering the covering factor and pocket geometry. However, the relatively simple geometries used in this study revealed a rich variety of flow dynamics that were highly sensitive to a few basic parameters. The complexity of the observed preliminary results suggested that a thorough investigation of these simplified geometries was needed before the flow hydrodynamics over more complex geometries could be unambiguously interpreted.

1.4 Objectives

The objectives of the present study are to numerically investigate the effects of fundamental geometry factors on hydrodynamic in pool-riffle units, and experimentally assess the fundamental mechanism of sediment transport, more specifically to: 1) identify and characterize turbulent structures in pool-riffle units based on an advanced transient turbulence modelling; 2) study the effect of pool-riffle geometry on generation, transport and dissipation of turbulent structures, and 3) study the influence of turbulent structures on non-cohesive sediment entrainment. By achieving these objectives, this research can

help engineers and researchers to understand better the hydrodynamics and turbulence in pool-riffle units. This study can clarify the pool-riffle hydrodynamics and maintenance hypotheses, while also helping to guide a more rational design. The experimental part of this research can provide a better understanding of sediment transport mechanism; moreover, by linking the transient numerical results and experimental data, a better understanding of turbulence effects on pool-riffle maintenance can be achieved. It is hoped that the results from the current study can be an important step in the understanding of complex hydrodynamics in pool-riffle units and provide a base framework for further researches.

Chapter 2: Literature Review

2.1 Definition of pools and riffles

Many researchers have tried to propose an accurate and comprehensive definition for pools and riffles, but their definitions remain problematic (Thompson, 2013). Pools and riffles can be considered either as a single morphological element or as distinct subunits because of their distinct influence on the flow (Clifford 1993; Thompson 2001). Pools can form by scouring in a particular location or where the flow is slowed by bars of deposited sediment (Clifford 1993). “Forced pools” can be formed by obstruction to flow and “free-formed pools” can be shaped freely by flow pattern (Lisle & Hilton, 1992; Montgomery et al., 1995; D. M. Thompson, 2013). Based on the hydraulic characteristics of the stream, riffles are those regions with steeper water-surface slope and pools are deeper part with horizontal water-surface in low discharge conditions (Lisle & Hilton, 1992; Lisle, 1979a). Another method for describing pools and riffles is “residual-depth criterion” that says if the flow at the upstream is ceased, after reaching to complete stable condition, those regions where are inundated with water are pools (Lisle, 1979b). However, this method cannot explain the definition of riffles (Thompson, 2013). Moreover, a quantitative method is needed to distinguish pools and riffles from common undulations in the streambed. A statistical approach based on the elevation distribution of streambed and a limit for the ordinary variation of elevation can help to distinguish pools from small-sized depressions.

Another method for defining pools and riffles in addition to previous methods is based on the bed grain size. Because of the maintenance or formation mechanism in pools and riffles, the material of riffles is coarser than that in pools (Leopold et al. 1960).

Most of these methods can only define pools and riffles; they cannot be extended to all morphological components such as runs and glides (Thompson, 2013). Runs and glides are small common undulations in the streambed that they are made because of small local scouring around boulders in streambed (Dietrich et al. 1979). Runs and glides do not have an influential impact on the hydraulic characteristics of the flow. They can only increase the turbulence because of their heterogeneity and roughness in the streambed. However, they can be vital for the quality of small species aquatic habitat (Halwas & Church, 2002; Lisle, 1982; Thompson, 2013; Wyrick & Pasternack, 2014).

2.2 The formation of pools and riffles

Most researchers agree with the concept that the scouring of pools and aggrading of riffles happens in high flow discharges (Thompson, 2013). Some researchers believe that the regular formation of spaced pools and riffles is a fundamental feature of many streams, and it does not depend on the main streambed material (Keller & Melhorn, 1978). Another issue is that most hypotheses for the shaping of pool-riffle units cannot explain the formation and stability of small undulations (e.g. runs and glides) in the streambeds (Thompson, 2013). A more clear idea about the shaping of pools and riffles is that the scouring of the streambed, which creates pools, and formation of bars from deposited sediments, which creates riffles, are the morphological response of streambed to the external forces from the flow (e.g. excessive shear stress) (Dolling 1968). These principles can illustrate the variety of pool-riffle types based on the diversity of the hydraulic characteristics of streams. Some researchers suggested that the geometric characteristics of pools, for example, higher length, are the result of streambed response for the minimization of stream power in the presence of a higher inlet stream power (Thompson, 2002). Some researchers showed that the geometric

characteristics of pools and riffles helped to maximize the resistance to the energy of flow then it limits the increase of velocity in high stage flows (Wohl & Merritt, 2008).

At the first stage in the study of pools and riffles, most of the researchers focused on the formation of them in meandering channels, and they tried to find a similarity between the helical flow pattern in meandering channels and the reason of pools formation in straight ones (Thompson, 2013).

2.2.1 Meandering development

In early studies, there was an idea that the flow and bed pattern in straight channels and meandering ones have some similarities; therefore, they started to describe the formation of pools and riffles in the straight ones based on the concept of helical flows in meanderings (Thompson, 1986).

As described by Thompson (1986), the formation and geometry of bars in the natural straight streams vary based on the flow stages and the types of channels. The form of bars in meandering channels is slightly different but shows many similarities with those from straight channels (Figure 2-5).

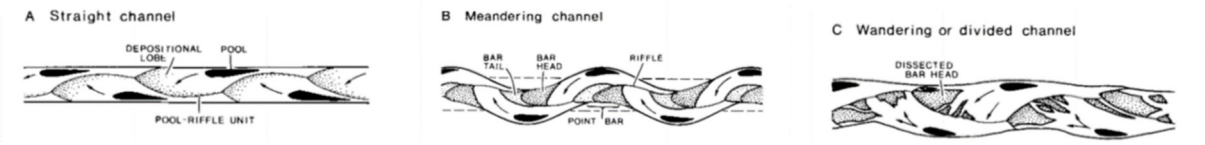

Figure 2-1- Morphological similarities between straight, meandering, and wandering channels

(Thompson 1986)

For instance, the bar head in the meandering channels has a larger flat area at the top and steeper ramp at the upstream and larger bar tail. In "wandering channels" the bar tail is faded. However, the order of elements based on the flow pattern is the same. They suggested that an ordered sequence of scouring and deposition of sediment were needed for the shaping of pools and riffles, and it can be the result of convergence and divergence flow. The helical flow that is shaped by meandering thalweg in straight

channels can produce those convergence and divergence flows. Those helical vortices are generated because of turbulence and vortex shedding in near-wall regions. The shedding and length scale of those vortices can shape the meandering thalweg (Figure 2-2). The interaction between the shaped thalweg and flow pattern can have a secondary effect on the formation of final and stable pools and riffles (Thompson, 1986).

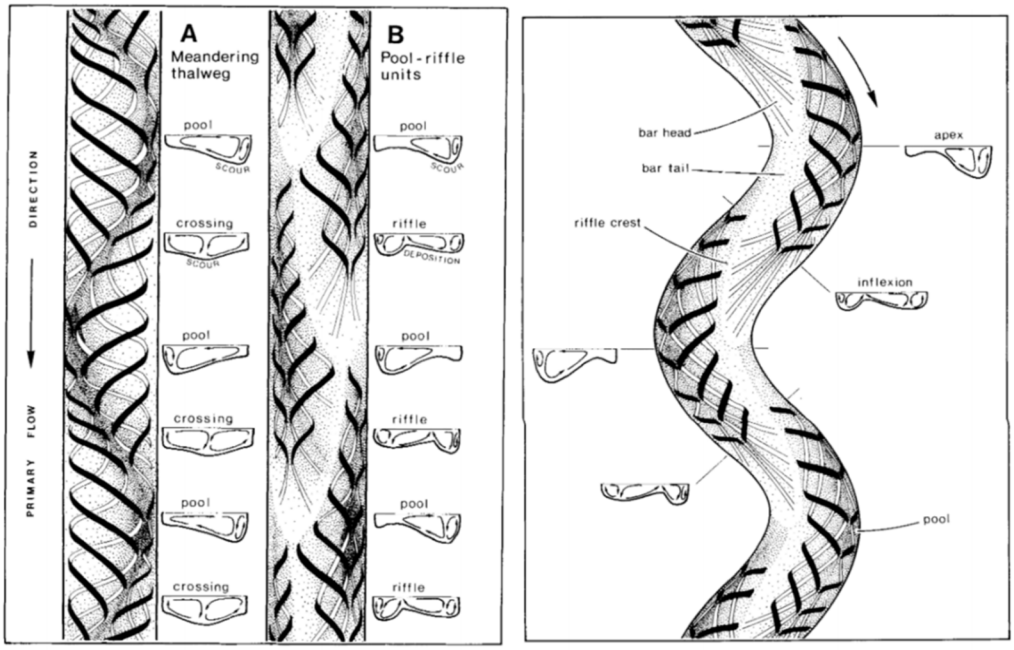

Figure 2-2- Helical flow in straight and meandering channel (Thompson, 1986)

One of the most important factors in forming and developing of meandering is pools and riffles. Several researchers suggested five steps developing stage from straight channel to meandering channel. All of the models consider pools and riffles as the most significant part of developing because of their impact on flow structure, sedimentation, and erosion. As illustrated in Figure 2-3, at the first stage the meandering thalweg is shaped because of turbulence structures and oscillation of flow in the near-wall region. At the second stage of the development of pools and riffles, helical vortices become stronger, and the erosion of the wall near the pool becomes faster. At the third and fourth stages, the curvature of the stream becomes higher by

the growth of pools and the translation of riffles. At stage five, because of growth and development, the distance between two pools becomes higher, and then the stages one to four happen again for the semi-straight part between two bends. At the fifth stage the complex shape of meandering shapes. The stages one to five repeatedly happen for different parts until the equilibrium state is shaped for the streambed (Lotsari et al., 2014; Thompson, 1986).

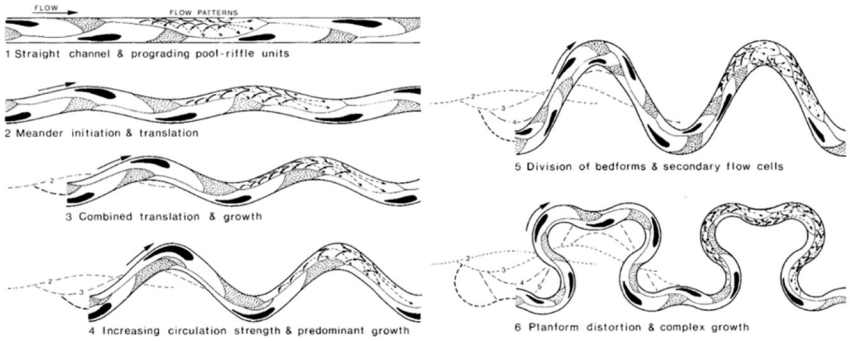

Figure 2-3- Development of meandering from the straight channel (Thompson, 1986)

2.3 Hydrodynamics in pools and riffles

2.3.1 Mean flow

One of the most famous hypotheses in pool-riffle hydrodynamics is "velocity reversal." It says that by increasing the flow discharge the increasing rate of near-bed velocity in riffles is lower than the one in pools and there is a point that the near-bed velocity in the pool is equal to the one in the riffle, in addition, the shear stress is projected to be higher in pools in high flow rate conditions (Keller 1971) (Figure 2-4).

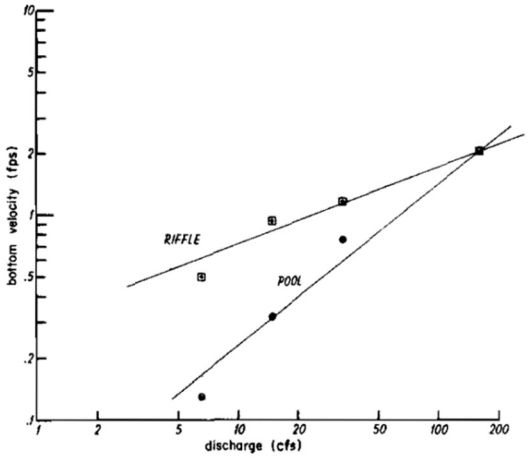

Figure 2-4- Near bed velocity (0.05 ft above the bed) versus total discharge in a pool-riffle unit

(Keller, 1971)

Although this was not observed in the field due to the difficulty of measuring at high water levels; however, a few studies in the field have found a reversal flow (Heritage & Milan, 2004; Thompson, 2013). Another set of findings illustrated that in the bankfull stage, the near-bed mean velocity in both riffles and pools tend to converge (Kieffer, 1989; Thompson, 2013). Other researchers showed that the occurrence of a velocity reversal is dependent on the "residual depth" of pools (depth between the top crest of the downstream riffle and the pool bed) for narrower pools (Thompson et al., 1996). Reversal flow is less likely in deeper pools, or it can happen intermittently. Still, other researchers showed that the likelihood and the magnitude of the reversal velocity were functions of width variations between the riffle and pool (Caamaño et al., 2012; Diego Caamaño et al., 2009; Jackson et al., 2015; Wilkinson et al., 2004). The focus on width is a focus on the 1D analysis of velocity reversal, which may not be the most relevant. MacVicar et al., (2010) argued that partial flow reversals may be possible even if the section-averaged velocity is not reversing. This point was made much earlier by Clifford & Richards, (1992). Some researchers showed that the convergence of near-bed mean velocity in pools and riffles created a jet-like flow that can make a

scour hole in the pools (Kieffer, 1985). They showed that the location of convergence shifts from the riffles to pools by increasing the flow level.

More recently, researchers have tried to restructure the reversal flow hypothesis by introducing the concept of lateral flow convergence (MacWilliams et al. 2006; Sawyer et al. 2010). MacWilliams et al., (2006) stated that the flow is uniform at the upstream riffle. The flow is funnelled in the constriction, which is shaped by the point bar at the pool. The constricted flow has a high-velocity core that increases the sediment transport. In addition, this high core velocity transports the sediment through the pool reach. The flow diverges at the downstream of the point bar. The flow becomes uniformly distributed across the width if the downstream riffle is far enough (Figure 2-5). These results were developed from a 3D steady-state model. This hypothesis, which is called "flow convergence routing," appraised by other researchers as well (Milan, 2013).

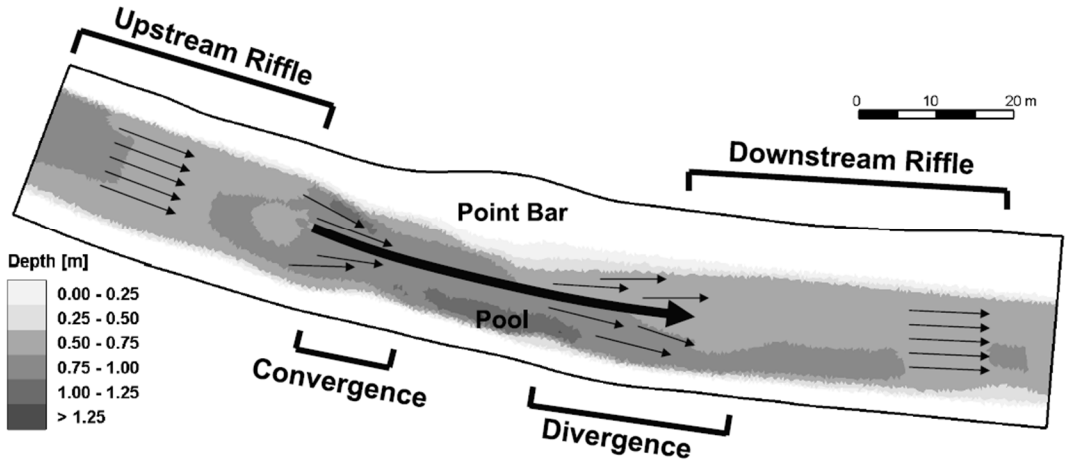

Figure 2-5 Conceptual model of flow convergence routing for pool-riffle sequence (MacWilliams et al. 2006)

2.4 Turbulence

Some detailed studies of hydrodynamics in pools and riffles have argued that turbulence plays a significant role in sediment transport, formation, and maintenance of pools and riffles (Clifford 1993; Clifford and Richards 1992; MacVicar and Roy 2007b). The turbulence in most natural streams is the result of the interaction between flow and irregularities in bed morphology (Thompson, 2013). Turbulent flows increase the pulsation in shear stress exertion and due to the dynamic loading of grains; the sediment transport rate will be increased (Roy et al., 1999). Pools and riffles make flow accelerate and decelerate, and the resulting pressure gradients act as perturbations on the flow and generate significant amounts of turbulence as a result of high strain rates (Smits and Wood 1985). As reported by MacVicar and Rennie (2012) and MacVicar and Best (2013), at the pool head, velocity can peak near the free-surface while turbulence peak near the bed. Moreover, the authors hypothesized that the turbulence that is generated in pool-head could maintain the geometry of pool-riffle units. They called pool head as convective decelerating flow (CDF) and pool tail as convective accelerating flow (CAF) (Figure 2-6). They stated that the redistribution of flow is a consequence of streamwise pressure gradients. Moreover, in CDF zones due to the positive streamwise pressure gradient, the flow becomes perturbed and get recovered by travelling downstream in the pool. Other sources for generating disturbances can be obstacles in forced-pools, bed roughness, flow convergence effect, and interaction of helical vortices in meanderings (Wohl & Thompson, 2000).

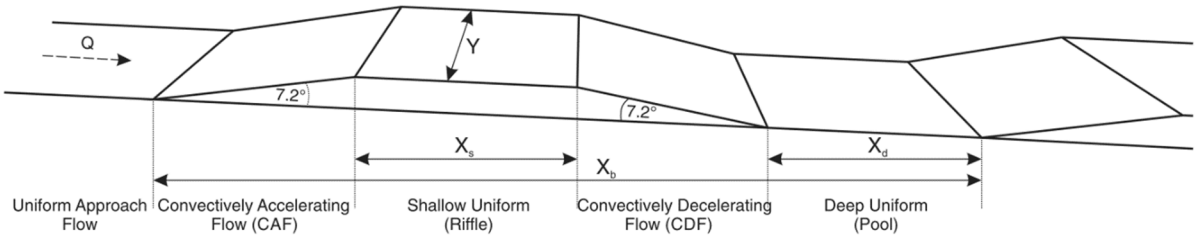

Figure 2-6- Schematic figure of pool-riffle unit with CAF and CDF zones (MacVicar and Obach 2015)

Some experimental and field studies showed that because of the variability of turbulence, dynamic loading and higher instantaneous shear stress exertion, the time-averaged results could not predict the strength of sediment transport precisely (Roy et al., 1999). Despite the importance of turbulence role in sediment transport, most hypotheses of pool-riffle formation and maintenance do not consider turbulence in their modelling. For example, MacWilliams et al. (2006) argued that the deepest part of pools has lower shear stress in comparison to shallower parts because of lower velocities (Figure 2-7), but they did not consider the spatial and temporal variability of turbulence that is now shown in the literature (MacVicar & Obach, 2015; MacVicar & Rennie, 2012; MacVicar & Roy, 2007b; Thompson, 2013). For example MacVicar and Best (2013), showed that lower near-bed velocities in a riffle or pool do not mean lower turbulence or shear stress in that region; in fact, the total and turbulent stresses appear to peak where the mean velocity is at minimum (Figure 2-8).

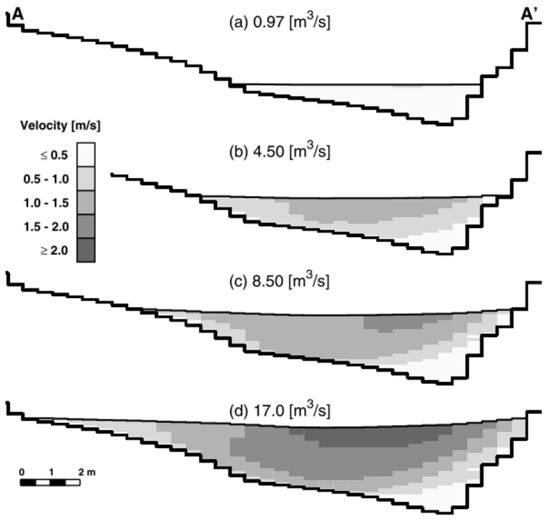

Figure 2-7 - Velocity domains at pool section for four different flow rates using a 3D numerical model (MacWilliams et al. 2006)

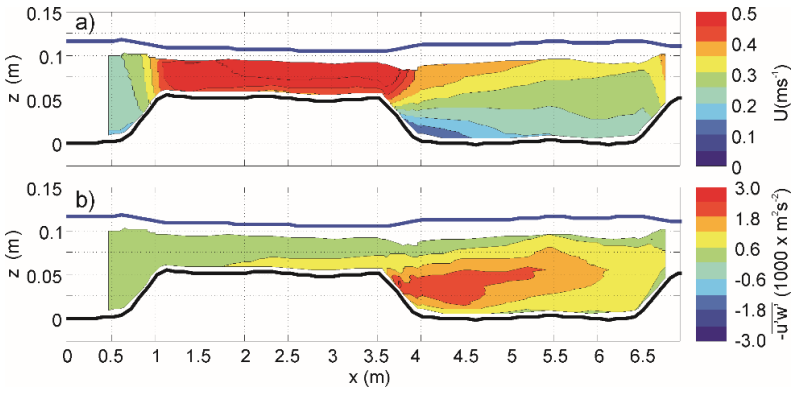

Figure 2-8 a) mean streamwise velocity b) Reynolds stress in a section crossing centerline of a pool-riffle unit (MacVicar & Best, 2013)

The current hypotheses rely on redistribution of flow and generation of turbulence that is not thoroughly understood. A number of studies on the effect of channel geometry or constriction on the turbulence and flow pattern have been performed, but there is not enough systematic analysis that answers why different geometries might produce the same or different results.

2.5 Sediment transport in pools and riffles

The stability of channel morphology is the main challenge of restoration projects. The instability of channels can affect the unwanted development of meandering, instability of bridge piers, the operation of weirs and culverts, and even the quality of aquatic life. For example, the high mobility of bed material can wash away or bury small species and fish eggs. On the other hand, an immobile or armoured bed can make the bed be rough and coarse for fishes to live and spawn. For these reasons, a mobile equilibrium bed should be the goal of restoration projects (Yager and Schott 2013). For rational design of pools and riffles, the sediment dynamic should be considered.

2.5.1 Sediment entrainment

The stability of a channel can be evaluated by assessing sediment entrainment. As reported in early studies, the most important factor in sediment transport and scouring is bed shear stress (Shields 1936). Shear stress is a function of turbulence intensity, flow depth, channel slope, roughness, and flow pattern. If the applied shear stress is equal to the shear strength of bed (critical shear stress), then sediment transport would be initiated. Shields diagram remains the most common method for estimating the threshold of shear stress for moving the grains (Buffington 1999; Buffington and Montgomery 1997; Shields 1936). In some previous studies and channel design manuals (Ancey et al., 2008; Lamb et al., 2015; Sear & Newson, 2004); researchers tried to use or modify Shields diagram for finding the critical shear stress (Milan et al., 2001). The fundamental issue with Shields stress criterion is that it is based on mean shear stress, which was determined based on experiments in uniform channels (Buffington 1999). In the uniform channel, there is a relatively predictable relation between turbulence and shear stress, meaning that the calibration is accurate for turbulence as well in these flow conditions. Over non-uniform flow the relation between mean and turbulent stress is different, and so the relation is less accurate and may even produce systemic errors where turbulence is high and mean velocity is low, conditions which occur in pools. As reported by Wiberg

and Smith (1987) the effect of shear stress on sediment entrainment can be interpreted by force balance on grains. Figure 2-9 shows that there are four major forces acting on a grain: drag and lift forces applied from the flow; resisting force from friction between particles, and gravity, which is the immersed weight of the grain. When the applied forces to a grain are higher than the resisting strength, the motion of sediment will be initiated.

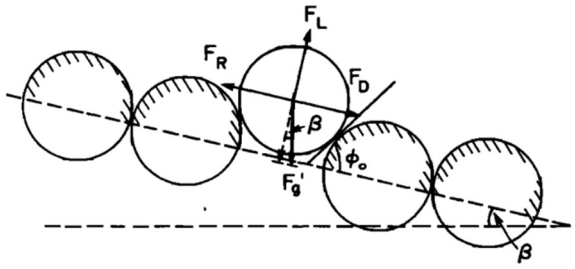

Figure 2-9- Force balance on a grain (Wiberg and Smith 1987)

At the moment of entrainment, the forces in at least one direction are in equilibrium, so either one of the following two conditions must be true:

$$F_g' \cos\beta = F_L \tag{2-1}$$

$$F_R = F_D + F_g' \sin\beta \tag{2-2}$$

$$F_R = \left(F_g' \cos\beta - F_L\right) \tan\emptyset_0$$

where F_R is resisting force, F_g' is the immersed weight of the grain, F_L is lift force, F_D is drag force, $\emptyset_0$ is repose angle, and β is channel slope. The drag and lift forces can be formulated as (Wiberg and Smith 1987):

$$F_D = \frac{1}{2}\rho C_D < u^2(z) > A_x \tag{2-3}$$

$$F_L = \frac{1}{2}\rho C_L(u^2{}_T - u^2{}_B)A_x \quad (2\text{-}4)$$

where ρ is water density, C_D and C_L are drag and lift coefficient respectively, A_x is cross-section area of the grain, $< u^2(z) >$ is square of mean velocity over the grain cross-section, u_T and u_B are top and bottom velocities over the grain. Drag and lift forces can also be determined by shear stress distribution over the grain instead of velocity pattern around them (Wiberg and Smith 1987).

$$F_D = \frac{1}{2}C_D\tau_b < f^2\left(\frac{z}{z_0}\right) > A_x \quad (2\text{-}5)$$

$$F_L = \frac{1}{2}C_L\tau_b[f^2\left(\frac{z_T}{z_0}\right) - f^2\left(\frac{z_B}{z_0}\right)] > A_x \quad (2\text{-}6)$$

where τ_b is the applied shear stress on the bed, $f\left(\frac{z}{z_0}\right)$ is velocity profile function, z_0 is bed roughness height, z_T and z_B are the top and bottom height of the grain. As shown from Equation 2-1 to Equation 2-6, the applied shear stress on the bed can be linked to the drag and lift forces on the grain. By considering Equation 2-2, 2-5, and 2-6 it can be shown that higher shear stress exertion on the bed increases the lift and drag forces, and then the resisting force will be reduced, and the streamwise applied force on the grain will be increased, which can increase the possibility of sediment entrainment. It can also be shown that a grain particle in well-sorted bed ($z_T \to z_0$ and $z_B \to z_0$) has lower exposure area to the flow then it has lower lift and drag forces, which increases the resisting force. For this reason, a well-sorted bed is more stable than poorly sorted one. As reported by Yager and Schott (2013) the applied force on a grain is not constant, it depends on the turbulence, eddies, and waves in the flow. Therefore, it can be interpreted by series of various periodical functions with different amplitudes and frequencies, and then it can be shown by a distribution. Some numerical and experimental studies showed that the threshold shear stress for entrainment (critical shear stress) is not exactly the same as the applied shear stress (Coleman and Nikora 2008). The sediment motion will be initiated if the applied shear stress exceeds the critical shear stress. As

illustrated in Figure 2-10 only those parts of the bed, which have lower critical shear stress than the maximum applied shear stress ($\bar{\tau}$), can move. It is important to note that it is possible to have sediment entrainments even if the mean of applied shear is lower than the mean of critical shear stress.

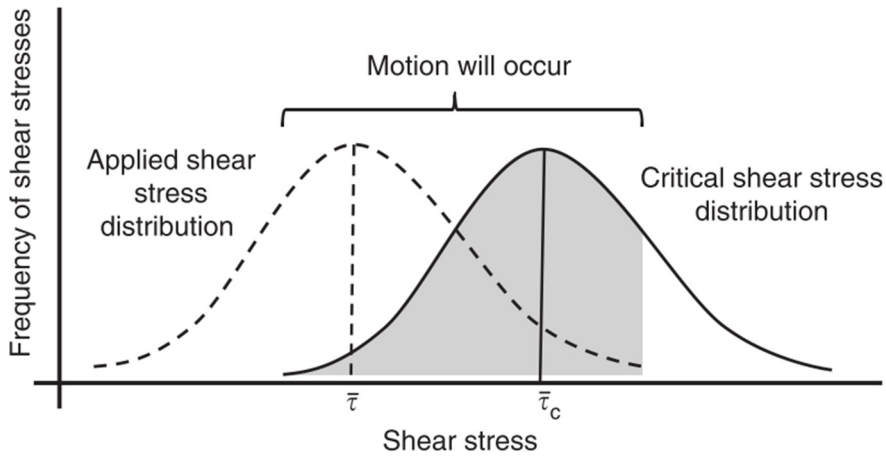

Figure 2-10- Schematic diagram of applied and critical shear stress (Yager and Schott 2013)

Some of the issues that researchers are trying to address are that they cannot theorize sheltering of fine sediments by coarse ones and their effects on the generation of fluctuations to move finer ones (Yager and Schott 2013). Moreover, the force balance between grains is not yet fully understood as, for example, even smaller particles can experience higher forces than their drag and lift forces would indicate because of contact with grains experiencing higher forces. The effect of turbulence on sediment entrainment has not fully understood yet because spatial and temporal parameters of turbulence and local characteristics of bed material cannot be predicted easily. Thus the findings of a particular case study cannot be generalized to all cases. However, parametric analysis with a wide range of mean and turbulent stress conditions could help designers to predict better sediment entrainment in different environments.

2.5.2 Bedload routing

When the applied force on a moving particle drops below the force required to keep it in motion the particle starts to deposit. The travel distance of particles depends on the flow behaviour and particle characteristics; therefore, the same particles with the same sizes tend to deposit in the same places. This mechanism is called sediment sorting. This is one of the most significant reasons for natural pool-riffle formation and maintenance based on the travel distance of particles, coarser material stores in riffle and finer in pools (Lisle 1979b). Some researchers showed that the transport of fine sediment from the center of pools was the result of the jet flow and flow convergence (Thompson & Wohl, 2009). The reason could be the higher turbulence condition, and dynamic loading of grain due to pulsation effect at the pools head after the deceleration part (MacVicar & Roy, 2011). The deposition of transported sediment from the center and head of pools at the tail of them can make the downstream riffle. And the deposition is the result of lateral flow divergence and boiling at the tail of pools (Buffington et al. 2002).

2.5.3 Effect of hydrodynamic on sediment transport

Despite limitations and issues related to scaling of sediment transport in the lab, it remains important due to the complexity of sediment transport and its interaction with the mean and turbulent components of the flow. Some researchers used the mobile bed for assessing the formation of morphological elements in rivers (e.g. pool-riffle). Lisle et al. (1991) used a poorly-sorted mixture of gravel and sand as bed material and inlet sediment in the flume for investigating the formation mechanism of bars in the steep channel. They saw a series of scouring and deposition in the flume that led to the formation and development of a meandering. Many researchers used completely or partially mobile bed in the flume to investigate sediment transport mechanism (Madej et al. 2009; Wilcock and Mcardell 1997; Wilcock and McArdell 1993). Diplas et al. (2008) used electromagnetic force to model drag force acting on steel spheres to investigate the effect of pulsation on motion initiation of sediment. They noted that because of turbulence

in the natural stream, the drag force, which is acting on the particles, has intensive fluctuations then they model this fact by making fluctuation in electromagnetic force. They stated that the sediment entrainment was not only depended on the magnitude of drag force, but also the duration of impulsion. Venditti et al. (2010) painted particles in a way that each colour was associated with particular grain size. They investigated the effect of flow pulsation frequency and amplitude on the transport of particular sediment sizes. They figured out that small transient pulses are more efficient in moving particles than a single large pulse.

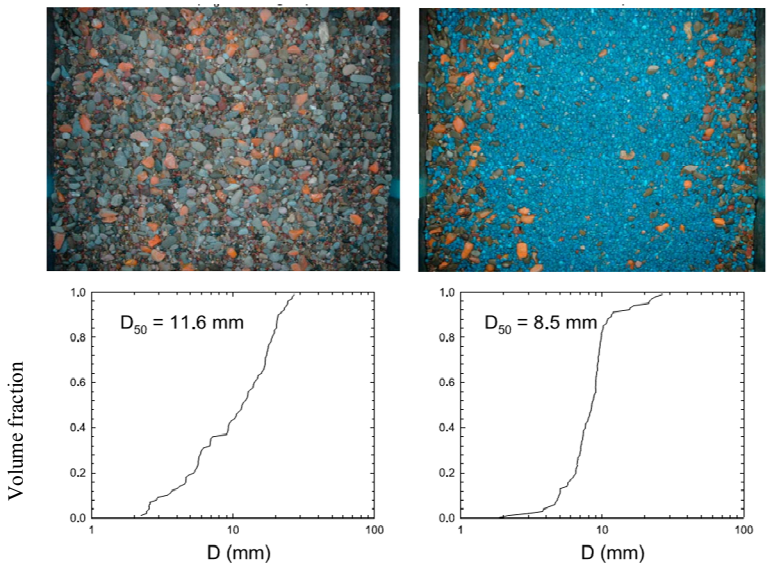

Figure 2-11 Bed picture and grain size distribution on a bed with a constant flow rate (Left) with pulsation (Right) (Venditti et al. 2010)**.**

2.6 Numerical analysis

In the last decade, many researchers used computational fluid dynamic (CFD) as a tool for hydrodynamic and geomorphological studies. Numerical methods have significant capabilities in compare with experimental and field studies, but the results must be validated with reliable data first. There are two

types of approaches in numerical analysis, steady state, and transient modelling. In steady state modelling, the variations of variables are zero in time. This kind of modelling is suitable for laminar flows and cases with steady, coherent structures. One of the advantageous of the numerical methods is that the velocity domain can be acquired for all regions, but in experimental and field studies, it is not possible due to the limitations of instruments. As stated before the most important parameters in hydrodynamic studies is shear stress; in numerical analysis, because of the possibility to measure velocity gradient in near-wall regions, the bed shear stress can be calculated precisely. The turbulence intensity is another important parameter for assessing the sediment transport rate and bed shear stress; therefore, numerical analysis is the best tool for this purpose. One of the limitations of using a steady state approach in hydrodynamic studies is that most of the phenomenon in this field is turbulent and containing dynamic behaviours. The capability of transient modelling enables researchers to study dynamic vortices and turbulent structures better. Another consideration in the modelling of the turbulent condition is that turbulence cannot happen in 2D modelling, and the case must be modelled in 3D because large-scale vortices must be stretched by all vorticity components before breaking into smaller scales. In the absence of one dimension, two component of vorticity is zero then large-scale eddies cannot be stretched. Viscosity cannot dissipate the energy of large-scale eddies; therefore, when they break into a smaller scale, by energy cascading the kinematic energy of large-scale eddies is transported to the smaller one, and then the viscosity can dissipate their energy. Constantinescu et al. (2013) performed three-dimensional transient large eddy simulations in an open channel with strong curvature. They detected strong transient helical flow in the bend by Q-criterion. As illustrated in Figure 2-12 they named strong vortices and defined their rotation direction by vorticity magnitude. Their results showed acceptable consistency with experimental data.

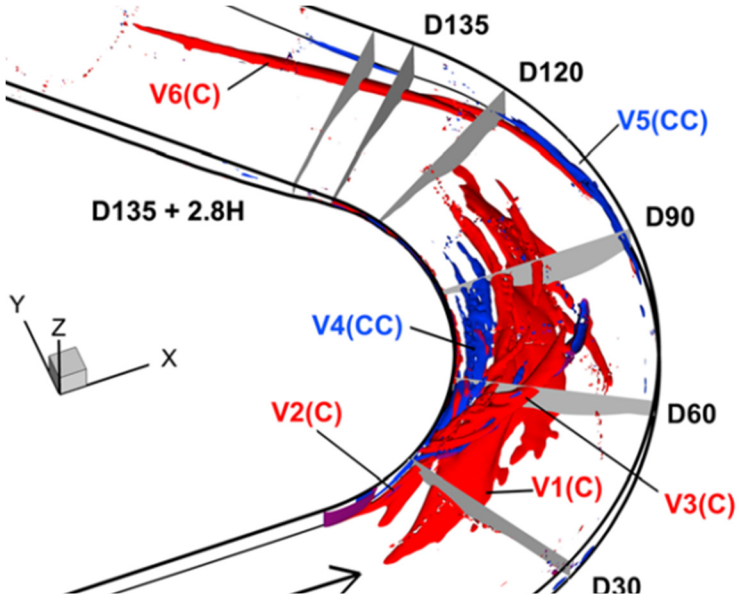

Figure 2-12- 3D visualization of strong vortices by Q-criterion, blue parts are rotating counterclockwise, and red parts are rotating clockwise (Koken et al. 2013)**.**

By reviewing literature, it can be concluded that the most of the researchers in this field, and especially in the field of water resources, did not pay attention to the limitation of numerical and experimental methods and there is a need for more advanced methods. Jackson et al. (2015) tried to evaluate the hypothesis of reversal flow in pools and riffles. They used 2D hydrodynamic modelling for simulating this case, but as stated before turbulence has a significant effect on the behaviour of the flow in pools and riffles and 2D modelling cannot simulate that condition. Another limitation of their study is that they tried to simulate this condition with steady-state approach, and as reported by many researchers (MacVicar and Roy 2007; MacVicar et al. 2012, 2013; Thompson 2013) this phenomenon is turbulent and unsteady, and then this case cannot be modelled by steady-state accurately. MacWilliams et al. (2006) performed 2D and 3D modelling of flow pattern in a pool-riffle sequence. The 2D model uses depth average velocity, and 3D model uses average near-bed velocity gradient for calculating the bed shear stress. These two methods were used to evaluate the flow convergence hypothesis. The point of convergence depends on the turbulence

condition; therefore, these two methods cannot precisely predict the flow convergence behaviour and shear stress exertion. They have stated that the deeper part of pools has lower shear stress in comparison to the shallower one, but they did not discuss the turbulence intensity and the effect of it on bed shear stress. They have stated that the highest bed shear stress only occurs in riffles, but as stated in the literature, pools have the most turbulent condition in pool-riffle units and because of turbulent condition the shear stress exertion could be higher in pools. de Almeida and Rodríguez (2011) used 1D unsteady flow for assessing the sediment transport rate and morphological changes. They used an empirical equation for calculating the sediment transport rate. Their empirical method was based on the ratio of bed shear stress and the strength of the bed. The shear stress in their model is based on the mean cross-section velocity. They did not consider the effect of turbulence intensity on sediment transport rate and shear stress exertion on the bed. It is not stated if they consider the secondary effect of scouring on flow pattern shaping or not.

2.7 Numerical methods

Due to the turbulent condition in most of the natural streams, it is better to use eddy-resolving techniques for more accurate results. In this chapter, the concepts of common techniques in CFD will be discussed briefly.

2.7.1 Numerical concepts

All numerical approaches to fluid flow try to solve the Navier-Stokes equations in some forms.

The Navier-Stokes momentum equation is:

$$\overbrace{\frac{\partial u_i}{\partial t}+\frac{\partial (u_i u_j)}{\partial x_j}}^{\textit{Inertial force}}=\overbrace{-\frac{1}{\rho}\frac{\partial p}{\partial x_i}}^{\textit{Pressure force}}+\overbrace{\frac{\partial}{\partial x_j}\left[\nu\left(\frac{\partial u_i}{\partial x_j}+\frac{\partial u_j}{\partial x_i}\right)\right]}^{\textit{Viscous force}} \quad (2\text{-}7)$$

where t is time, p is pressure and ν is kinematic viscosity. By choosing (i, j) as (1, 2), (1, 3), and (2, 3) then we have three coupled equations for a 3D model. The continuity equation for incompressible flow is:

$$\frac{\partial u_i}{\partial x_i} = 0 \qquad (2\text{-}8)$$

where (u,v,w) are velocity components in x,y,z directions, u_1, u_2, u_3 are streamwise, spanwise, and vertical components of velocity.

In direct numerical simulations (DNS), there is no turbulence closure scheme for approximation and all of the turbulence effects are simulated directly based on the exact behaviour of the flow. This approach requires high-resolution grids to simulate the viscous sub-layer and Kolmogorov's eddy scales. For example, Schlatter et al. (2014) used 4000 cores in parallel for simulating flow over a rough plate. In other approaches such as the Reynolds-averaged Navier-Stokes (RANS) equations, large eddy simulation (LES), and detached eddy simulation (DES) the effect of small-scale eddies are modelled separately and added to the Navier-Stokes equations as a means of reducing the computational requirements.

2.7.2 Reynolds Averaged Navier-Stokes (RANS)

By considering velocity as variable in time and averaging in time, each velocity component can be written as the sum of a mean part and fluctuating part:

$$u_i = \overline{u_i} + \acute{u}_i \qquad (2\text{-}9)$$

where $\overline{u_i}$ is mean part and $\acute{u}_i$ is fluctuation part of a velocity component. The RANS equations then combine the time averaged versions of Equations 2-7 to obtain the following:

$$\overline{u_j}\frac{\partial \overline{u_i}}{\partial x_j} = -\frac{1}{\rho}\frac{\partial \overline{p}}{\partial x_j} + \frac{\partial}{\partial x_j}\left[\nu\left(\frac{\partial \overline{u_i}}{\partial x_j} + \frac{\partial \overline{u_j}}{\partial x_i}\right) - \rho\overline{\acute{u}_i\acute{u}_j}\right] \qquad (2\text{-}10)$$

As can be seen in Equation 2-10, the most-right term ($-\rho\overline{\acute{u}_i\acute{u}_j}$) is the combination of fluctuation in velocity components. This term called the Reynolds stress, and it cannot be simulated in steady state modelling; therefore, researchers tried to approximate it with different methods. One of the most common for estimating Reynolds stress and modifying Equation 2-10 is using a turbulence closure scheme that is called k-ε. In k-ε two additional equations will be coupled with Equation 2-10 that are related to the kinetic turbulent energy and dissipation rate.

2.7.3 Large Eddy Simulation (LES)

In the RANS method, the filtration of velocity component is temporal by separating mean and fluctuation components. In LES models, the filtration is spatial, which means that each velocity component is separated into turbulent scales that are larger and smaller than the filter scale:

$$u_i = \widetilde{u_i} + \breve{u_i} \tag{2-11}$$

where $\widetilde{u_i}$ is velocity component of large scale and $\breve{u_i}$ is velocity component of sub-filter scale. By combining Equation 2-11 with the Navier-Stokes equation (Equation 2-7) it is possible to derive the LES momentum equation:

$$\frac{\partial \widetilde{u_i}}{\partial t} + \frac{\partial(\widetilde{u_i}\widetilde{u_j})}{\partial x_j} = -\frac{1}{\rho}\frac{\partial \tilde{p}}{\partial x_i} + \frac{\partial}{\partial x_j}\left[\nu\left(\frac{\partial \widetilde{u_i}}{\partial x_j} + \frac{\partial \widetilde{u_j}}{\partial x_i}\right) - \tau_{ij}^{SFS}\right] \tag{2-12}$$

τ_{ij}^{SFS} can be substituted by eddy viscosity (ν_t) equation:

$$\tau_{ij} = -\rho\overline{\acute{u}_i\acute{u}_j} = \nu_t\rho\left(\frac{\partial u_i}{\partial x_i} + \frac{\partial u_j}{\partial x_j}\right) \tag{2-13}$$

By using modified length scale (l_m), turbulent kinematic viscosity can be derived:

$$\nu_t = l_m^2\left|\frac{\partial \widetilde{u_i}}{\partial x_j}\right| \tag{2-14}$$

There are various methods for estimation of ν_t using some calibration constants.

2.8 Research gap

The overall research gap is that there is no comprehensive and unanimously agreed hypothesis on pool-riffle formation and maintenance. In addition, the effect and variation of pool-riffle geometry, which are the most important factors in hydrodynamics of pool-riffle units, is not investigated adequately, which makes it difficult to predict the success or failure of restoration designs. Limitations inherent in experimental and field studies mean that the understanding of hydrodynamics in pools and riffles can be improved with transient numerical studies. Due to the turbulent behaviour of the flow in pool-riffles, 3D and unsteady numerical approaches with appropriate turbulence closure schemes would be particularly insightful. Turbulence, temporal and spatial distribution of shear stress and their effects on sediment transport, which are the main gaps in pool-riffle research, can be investigated by linking of well-designed numerical simulations with experimental modelling. The most significant advantage of experimental and field studies is that they enable researchers to assess and evaluate the sediment transport mechanism. This objective cannot be addressed easily by numerical approaches; therefore, a targeted flume-experimental study could help to improve the understanding of the role of vortices in sediment transport and the relation between turbulence and pool-riffle maintenance.

Chapter 3: Effect of riffle height on turbulent structures and flow pattern in isolated pool-riffle units

This chapter is based on a manuscript that has been submitted to the Journal of Geophysical Research: Earth Surface. All the results were generated by myself, and I prepared the final document under the supervision of Dr. MacVicar.

Large eddy simulations of turbulent structures in plunging and skimming flow in straight pool-riffle bedforms

H. Dashtpeyma[1], and B. J. MacVicar[1]

[1] Department of Civil and Environmental Engineering, 200 University Avenue West, Waterloo, Ontario, Canada N2L 3G, University of Waterloo.

Corresponding author: Hamed Dashtpeyma (hdashtpe@uwaterloo.ca)

Key Points:

1-Four different types of vortical turbulent structures were detected in the zone of flow expansion in the pool head.

2-The turbulent structures steer the main flow by increasing the turbulent Reynolds stresses and the effective viscosity.

3-The degree of plunging or skimming of the main flow through the pool can be controlled by the height of the riffle and the Froude number at the riffle crest.

3.1 Abstract

Pool-riffle units are common topographical elements of rivers. Many hypotheses such as flow reversal and lateral flow convergence have been proposed for clarification of hydrodynamics in pool-riffle units. In this study, large eddy simulation (LES) is used to capture detailed information on flow characteristics in idealized pools and riffles. The Q-criterion is used to detect flow structures. The idealized structure is a straight channel with sloped bed rises and drops acting as zones of convective acceleration and deceleration. Four types of vortical structures are detected of these forms. Ramp rollers and corner eddies are shaped on the ramp and in the corners of the upstream part of the pool (i.e. the pool head), respectively. Surface turbulence is shaped at the free-surface of the pool-head. All the generated

vortices in the pool-head get stretched and form axial tail vortices. Interaction and combination of these vortices create three different types of incoming flow to the pool. If surface turbulence is strong it can interact with corner eddies and direct the incoming flow to plunge into the pool. If ramp rollers are strong, they can push the incoming flow away from the bed so that it skims the free-surface. If the ramp and surface rollers have similar strength, the incoming flow will be squeezed between the high turbulence zones so that streamwise velocity peaks in the middle of the flow depth.

3.2 Introduction

One of the most common topographical elements of rivers are pool-riffle units. The deeper parts of undulations in the bed are called pools, whereas the shallower parts are riffles (Figure 3-1). Pool-riffle sequences can be shaped naturally, but are also frequently used in river restoration projects (Bernhardt and Palmer 2007; Miller and Kochel 2009; Wohl et al. 2005). Many researchers have investigated the formation and maintenance mechanism of pool-riffle units (Keller, 1971; Keller & Florsheim, 1993; MacVicar & Roy, 2007; Wilkinson et al., 2008). One of the most famous hypotheses is "velocity reversal," which says that the near-bed velocity in pools will increase faster than the corresponding velocity in riffles, leading to higher shear stress and scour in pools at flood stages (Keller 1971). This hypothesis was not connected to a hydraulic analysis of flow over bedforms, however, and it has been difficult to confirm or refute, with several researchers finding rivers with stable pool-riffle units without velocity-reversal effects (Heritage and Milan 2004; MacVicar and Roy 2007a; Thompson 2013), and others qualifying that the likelihood and the magnitude of the reversal velocity are functions of width variations between the riffle and pool (Wilkinson et al., 2004). The importance of width variations has been reinforced by field, numerical, and laboratory demonstrations (de Almeida & Rodríguez, 2012; Nelson et al., 2015; White et al., 2010). The velocity reversal hypothesis has now largely been restructured by introducing the concepts of lateral flow convergence and sediment routing (MacWilliams

et al. 2006; Milan 2013; Sawyer et al. 2010), and considering the bulk flow properties in width restrictions (Caamaño et al., 2012, 2009). The flow convergence hypothesis does not explicitly consider turbulence, however, which is known to be strongly influenced by pool-riffle morphology (Clifford, 1993; Clifford & Richards, 1992; MacVicar & Roy, 2007b; Thompson, 2013), and influence in turn the scour and transport of sediment (Celik et al., 2013; Nelson et al., 1995; Sumer et al., 2003). Length scales of turbulent dissipation have also been shown to be similar to commonly observed scaling relations between channel width and the frequency of riffles and pools (MacVicar and Best 2013, MacVicar & Obach 2015), which suggests an appealing link between turbulence and macroscale morphology. More research is required to clearly understand turbulence generation and dissipation over pool-riffle bedforms in a way that integrates existing observations and considers both mean flow and turbulence induced stresses.

From a hydraulic perspective, the morphology of pools and riffles causes streamwise pressure gradients that forces flow to accelerate and decelerate. In such environments, turbulence is generated as a result of high strain rates during acceleration (Smits and Wood 1985) then spreads across the domain and dissipates when pressure gradients are removed. In a series of laboratory experiments in straight channels with low angle ramps (<7°) to simulate bedforms, MacVicar and Rennie (2012) and MacVicar and Best (2013) considered the convective accelerating flow (CAF) and convective decelerating flow (CDF) zones as flow perturbations and documented their effects on mean flow and turbulence. They found high turbulence intensities near the bed and channel sidewalls at the head of the pool in CDF, with the turbulent structures growing, expanding laterally from the side walls, and dissipating as they travelled downstream (MacVicar et al. 2013). Critically for theories of pool formation, they observed that the fastest mean flow occurs near the water surface along the centerline of the channel, i.e. that it ‘skims’ across the top of the pool rather than ‘plunging’ to the bottom of the pool where it could exert a strong influence on particle mobility. These patterns of mean flow and turbulence matched what occurred in the

head of a forced pool system (MacVicar and Roy 2007a, 2007b), which supported the hypotheses that the turbulence must be contributing to sediment mobilization and scour, particularly over the downstream riffle face and into the head of the pool (MacVicar and Roy, 2011). Limitations inherent to field and laboratory studies, however, mean that it is difficult or impossible to extrapolate these hypotheses to pool-riffles at different flow levels and with differing geometries.

In the last decade, many researchers have used large eddy simulation (LES) as a tool to understand the hydrodynamics over river morphologies (Bradbrook et al., 2000; Hardy et al., 2005; Keylock et al., 2012; Keylock et al., 2016; Stoesser et al., 2008). This method uses a subgrid-scale model to include the effect of small turbulent eddies on the mean and turbulent flow while allowing the larger turbulent eddies to be simulated explicitly investigated (Smagorinsky, 1963; Stoesser, 2014). In this way, it is possible to change parameters such as the flow or geometry that may be difficult in the field or physical models. Riffle height, for instance, requires multiple models to be constructed in the lab and is difficult or impossible to control in the field. Numeric simulations also have the advantage of allowing the instantaneous visualization and analysis of the entire flow field, which can be used to clarify the genesis and evolution of intermittent turbulent structures.

In the current study, transient turbulent flow is simulated using LES in isolated pool-riffle units with various riffle heights. Though many aspects of pool and riffle morphology are not investigated, the study is part of a larger effort to investigate turbulence generation and dissipation in pools and riffles that will increase the generalizability of the results. Given the novelty of the approach, we focused for the moment on a description of the turbulent structures and the key parameter of riffle height, which was found to exert an important control on the hydrodynamics, with observations of both plunging and skimming flow in pools. Specific objectives are to: 1) investigate, identify, and characterize turbulent structures in straight pool-riffle units; 2) demonstrate the effect of riffle height on flow patterns, and 3) illustrate the influence of turbulent structures on variation and mean bed shear stress. It is hoped that the results will

help to connect various observations of hydrodynamics in pools and riffles and contribute to better designs of pool-riffle structures that are sensitive to the local flow conditions.

3.3 Methodology

3.3.1 Model Geometry

The model geometry is based on one of the flume experiments completed by MacVicar and Obach (2015), which was in turn based on a geometric (1:10) and Froude scale (Fr ~ 0.6) matching of a field example (MacVicar and Roy 2007). The physical and numerical models use a simplified straight geometry of pool and riffle units in a 0.6 m wide channel (Figure 3-1). The simulated flume in the numerical model is 6 m long with a 1 m long uniform upstream section followed by a 0.52 m long upsloping ramp, a flat uniform shallow 'riffle' of 0.4 m, a 0.52 m long downsloping ramp, a flat uniform deep 'pool' of 2.4 m. A final upsloping ramp and short uniform shallow section were used to define the downstream boundary of the model. For the series of simulations in this study, the riffle height was varied as shown in Table 1. With the fixed length of the ramped sections, the change of riffle height also changed the ramp angles. The average inlet velocity (U_o), the flow depth in the pool (h) and the Froude number in the pool were 0.21 m/s, 0.12 m, and 0.2 for all cases, respectively. For reference, X, Y, and Z represent the streamwise, vertical, and spanwise directions, respectively.

The cases described in this study were designed to approach and slightly exceed the thresholds for choking flow based on a specific energy analysis. By considering the velocity variation in only the streamwise direction, the specific energy m is calculated as $E = h + \alpha U^2/2g$, where α is the energy coefficient, U is the cross-section average flow velocity, and g is the gravitational constant (9.81 ms^{-2}). A critical height for a bed rise that is just sufficient to induce choking flow (ΔZ_c) can then be found as the difference between the critical specific energy (E_c) and E, where $E_c = 3/2\sqrt[3]{Q^2/gW^2}$, Q is the total

discharge and W is the width of the channel. For $Q = 0.0151$ m^3/s, $h = 0.12$ m, $W = 0.60$ m and assuming $\alpha = 1.0$, $E = 0.122$ m, $E_c = 0.060$ m and $\Delta Z_c = 0.062$ m. For real flows the threshold for choking flow may vary because of nonuniform distributions of velocity ($\alpha > 1.0$), and the effects of turbulence, sidewall and surface roughness, and transitions at sharp edges.

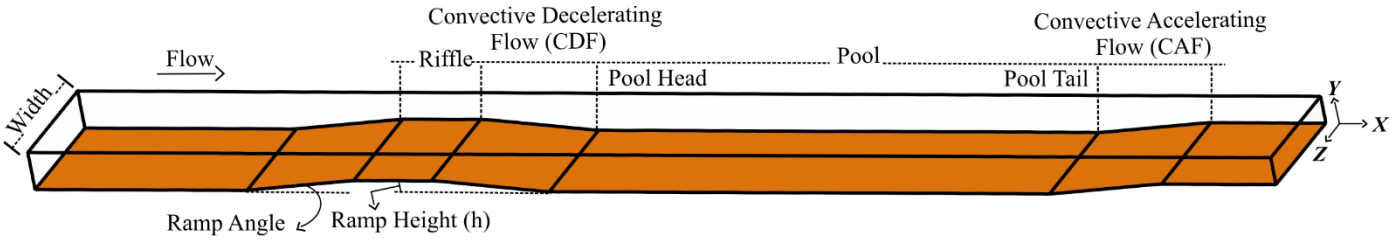

Figure 3-1- Simplified geometry of a pool-riffle unit as used in the current study

Table 3-1- Simulation parameters

Case name	Riffle height [m]	Ramp angle [°]	Fr at riffle
R45	0.045	4.95	0.5
R50[a]	0.05	5.49	0.6
R55	0.055	6.04	0.7
R60	0.06	6.58	1
R65	0.065	7.13	1.1

Note: [a] case R50 is the same as case R40P240 in MacVicar and Obach (2015).

3.3.2 Numerical Method

Simulations used the commercially available ANSYS CFX Version 16.2 software. In ANSYS CFX, large eddy simulation (LES) was used to model the flow. The initial condition for the distribution of

flow and turbulence intensity was determined by first modelling the system with a steady state Reynolds average Navier-Stokes (RANS) approach and a K-epsilon model for turbulence. Because of smooth and non-slip walls and bed, a wall-function is not required. Instead, the LES Smagorinsky (1963) method was chosen, which has been widely used in similar geomorphic research (Keylock et al., 2005, 2012). For more detailed information about formulations and equations of LES see Rodi et al., (2013). The simulations were 3D, with a structured mesh generated using ICEM Version 16.2, and a total number of elements equal to 48.5×10^6. Minimum cell size in the near-wall region was 1×10^{-3} m, which was selected to satisfy the criteria suggested by Keylock et al. (2012), who recommended at least six points for resolving small eddies generated in this region, which they have the same scale as the height of the riffle. Also following Keylock et al. (2012), cell sizes were 1/40 of the depth, which meets the recommendation to keep the free surface cells to less than 1/20 of the flow depth. The total time for transient modelling was 250 s, which is > 300x the largest eddy scale ($\sim h/U_o$) and easily exceeded the recommendation of 20x the eddy time scale by Keylock et al. (2012). The first 50 s were not considered because of initial condition effects, so only the results between 50 s and 250 s were recorded for analysis. On the machine we used, which has dual CPUs, each with ten cores of 2.3 GHz with CPU model Intel(R) Xeon(R) 2650 V3, and 192 GB RAM, one complete simulation took approximately 240 hours. Post processing was completed with CFD-POST Version 16.2 and MATLAB R2017b.

3.3.3 Boundary Conditions

Following (Hirt and Nichols 1981), the volume of fraction (VOF) method was used to model the multi-phase flow and locate the free surface. In VOF, the assumption is that the fluid occupies the entire domain with the characteristics that are a function of the fractional volume of the primary fluid (i.e. water in this study), which its value is one at any nodes that are occupied by primary fluid and zero when they are empty or occupied by the secondary fluid (i.e. air). Considering free surface is moving with the fluid,

by adding a kinematic transport equation for fractional volume to other equations, the free-surface can be located in transient models as well. By using this method, there is no need to solve two sets of equations for each phase. Therefore the calculation can be done with lower computational cost. For more details and formulation see (Hirt and Nichols 1981).

Using VOF, the inlet was separated into air and water zones at the experimental flow depth (h = 0.12 m). The air zone had zero velocity inlet and the constant pressure of zero. The water zone was defined as having a hydrostatic pressure distribution with a fully developed steady water velocity profile. To define the inlet velocity profile, a separate simulation was done with uniform velocity inlet (U_0 = 0.21 m/s) in a ten meter long uniform channel (i.e. without pools and riffles) with the same slope, width, flow height and simulation adjustments. The time-averaged velocity profile at the end of the plain channel was used as the inlet profile of pool-riffle simulations. The outlet was defined as having a constant hydrostatic pressure distribution for water and constant zero pressure for air. In all locations, a distance of at least 4 cm was maintained between the water surface and the top of the simulation space, which allowed the free surface to be shaped based on the hydraulic characteristics alone.

3.3.4 Q-criterion for detection of vortex cores

One of the most challenging problems in hydrodynamic studies of open channel flows is the detection of dynamic vortices and turbulent structures. Moreover, in turbulence and transient modelling, the core of dynamic vortices are not detectable in the streamlines or vectors of mean or instantaneous velocities. In addition, even the vorticity cannot give sufficient information about them near the wall-region due to high velocity gradient (Dubief and Delcayre 2000; Roy et al. 2004; Schlatter et al. 2014). Dubief and Delcayre, (2000) showed that the dynamic vortices in turbulence could be detected by Q-criterion, even in regions with high strain rates, defined as:

$$\mathrm{Q} = \frac{1}{2}(\Omega_{ij}\Omega_{ij} - S_{ij}S_{ij}) \tag{3-1}$$

$$\Omega_{ij} = \frac{u_{i,j} - u_{j,i}}{2} \quad (3\text{-}2)$$

$$S_{ij} = \frac{u_{i,j} + u_{j,i}}{2} \quad (3\text{-}3)$$

where u_i is instantaneous velocity in i direction, $i \in \{X, Y, Z\}$, and j related to different spatial coordinate, $u_{i,j}$ is the spatial gradient of u_i in j direction. Positive values of Q occur where the rotation term of equation (2) ($\Omega_{ij}\Omega_{ij}$) exceeds the strain rate ($S_{ij}S_{ij}$) and indicate the presence of rotational flow or vortices. This method has been used recently in several hydrodynamic and geomorphological studies to identify and describe vortices in channel confluences, around groynes, and in channel bends (Beheshti et al., 2017; Ettema et al., 2017; Guillén Ludeña et al., 2017; Keylock et al., 2012, 2016; Zeng & Constantinescu, 2017). Based on its success in similar studies in rivers and the utility of comparing structures between morphologic environments, the Q-criterion was applied in the current study.

3.3.5 Validation

The experimental data for the case of R40P240 from MacVicar and Obach (2015), corresponding with case R50 (Table 1), was used to validate the flow behaviour, water surface elevation, and the distribution of time average streamwise flow velocity (U_x) in the numerical simulations. As a note, the ramp angle of 7.2° reported by MacVicar and Obach (2015) referred to the design rather than the as-built angle of the physical model, which was in fact 5.5°. Time-averaged numerical results and experimental data are compared in Figure 3-2. Water surface level is similar in both numerical and experimental results, with a drop at the riffle that is consistent with what is expected from a specific energy analysis for subcritical flow (Figure 3-2a). Froude numbers from simulated models calculated at the top downstream edge of the riffle match the analytical calculations (Table 1). Seven time-averaged streamwise velocity profiles normalized by the inlet velocity (U_x/U_o) are shown at different points along the channel centerline between the middle of the riffle and middle of the pool (Figure 3-2b). Numerical results are generally

consistent with experimental data, especially in the pool, which is a key area for assessing existing hypotheses for pool-riffle hydrodynamics. The numerical results show higher velocity near the surface and lower near the bed, which are similar to the experiments. The numerical and experimental profiles of U_x diverge near the bed at the middle of the ramp (profile 3). This divergence is thought to be related to experimental uncertainty in the measurement technique of MacVicar and Obach (2015), which used single beam ultrasonic velocity Doppler profilers (UDVPs) and interpolated profile results measured at different angles to estimate the orthogonal velocity components. The UDVPs were more accurate where turbulence intensity was low, and the interpolation was more accurate where gradients in velocity and turbulence intensity were low, conditions that were not met close to the bed within the flow expansion.

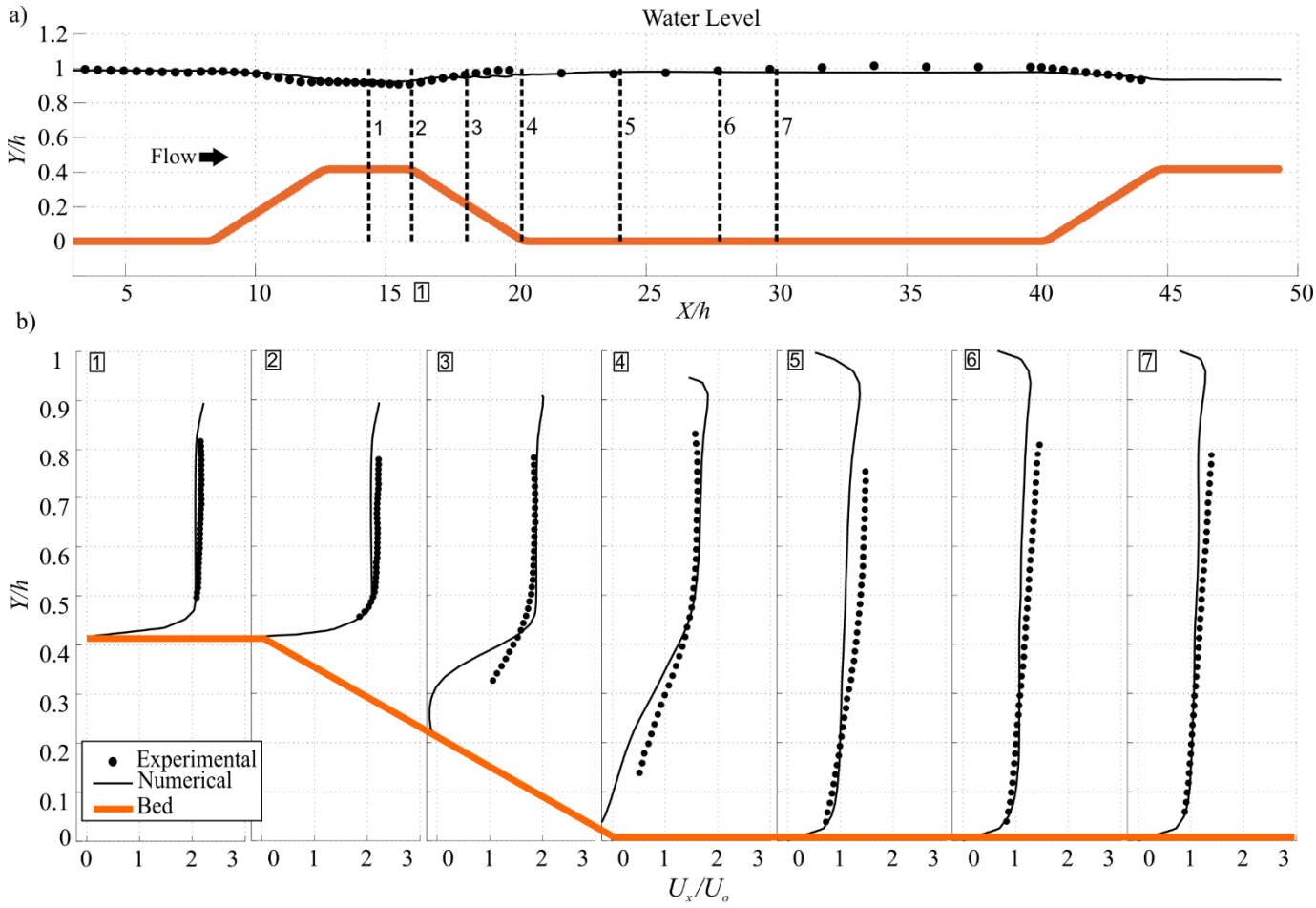

Figure 3-2- Validation of numerical results with available experimental data, a) water surface elevation at centerline, b) profiles of time-average streamwise velocity (Ux) for locations shown in a)

3.4 Results

3.4.1 Skimming and plunging flow over bedforms of different heights

The height of the riffle in the simulations exerts a strong control on the overall patterns of flow and turbulence distributions in the pool. In case R45, for example, the contour of time-average velocity magnitude (U) shows higher velocity near the surface and lower velocity near the bed (Figure 3-3a). Moreover, higher turbulence intensities (U_{stdv}/U_o) can be seen near the bed in CDF zone where the

average-velocity is low (Figure 3-3b). The flow pattern for case R45 is broadly similar to what was observed by MacVicar and Best (2013) in flume experiments over similarly sized bedforms. Based on the similarity with Nowell and Church's (1979) description of flow interaction with micro-roughness elements, we refer to this type of flow pattern as ‘skimming’ flow herein. By increasing the riffle height, in case R55, skimming flow occurs at the upstream end of the pool, but the highest time-average velocity tends to dip towards the middle of the pool depth by the middle of the pool length (Figure 3-3a). High turbulence intensities are initially observed near the bed in the pool, but as flow travels downstream, the distribution of turbulent intensity becomes more evenly distributed across the flow depth (Figure 3-3b). Based on the observed tendency for higher velocity fluid to push through the middle of the flow profile, we refer to this flow pattern as ‘rifting’ flow herein. In case R65 the flow pattern is nearly completely reversed from case R45, with higher time-average velocity near the bed of the pool and higher fluctuations near the surface (Figure 3-3). The zone with high turbulence intensities begins near the water surface at the downstream riffle crest and extends down through the pool as it expands vertically. A small region with high fluctuations occurs near the bed in the decelerating flow, but these fluctuations appear trapped in a relatively small region of the flow by the strong jet-like flow moving toward the bed of the pool. Because of this strong downward motion, we refer to this flow pattern as called ‘plunging’ flow.

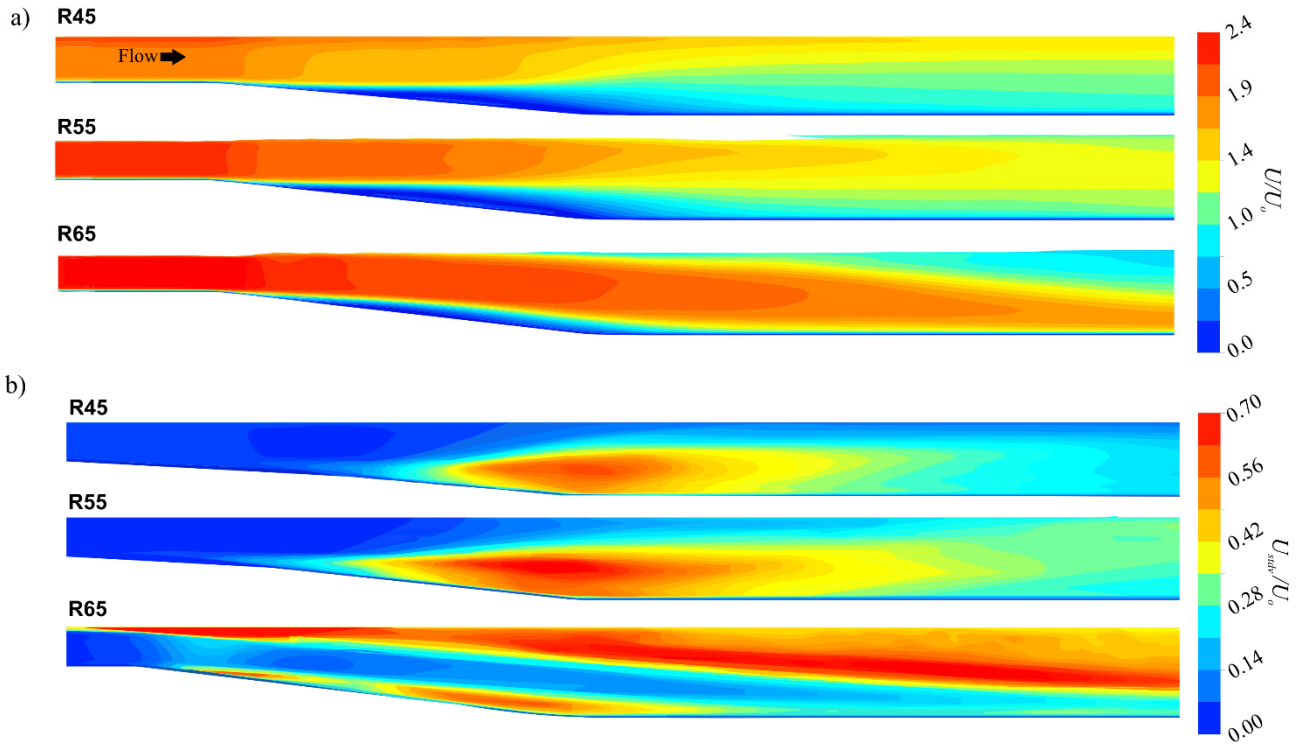

Figure 3-3- a) time-average velocity magnitude (*U*) in the *X-Y* plane at channel centerline, b) total velocity standard deviation (U_{stdv}) in the *X-Y* plane at the channel centreline.

The type of velocity profile has implications for the distribution of Reynolds's stresses in the pool. In skimming flow (cases R45 and R50), Reynolds stresses tend to peak in the lower half of the profile and decrease towards the bed and the water surface as is common in uniform flow channels (Figure 3-4b). Even in the 'rifting' flow, which the profile in the middle of the pool shows is relatively weak, with a nearly constant velocity from y/h =0.1 to the water surface (case R55), the Reynolds stress tends to similarly peak at y/h ~ 0.35. However, for plunging flow (cases R60 and R65), the peaks in Reynolds stress are stronger and closer to the bed, while negative Reynolds stresses generally occur above y/h ~ 0.25.

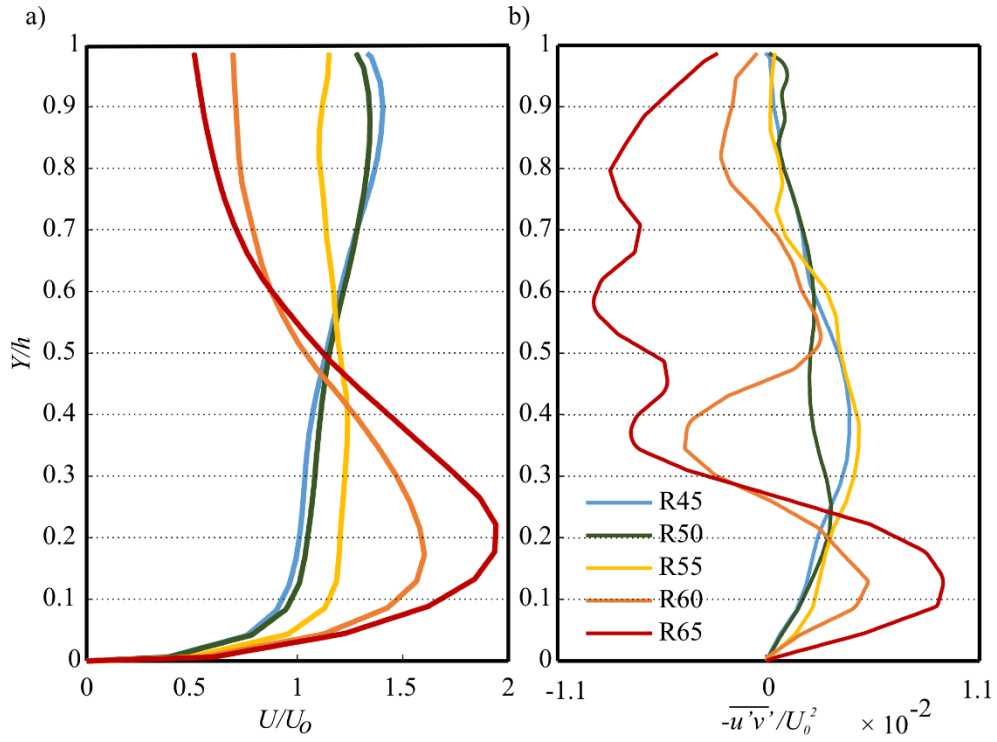

Figure 3-4- a) time-average velocity, and b) Reynolds stress profiles at the centre of the pool for the five cases listed in Table 3-1.

3.4.2 Vortical turbulent structures in the decelerating flow

Many powerful vortical turbulent structures are generated in the region of decelerating flow at the head of the pool (Figure 3-5). Looking over the whole width for the example case R50, Q-criterion thresholding shows that the turbulent structures generated in this area are physically larger and more powerful than those generated anywhere else in the test channel. From this example, two types of generative structures and one type of dissipative structure are identifiable. One type of generative structure is formed close to the bed of the ramp and oriented across the width of the channel, which we refer to herein as 'ramp rollers' (RR). RR have a hairpin structure, with the tails attached to the bed while the heads are elevated. Figure 3-5b shows one example of a growing, stretching, and dissipating structure in four time steps. The head of hairpin vortices dissipate quickly as they grow and are ejected into the main flow (head is not

visible for t = to+0.6 s), but the legs remain identifiable as vortices a bit longer and get stretched as they travel through the pool near the bed. Without the connecting head, we refer to the residual legs of the structure as 'axial tails' (AT). The second type of generative structure in the flow expansion zone is formed in the corner between the bed of the ramp and the sidewall of the channel, which we refer to as 'corner eddies' (CE). In contrast with RR, their structure is more complex because they are formed due to interactions with both the bed and the sidewall boundary layers, and they can occupy the full flow depth. Similar to RR, CE tend to grow in the flow expansion zone before breaking into smaller scales, with the largest elements losing the vorticity that makes them visible using the Q-criterion as they move downstream. Also similar to RR, the legs of CE tend to remain visible longer as they are stretched downstream to form AT. Residual structures from the CE remain near the surface, similarly angled away from the sidewalls as they travel downstream. These structures are referred to simply as 'surface turbulence' (ST). AT finally dissipate further downstream in the uniform flow section, likely due to viscous forces in the flow.

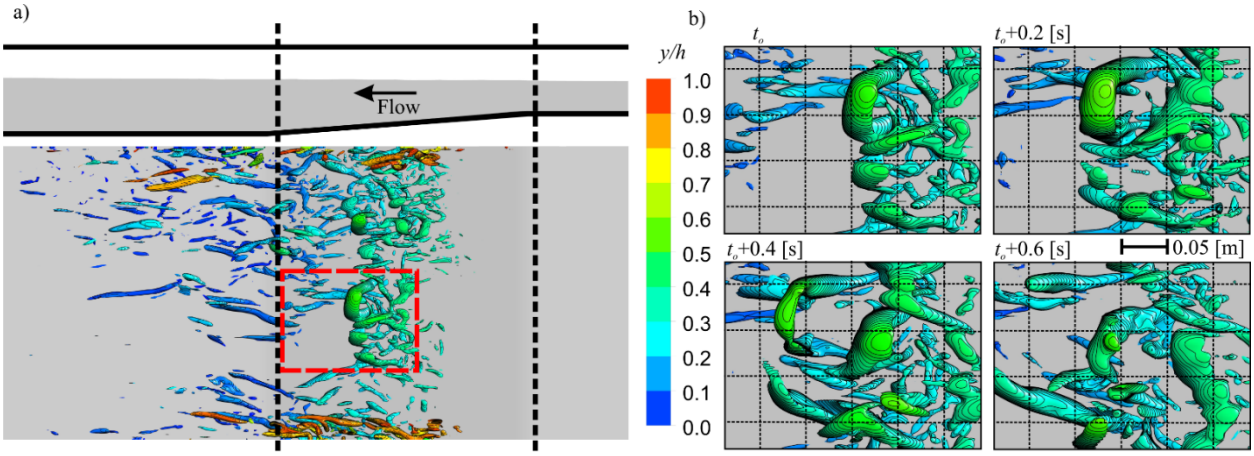

Figure 3-5- a) Instantaneous flow structure in case R50 defined by iso-surface of Q=15 s^-2 and shaded by relative depth, b) development and breakage of a ramp roller over time.

3.4.3 Effect of riffle height on dynamics of turbulent structures and stresses on the bed

Despite different riffle heights and significant changes in the types and strengths of turbulent structures that are observed, the CDF zone remains the main origin of turbulence in a pool-riffle unit for the geometries investigated in this study. Figures 3-6, -7, and -8 show a section of the simulation domain from the middle of the riffle to the middle of the pool for simulation cases R45, R55 and R65, respectively. Each figure is comprized of three subfigures showing an instantaneous view of the flow including a) *X*-*Z* plane views of the iso-surface of Q-criterion =12 s^{-2} over the bed relative vertical pressure gradient in the Y direction (defined below), b) *X*-*Z* plane views of contours and direction of applied bed shear stress, and c) an image of Q-criterion for three *Z*-*Y* sections of the flow. The relative vertical pressure gradient is defined as the difference between the actual instantaneous pressure gradient in *Y* and the hydrostatic pressure gradient. Strongly negative dynamic pressure gradients are relevant for a discussion of sediment mobility and scour in pools because they would correlate with high lift forces on the bed.

The vortical structures in case R45 are similar to those in case R50; however, CE and RR are weaker and smaller (Figure 3-6). RR are again hairpin-like vortices that grow over the ramp and dissipate in the deep uniform section. They mostly have negative *Z*-vorticity (rolling in the flow direction). Figure 3-6a shows that RR are preceded by a zone of strongly negative relative pressure gradient in the vertical direction and followed by strongly positive relative pressure gradient in the vertical direction. The RR thus apply strong vertical pulsations in force to the bed. The structures also increase bed shear stress in CDF zone, and their effects become stronger if they are closer to the bed (Figure 3-6b). Directly beneath the head of the hairpin-like structure, a negative shear stress (opposite to flow direction) is exerted on the bed, which applies strong bed-parallel pulsations in bed shear stress as they rolling downstream. CE do not have a dominant spin direction because they are shaped by momentum exchange between the main flow and

both the near bed and the near side wall regions, complex effects of secondary flows to the walls, Kelvin-Helmholtz effect in shear layers, or vortex induction result in smaller pulsations in both vertical pressure gradient and the bed shear stress. The CE mix with other vortices (e.g. RR) and transition to AT as they travel the downstream. The AT tend to produce parallel areas of strongly positive and negative relative vertical pressure gradients (Figure 3-6a) and high and low bed shear stress (Figure 3-6b). High and low shear stress around the AT tend to occur where shear vectors diverge and converge, respectively. The strong AT indicated in Figure 3-6c for section C, does not result in high pressure gradients or shear stress at the bed because it is located closer to the middle of the depth. In contrast, the AT structures located just downstream of section B are closer to the bed and have a more significant impact on the bed pressure and stress.

By increasing the riffle height to 0.55 m, the Froude number increases at the riffle crest and the relative strengths of CE and RR change (Figure 3-7). Most significant is that the CE become stronger and the region of flow characterized by complex turbulence as a result of interactions between the near-bed and near-sidewall regions increases over the ramp and downstream into the deep uniform pool. Though somewhat obscured by the number of vortices detected with the Q-criterion, the CE are associated with strong pulsations in relative vertical pressure gradients (Figure 3-7a) and, more clearly, with high bed stresses oriented towards the walls (Figure 3-7b). Moreover, the CE appear first near the surface of the water rather than in the corner over the ramp and then extend towards the bed as the flow travels downstream (Figure 3-7c sections A and B). The patterns of bed shear stress and flow are not symmetric in this case. The RR are similar to the previous case but are confined to a narrower region in the centre of the channel (Figure 3-7a). As for the previous case, they are associated with strong pulsations in relative vertical pressure gradient and bed shear stress. The AT extending into the deep uniform pool are relatively small and weak compared to the large numbers of vortices near the water surface and channel

sidewall in this area (Figure 3-7c). Vortices generated near the walls and free-surface extend into the pool to create these vortices (Figure 3-7a and c).

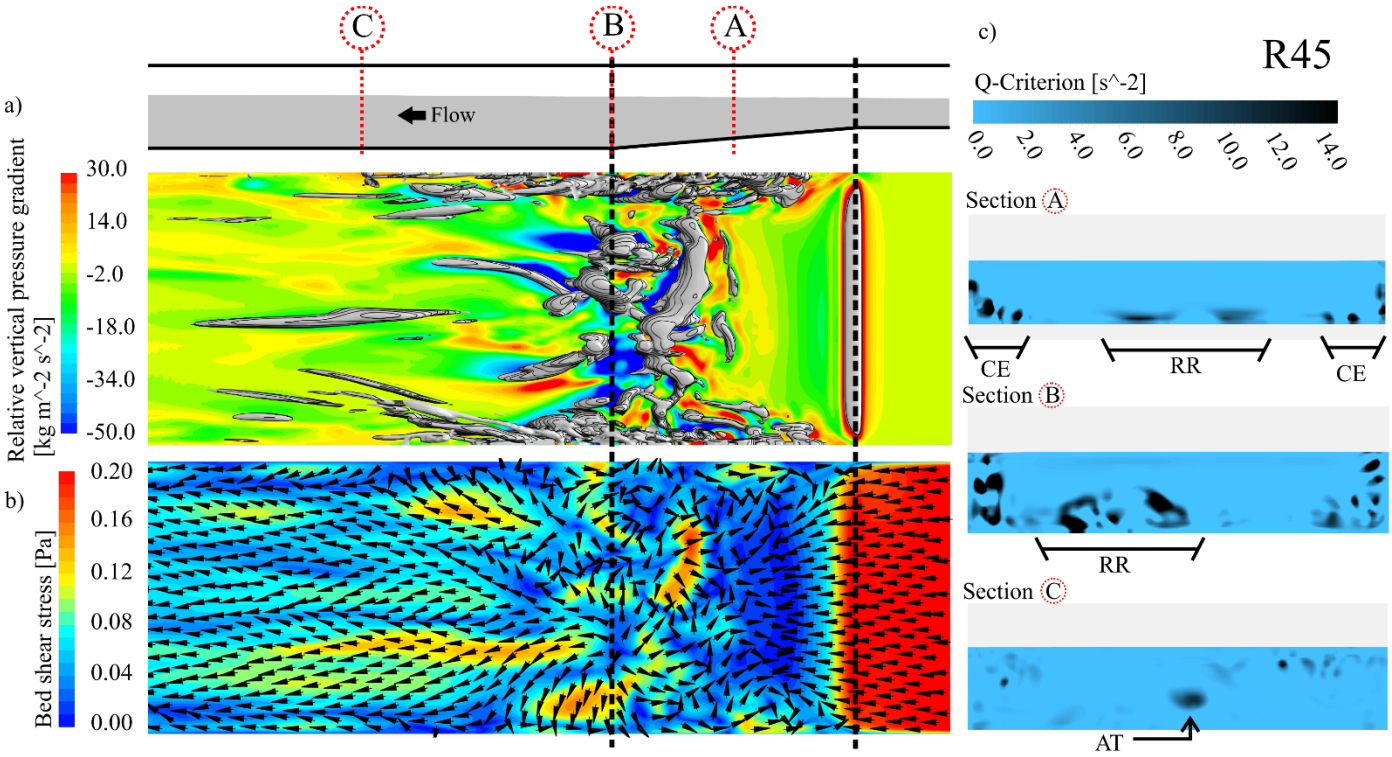

Figure 3-6- Instantaneous vorticity and hydrodynamics for case R45, showing: a) Iso-surface of Q=12 s^-2 showing flow structures, and contour of relative vertical pressure gradient at the bed, b) contour and vector of bed shear stress magnitude, c) contour of Q in three cross-sections.

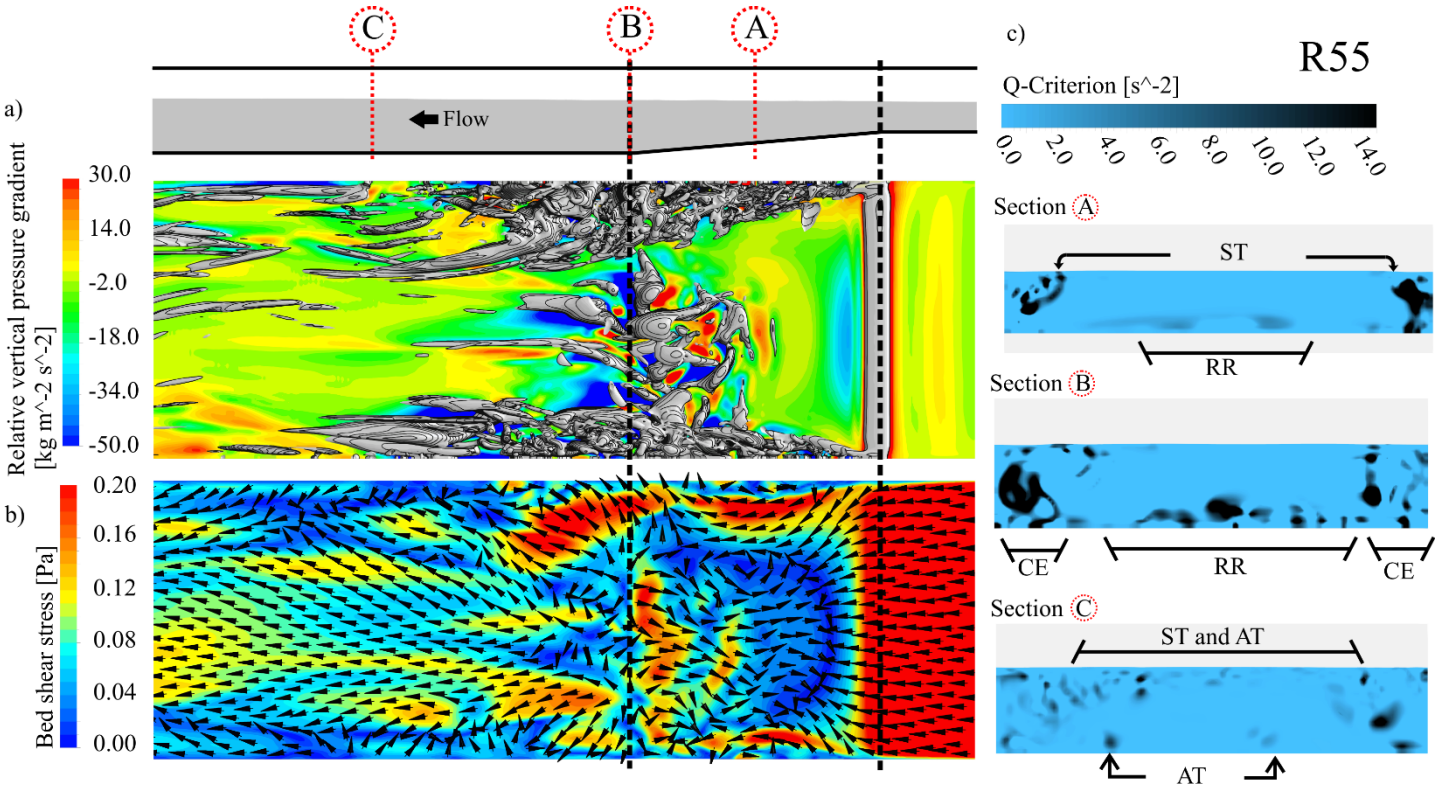

Figure 3-7 Instantaneous vorticity and hydrodynamics for case R55, showing: a) iso-surface of Q=12 s^-2 showing flow structures, and contour of relative vertical pressure gradient at the bed, b) contour and vector of bed shear stress magnitude, c) contour of Q in three cross-sections

R65 is the case with the highest riffle height, and the Froude number at the riffle crest (Fr~1.1) indicates a super-critical condition in the riffle, and is followed by a surface undulation hydraulic jump at the pool head. Many of the differences described between cases R55 and R45 are extended between cases R65 and R55 including large and asymmetrical CE regions, strong lateral funneling of the flow, and the suppression of RR to the point that they do not exceed the Q threshold used for visualization (Figure 3-8a). The relative vertical pressure gradient is strongly negative in the middle of the channel at the bottom of the ramp, but this effect appears to be related to the high velocity of the mean flow rather than the passing of turbulent structures. The bed shear stress is high over a large area of the ramp and deep uniform pool, with all of the stress directions pointing downstream in this area. A cross section of the Q-

criterion in the sections B and C shows an asymmetric distribution of strong vortices near the water surface of the flow, with an area of low vorticity near the bed that delineates a zone of high velocity flow plunging under the highly turbulent flow, which is characteristic of hydraulic jumps.

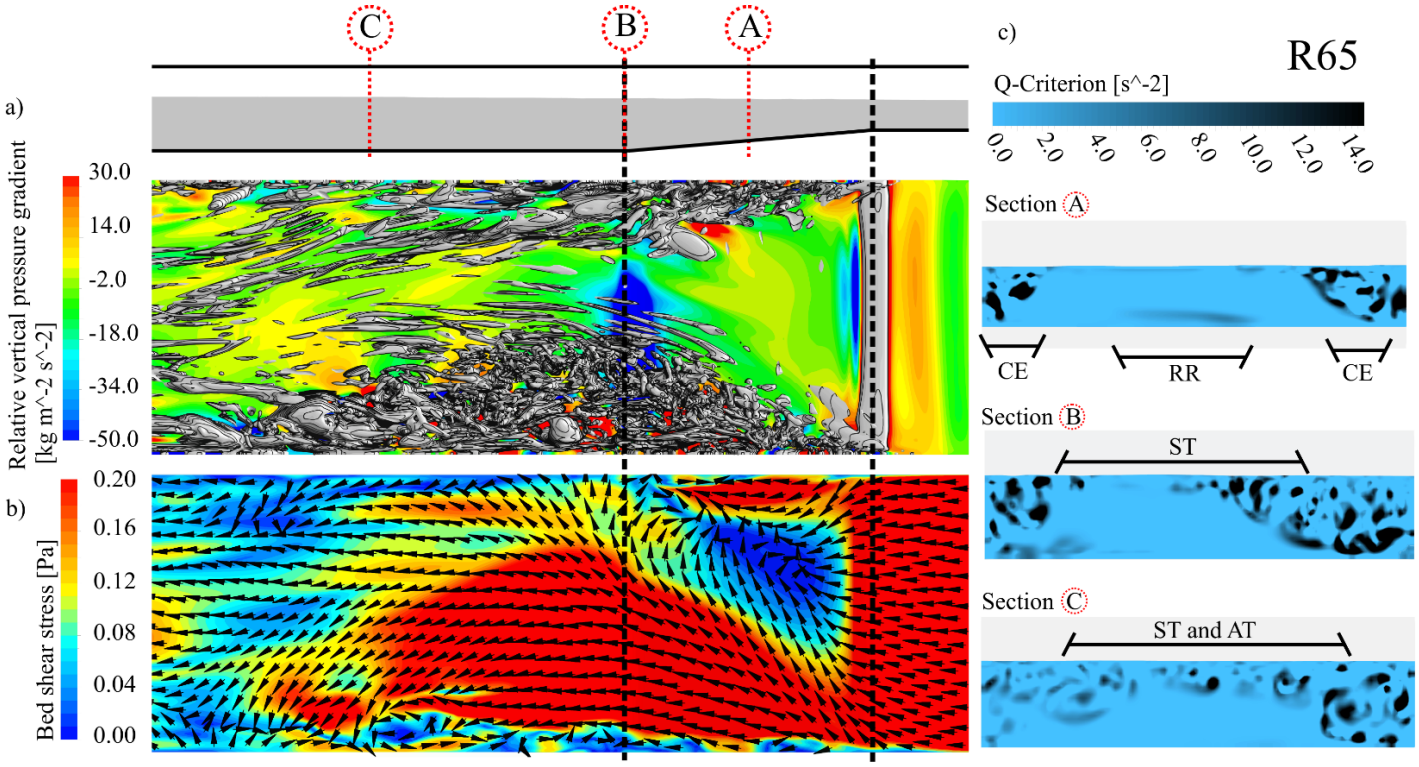

Figure 0-8- Instantaneous vorticity and hydrodynamics for case R65, showing: a) Iso-surface of Q=12 s^-2 showing flow structures, and contour of relative vertical pressure gradient at the bed, b) contour and vector of bed shear stress magnitude, c) contour of Q in three cross-sections

3.4.4 Bed shear stress

By increasing the riffle height, the magnitude and fluctuation of bed shear stress increase in CDF and pool head. Figure 3-9 shows the time-average and 95% confidence range of shear stress at the centreline between the middle of riffle and the middle of the pool. In the case R45, the average of shear stress in the pool is lower than that of the riffle; however, because of higher fluctuations, the upper bound

of shear stress reaches to the same magnitude in the riffle, despite lower velocity average in the pool. The fluctuations of shear stress decrease further downstream in the pool, but the average remains relatively flat. Similar dynamics are observed for case R55, despite average shear stress in the riffle and shear stress fluctuations in the pool that are higher than those in case R45. In case R65, the maximum shear stress in the riffle is almost four times the value in case R45. For this last case with the relatively high riffle, the flow is supercritical by the time it reaches the upstream limit of the ramp and the rapid increase in shear just upstream of the ramp is likely due to a decreasing depth as would occur at the downstream lip (i.e. the brink depth) of a broad-crested weir. The average shear stress decreases in the upper part of the ramp as was observed in cases R45 and R55, but then increases at the bottom of the ramp and slightly downstream. Shear stress fluctuations are higher than for the previous cases, and their magnitude decreases only slightly through the section of the pool shown in Figure 3-9.

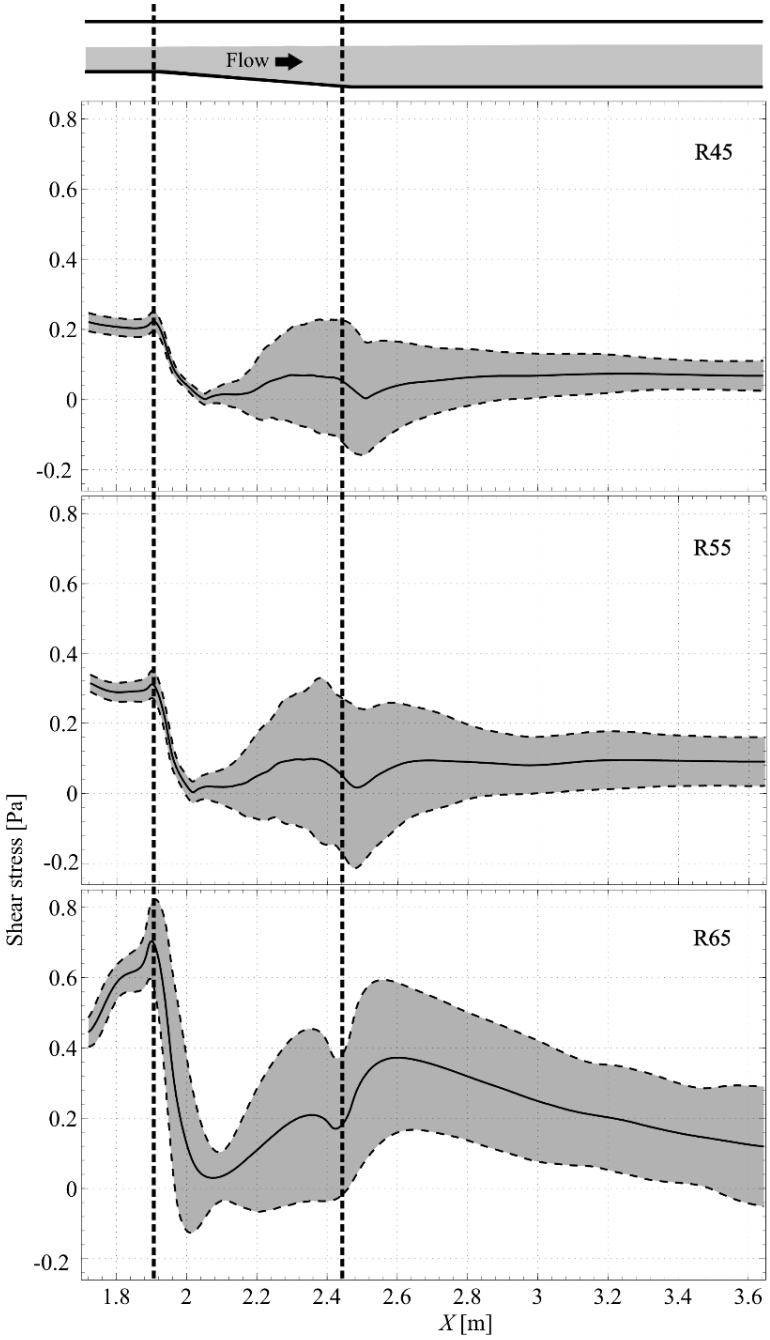

Figure 0-9- Time-average (black line) and 95% confidence range (dashed line) of bed shear stress at centreline for cases R45, R55, and R65.

3.5 Discussion

The simulations described in the current study offer a detailed look at turbulence generation and mean flow in a simplified pool-riffle morphology in open channels. The novelty of the work is the application of an advanced turbulence scheme that uses transient, three-dimensional, and deformable free-surface approaches to the studied morphology, which exceeds what has been applied to date with comparable bed morphologies (Jackson et al., 2015; Keller & Florsheim, 1993; MacWilliams et al., 2006; Stoesser et al., 2008). This modelling approach allows a unique examination of the interplay between areas of high velocity and areas of high turbulence over time and allows the magnitude and pulsation of shear stress and pressure gradients on the bed to be approximated. It is shown that there is a hydraulic reason to expect fundamentally different flow dynamics in riffle-pools dependant on the discharge, flow depth, and the relative height of the riffle. As the critical condition is approached, the mean flow can switch from a state where the high velocity core skims across the surface of the pool to one in which it plunges towards the bed. This bifurcation fundamentally alters the distribution of mean and fluctuating shear and pressure forces on the bed and provides a foundation for reconciling patterns of flow and turbulence that have been observed in pool-riffles with different geometries.

The results of the current study most directly help to explain the distributions of velocity and turbulence that were reported in previous laboratory studies of flow in straight pools (MacVicar & Rennie, 2012; MacVicar & Best, 2013; MacVicar & Obach, 2015). Four types of flow structures (CE, RR, ST, and AT) are seen developing and dissipating in a pool-riffle unit, while momentum exchange near the walls can shape CE and RR due to the development of secondary flow in vertical expansion in CDF and instabilities in shearing flow downstream of the riffle crest. In the lab, MacVicar & Rennie (2012), found that sweeps tended to be angled towards side-walls with ejections angled towards the middle of flow in CDF zone. These series of sweeps and ejections in CDF near the walls are identifiable as vortical structures (CE) in

the current simulations. They also found that specific discharge was higher in the middle of the pool and hypothesized that the higher turbulence near the wall was acting to steer the flow towards the middle, a result that was reproduced here. MacVicar and Best (2013) showed how high strain rates were correlated with high Reynolds stresses and higher bed shear stress in the expansion of flow at the head of the pool, while further downstream an area of enlarging but weakening structures was convected away from the boundary. The current study largely confirms their conceptual model, with both higher average and fluctuations of shear stress in the pool-head than in the rest of the pool for cases R45 and R55 (Figure 3-9). The patterns of turbulent fluctuations are explained by the generation of vortical structures in the areas of high strain (CE and RR) and their weakening and dissipation in the pool where only occasional AT remain visible (Figures 3-5 and 6). The results thus offer greater clarity than the simulations of Kara et al. (2008), which did not include the effect of the side walls and so could not show the generation and dissipation of the CE structures and their effect on steering the main flow. However, the current study also shows the limit of the conceptual model presented by MacVicar and Best (2013), as the observed hydrodynamic cs are characteristic of only one of the possible regimes in straight pools and riffles.

In total, three types of flow patterns were seen in pool-riffle units. By varying the riffle height, it was possible to affect both the maximum velocity (Figure 3-10a) and the vertical location of the maximum velocity (Figure 3-10b) in the pool. For the purposes of this numerical study we looked a section in the middle of the pool and defined ‘skimming’, ‘rifting’, and ‘plunging’ flows based on whether the elevation of maximum velocity in profile at the centre of the pool was in the top 30%, middle 40%, or bottom 30% of the flow depth. For lower riffles, the skimming flow regime is characterized by turbulence generated near the boundaries and high velocity main flow in the middle of the channel. The flip from skimming to rifting and then plunging flow is based on flow specific energy, where the critical flow condition is approached as the riffle height increases, eventually causing a choked flow condition. In a 1D analysis (see, e.g. Sturm, 2010), the choked flow causes a local increase in potential energy upstream of the riffle

and higher kinetic energy in the pool. This choked flow condition also results in more downward momentum into the pool and is known to result in a transition from sub to supercritical flow. In locations where the depth in the pool is sufficiently high, the supercritical flow will be forced to jump back to a subcritical condition in the pool, either as a free or submerged jump. In profile, the water surface profile appears to be characteristic of an undular jump, which are 'weak' jumps that occur for Froude numbers < 1.7 (Sturm, 2010), with a zone of high turbulence on top of the high velocity flow (Figure 3-3b – R65). Viewed in the plan form, however, the picture becomes more complex as the area of high velocity flow is laterally restricted by zones of high turbulence that gradually cover the plunging flow (Figure 3-8). Plunging flow is significant because it may corroborate observations of plunging flow in the field (Carling 1991; Keller and Florsheim 1993; Thompson et al. 1996) and support the hypothesis of velocity reversal (Keller, 1972), demonstrating that a local velocity reversal can happen as a result of the redistribution of flow in a cross-section, as argued by MacVicar et al. (2009), and that the shear stresses on the bed are very high for such a condition (Figure 3-8). As has been done for flows in confluences (Guillén Ludeña et al. 2017), future work should examine the effect of more realistic pool and riffle geometries on turbulence generation and the redistribution of flow to more fully understand the hydrodynamics in pool formation and maintenance in natural channels.

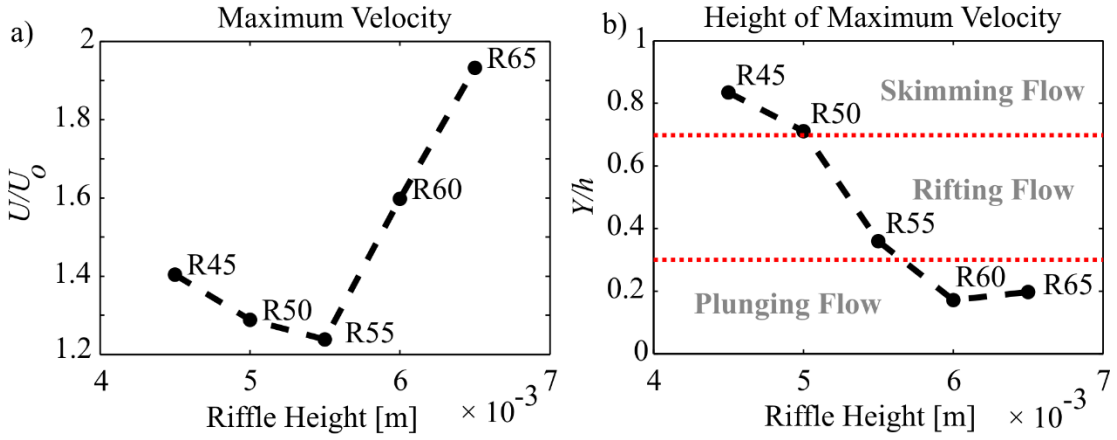

Figure 3-10- a) the maximum velocity magnitude in the profile at the centre of the pool, b) the elevation of the maximum velocity point in the profile at the centre of the pool

We propose that the concept of vortex-resistance can be used to understand how mean flow is steered through the area of flow expansion in the head of a pool. To understand this concept, it is important to conceptualize turbulence as both a cause and an effect. In a fundamental sense, turbulence is an effect of (i.e. generated by) velocity gradients or strain in fluids. In uniform flows, turbulence is thus generated near the bed where velocity gradients are highest. Following the theory of turbulence (Lohse and Grossmann 2002), however, turbulence can be considered as a cause by formulating it as a matrix of stresses. The well-known Boussinesq (1877) assumption used in Reynolds averaged models introduces a term called the eddy-viscosity (μ_t) to model the effect of turbulent stresses (τ_{ij}) on the mean flow (U_i) as follows:

$$u_i = U_i + u_i' \tag{3-4}$$

$$\tau_{ij} = -\overline{\rho u_i{}' u_j{}'} = \mu_t \left(\frac{\partial U_j}{\partial x_i} + \frac{\partial U_i}{\partial x_j} \right) \tag{3-5}$$

where u'_i is the fluctuating part of velocity in i direction, $i \in \{X, Y, Z\}$, j related to different spatial coordinate , x_i is Cartesian space coordinate, and ρ is fluid density. In LES modeling, an eddy viscosity is

applied on the subgrid length scale (Δ_g) to model subgrid scale eddy viscosity (μ_{t_SGS}) and filtered velocity ($\widetilde{U}_i$) gradients.

$$u_i = \widetilde{U}_i - u'' \tag{3-6}$$

$$\mu_{t\_SGS} = \rho(C_s\Delta_g)^2\sqrt{2S_{ij}S_{ij}} \tag{3-7}$$

$$S_{ij} = \frac{1}{2}\left(\frac{\partial \widetilde{U}_i}{\partial x_j} + \frac{\partial \widetilde{U}_j}{\partial x_i}\right) \tag{3-8}$$

where C_s is a constant and u'' is subgrid scale component of the fluctuating velocity. With increasing grid resolution, the model approaches to direct numerical simulation (DNS) method and μ_{t_SGS} approaches zero. For the current study, instantaneous contours of velocity magnitude ($\bar{u}$) and μ_{t_SGS} were compared for three cases (Figure 3-10), with $\bar{u}$ normalized by the bulk velocity (U_o) and μ_{t_SGS} by the dynamic viscosity (μ_o). In all cases over the riffle, the eddy viscosity is high near the bed as expected. As flow expands in the pool-head, however, bands of high eddy viscosity are formed along lines of high shear within the flow where velocity gradients are also high. Skimming and plunging flow are thus steered at the subgrid scale by the modeled turbulence. In the case of R65, high eddy-viscosity near the water surface creates a region that has an effective viscosity ($\mu_{t\_SGS} + \mu_o$) is locally up to ten times higher than the viscosity of the fluid itself (Figure 3-10b). Once the flow expansion is completed, the lines of high vortex resistance tend to decrease in magnitude and become discontinuous. This breakup leads to increased turbulent mixing of high and low velocity fluid in the pool and supports the idea that the flow will recover towards the distribution of flow and turbulence found in uniform channels once the streamwise pressure gradient is removed (MacVicar & Best, 2013).

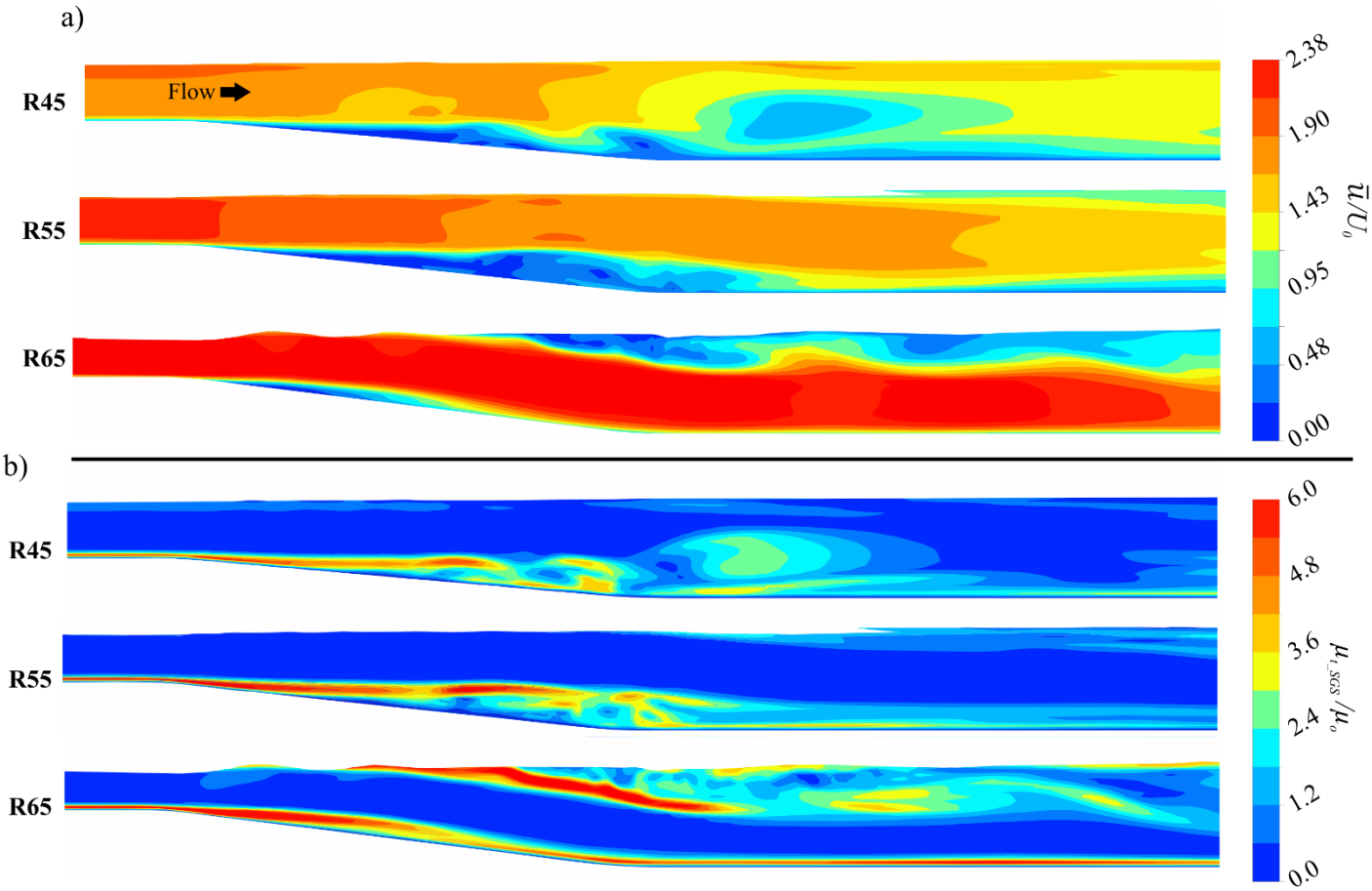

Figure 3-11-Instantaneous a) velocity magnitude, b) ratio of eddy viscosity and dynamic viscosity

The eddy viscosity of K-epsilon method (μ_{t_Ke}), or the turbulence that is greater than the grid scale, shows similar patterns to μ_{t_SGS} (Figure 3-11). Following the standard K-epsilon model (Launder and Spalding 1974), turbulent kinetic energy (K) and turbulent dissipation rate (ϵ) are calculated as:

$$K \equiv \frac{1}{2}\overline{\acute{u}_\iota \acute{u}_\iota} \tag{3-9}$$

$$\epsilon = \nu \overline{\frac{\partial \acute{u}_\iota}{\partial x_k}\frac{\partial \acute{u}_\iota}{\partial x_k}} \tag{3-10}$$

Using LES results, μ_{t_Ke} is calculated as:

$$\mu_{t\_Ke} = \frac{C_\mu \rho K^2}{\epsilon} \tag{3-11}$$

where ν is kinematic viscosity and C_μ is a constant (~ 0.09).

The contour of *K* (Figure 3-12) shows that in case R45, which is associated with skimming flow and strong RR, there is a region with high *K* in the pool-head, and ϵ is high at the upstream and around that region. Therefore, eddy viscosity peaks at the centre of that region as expected. This pattern of *K* and ϵ can be found in case R55 with higher values, and additional slightly high values in a narrow region near the free surface. Case R65 is completely opposite to case R45, with higher *K* near the free surface. The region with high eddy-viscosity applies a stress to the mean flow that helps to guide the flow to plunge into the pool.

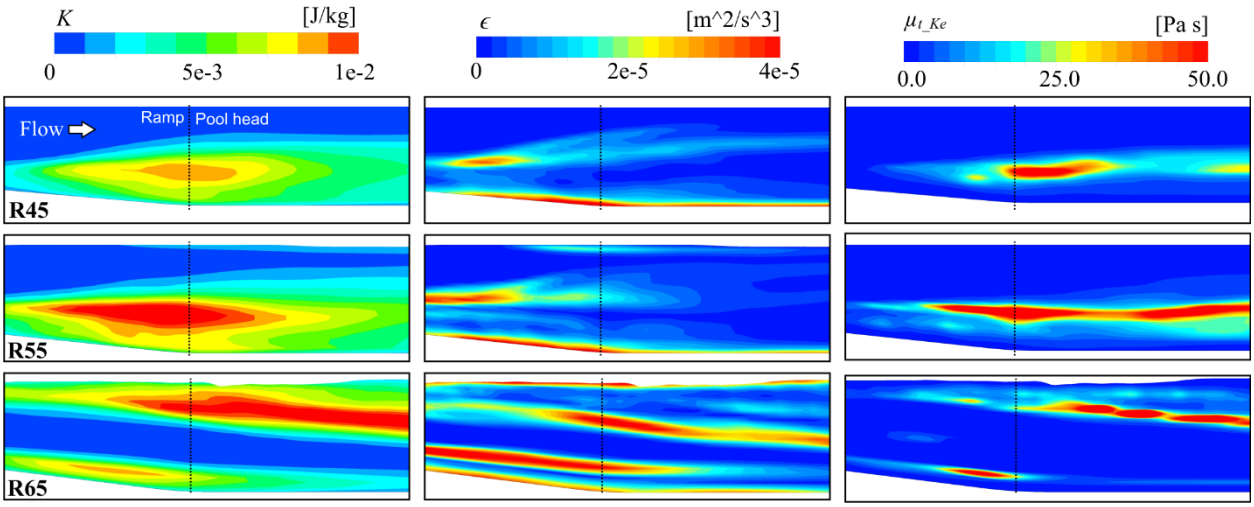

Figure 3-12- Turbulent kinetic energy (*K*), turbulent dissipation rate (ϵ), and turbulent viscosity based on K-epsilon concept in the pool-head of cases R45, R55, and R65.

This concept of vortex resistance also leads to an important bifurcation in the lateral dimension of pools with plunging flow. As shown by the growth of high turbulent zones near the side wall of the channel during flow expansion, the mean flow is increasingly funneled into the centre of the channel in this area (Figure 3-8). The instantaneous patterns are clearly asymmetric, however, as would be expected due to the intermittent growth and detachment of larger packets of low momentum fluid. Any instantaneous

asymmetry, however, has the potential for positive feedback by steering more flow away from the region, which was observed to lead to an asymmetric time average state for some simulations with plunging flow in the pool. Lateral flow bifurcations in a straight pool-riffle unit, which distribute bed shear stress biasedly to one side of the channel, suggests a physical mechanism for the link between pools and the initiation of meandering in a straight channel. Such a result is also significant because it indicates that a small bias in the laterally funnelled flow, such as a minor geometrical deviation, could preferentially expand the recirculation at one side and deflect the main flow away from this area. In field cases such as the study by MacWilliams et al., (2006), a jet-like flow was observed in a pool-riffle unit, which led to the "flow convergence routing" hypothesis for pool maintenance. As part of this hypothesis, however, the authors assumed a need for an upstream constriction to induce the jet-like flow into the pool. The current study shows that the resistance of CE and ST in CDF zone can act as a constriction and shape this jet-like flow (i.e. 'plunging' flow in the current study) as well as a function of the chaotic behaviour of turbulent flow. Investigations into the role of turbulent vortices in more realistic pool geometries are again warranted to determine how they affect pool formation and maintenance in natural channels.

3.6 Conclusions

The transient numerical simulations of turbulent flow in isolated pool-riffle units showed that:

1) Four different types of vortices are shaped in the convective decelerating zone: surface turbulence, ramp rollers, corner eddies, and axial tails;

2) Ramp and corner eddies are dominant near the bed and responsible for high bed shear stress in skimming flow;

3) Based on this finding that, vortices exert resistance to the flow by increasing the mixing effects, and changing the pressure domain, the vortex-resistance hypothesis has been suggested;

4) Froude number close to one at riffle can make surface undulation hydraulic jump, which steers the flow to plunge into the pool near the bed;

5) If ramp rollers are strong enough, they push the flow to skim the free-surface and increase near bed turbulence;

6) Axial bifurcation occurs where strong plunging flow happens, such one side of the channel experiences higher velocities and shear stresses while the opposite side is dominated by flow recirculations.

Chapter 4: Effect of width variations on turbulent structures and flow patterns in isolated pool-riffle units

4.1 Introduction

Macromorphological variations in natural and restored streams have significant effects on sediment transport, flow pattern, and bed stability. Pools and riffles, which are respectively deeper and shallower part of the bed, are known as the main reason of channel deformation and meandering developments (Hooke 2013; Montgomery 1995; Stoesser et al. 2010). They are mostly found in gravel bed streams, but they can shape and become stable in both alluvial and bedrock channels (MacVicar and Roy 2007b; Sear 1996; Thompson 2013). They play essential roles in the quality of aquatic habitats by providing enough volume of water during low discharge seasons or protect them from freezing during ice developing seasons (Gorman and Karr 1978). Pools and riffles increase the turbulence that can protect the channel from the unwanted deposition of sediment, or causes erosion and make the channel unstable (MacVicar & Roy, 2007b, 2007a, Thompson, 2001, 2004; Thompson et al., 1999). Another important geometry factor in natural and restored streams is the size and variation of channel width. The spacing and frequency of

some of the large bedforms are thought to be a function of the channel width. For example, the frequency of pool-riffle unit is five to seven times of the channel width (Keller & Melhorn, 1978). Also, the curvature and wavelength of meanderings are two to three, and ten to fourteen times of the channel width, respectively (Hooke 2013). Local variations in the width of the channel, which are known as constrictions and expansions, are also a primary control on pool formation (Buffington et al., 2002; Thompson et al., 1999). Channel constrictions; by shaping jet flows, flow convergences, increasing bed shear stress, and generation of strong turbulent structures, have influential effects on sediment transport and pool maintenance mechanism (Buffington et al., 2002; MacVicar & Roy, 2007b, 2007a, Thompson, 2001, 2004; Thompson et al., 1999). Most of the studies on pool-riffle maintenance and shaping mechanism did not consider the effects of width size and variation; therefore, there is a need for more hydraulic studies to demonstrate the effects of basic geometry factors on flow patterns in pools and riffles.

The mechanisms underlying the formation and maintenance mechanism of pool-riffle units have many uncertainties due to the variability in the field, complexity of flow interaction with the morphology and the chaotic behaviour of turbulence. One of the first hypothesis in pool-riffle formation and maintenance is “velocity reversal.” It says that by increasing the flow discharge, the increasing rate of near-bed velocity in riffle is lower than the one in the pool and there is a point that the near-bed velocity in the pool is equal to the one in the riffle (Keller & Florsheim, 1993). They suggested that high near bed velocity in the pools exerts high shear stress to the bed and increases the sediment transport rate. They defined this scouring process as the maintenance mechanism in pools and riffles. Another hypothesis in this field is “flow convergence.” It says that the high near bed velocity and bed shear stress in the pools are the results of a jet-like flow, which is induced by upstream constrictions (MacWilliams et al. 2006). These two hypotheses are based on the spatial distribution of time-averaged velocity in the pools and riffles, without considering the effects of turbulence. MacVicar and Rennie (2012) and MacVicar and Best (2013) treated the convective accelerating flow (CAF) and convective decelerating flow (CDF) zones as perturbations.

They used the idea of recovery from perturbation to assess the impact of macro bed forms (i.e. riffles) on flow behaviour. They defined 'recovery length' that is a required length for dissipating the perturbation effects (e.g. Reynolds stresses). They found that recovery length is higher in wider channels with the same vertical expansion geometry. They have stated that in the CDF zone, adverse pressure gradient shapes the flow in a way that high turbulence shapes near the bed and high velocity peaks near the free-surface.

The up-scaled geometry of pool-riffle units, with or without constriction, can be found in the field as well. Venditti et al., (2014) found the similar geometry of pool-riffle units with a constriction in Fraser Canyon, British Columbia, Canada. They did the first three-dimensional measurement of velocity domain in bedrock canyons (Hunt et al. 2018). They observed a plunging flow into the pool and boiling structures on the free-surface. They argued that the CDF zone and lateral constrictions form upwelling flows, which are seen as boiling structures when they reach the free-surface. They stated that the upwelling flows, by reducing the local dynamic pressure near the bed, guide the incoming flow to plunge into the pool. Moreover, this plunging flow intensifies the upwelling flow as positive feedback. Hunt et al., (2018) conducted a series of flume experiments in support of Venditti et al., (2014). Their flume model was a constriction varying from 20 to 50% and a downslope ramp entering the pool. In the experiments, however, the Froude number in the constriction ($0.61 < Fr < 1.21$) is not matched with the field value ($Fr = 0.3$), which means that the lab case largely considered choked flow conditions rather than matching what occurs in a subcritical flow in the field.. Thompson & Wohl (1998) used a sharp plate as constriction downstream of the riffle at pool-head. They argued that the constrictions make a vena contracta at the downstream, which is necessary to the maintenance mechanism of pools, and that the characteristics of the vena contracta were primarily controlled by pool length. The creation of vena contracta because of the sharp plate may not replicate the actual geometry of constrictions and pool-riffle units in the field.

Using large eddy simulation (LES) of turbulent flow in isolated pool-riffle units with various riffle height in the previous chapter, four types of vortices were detected. The Q criterion was used to detect vortices cores. In the cases with Froude number lower than 1 in the riffle crest, a series of vortices were found near the bed on the ramp, called 'ramp rollers' (RR), which were found to have a similar generation and dissipation mechanisms as hairpin vortices that form at the top of the viscous sublayer in boundary flows (Kline et al. 1967). As they travel downstream, their head elevates from the bed and dissipates quickly, but the legs remain longer and form stretched tube-like vortices called 'axial tails' (AT). Near the corners in CDF zone, 'corner eddies' (CE) were detected. By increasing the riffle height, RR become weaker, and series of vortices appear near the free-surface in CDF zone, which are called 'surface turbulences' (ST). ST mix with CE and occupy the top and both sides of the channels; they steer the flow to plunge into the pool. This flow pattern with high velocity core in the bottom 30% of the flow depth, in the centre of the pool, was called 'plunging flow.' In the absence of ST, RR push the flow to skim the free surface. This flow pattern with high-velocity core in the top 30% of the flow depth was called 'skimming flow.' If ST and RR have similar strength, flow velocity peaks in the middle 40% of the flow depth in the centre of the pool. This flow pattern was called 'rifting flow.' The results are significant because they show that dramatically different flow patterns can occur in pools and riffles depending on the channel geometry and the flow regime in the riffle. More research is needed to understand how the overall width and local constrictions affect the channel hydrodynamics.

The current chapter aims to continue the study of vortical structures in pool-riffle units with different geometrical parameters with an advanced transient, and turbulent numerical approach. The specific objectives are to: 1) study the effects of width variation on flow pattern and vortical structures in isolated pool-riffle units 2) study the effects of lateral constrictions on flow pattern, 3) detect and study the constriction-induced vortical structures, 4) investigate the interactions of constriction and pool-riffle induced flow structures. The geometry of the models is based on the previous experiments in pool-riffle

units by MacVicar & Obach, (2015), which is a simplified geometry of common pool-riffle units found in the field. Pool-riffle units are considered to be in a straight channel with a lateral constriction in the riffles. It is hoped that this research will provide a clear visualization of hydrodynamics in pool-riffle units and lead to a more complete understanding of the formation and maintenance mechanisms of pool-riffle units.

4.2 Methodology

4.2.1 Model Geometry

The model geometry is based on one of the flume experiments completed by MacVicar and Obach (2015), which was in turn based on a geometric (1:10) and Froude scale (Fr ~ 0.6) matching of a field example (MacVicar and Roy 2007). The physical and numerical models use a simplified straight geometry of pool and riffle units with and without constriction in a 0.6 m wide channel. The constrictions are placed in the upstream riffles, and there are some cases that have constrictions alone. The simulated flume in the numerical model is 6 m long with a 1 m long uniform upstream section followed by a 0.52 m long upsloping ramp, a flat uniform shallow 'riffle' of 0.4 m, a 0.52 m long downsloping ramp, a flat uniform deep 'pool' of 2.4 m. In the cases with constriction, the constriction and riffle are in phase. A final upsloping ramp and short uniform shallow section were used to define the downstream boundary of the model. For the series of simulations in this study, three riffle heights (h_R= 40 mm, 50 mm and 60 mm) was chosen to model skimming and plunging flows (Table 4-1). With the fixed length of the ramped sections, the change of riffle height also changed the ramp angles. The average inlet velocity (U_o), the flow depth in the pool (h) and the Froude number in the pool were 0.21 m/s, 0.12 m, and 0.2 for case R50, respectively. For other cases, the average inlet velocity (U_o), the flow depth in the pool (h) and the Froude

number in the pool were 0.21 m/s, 0.115 m, and 0.2, respectively. For reference, *X*, *Y*, and *Z* represent the streamwise, vertical, and spanwise directions, respectively.

The cases with h_R= 60 mm had already choking flow condition; therefore these cases were not modelled with constrictions. By considering the velocity variation in only the streamwise direction, the specific energy is calculated as

$$E = h + \alpha U^2/2g \tag{4-1}$$

where α is the energy coefficient, U is the cross-section average flow velocity, and g is the gravitational constant (9.81 ms^{-2}). A critical height for a bed rise that is just sufficient to induce choking flow (ΔZ_c) can then be found as the difference between the critical specific energy (E_c) and upstream specific energy (E_1) where E_c is given by:

$$E_c = 3/2\sqrt[3]{q^2/g} \tag{4-2}$$

and q is the specific discharge. For q = 0.02415 m^2/s, h = 0.115 m, and assuming α = 1.0, E_1 = 0.117 m, E_c = 0.058 m and ΔZ_c = 0.06 m. Critical width constrictions (W_c) that will induce choking flow in a channel can be found as

$$(W - W_c)/W = 1 - \sqrt{(qW)^2/\left(\frac{2}{3}(E_1 - h_R)\right)^3 g} = 60\%. \tag{4-3}$$

where h_R is the riffle height. For the modelled channel (W = 0.60 m) in a flat bed (h_R =0) and a small riffle (h_R =0.04 m) for q = 0.024 m^2/s, Wc = 0.14 m and 0.24 m, respectively, meaning that constrictions of 60 % would be required to induce critical flow in the respective cases and assuming 1D ideal flows. For real flows, the threshold for choking flow may vary because of non-uniform distributions of velocity (α > 1.0), and the effects of turbulence, sidewall and surface roughness, and transitions at sharp edges. The cases in this chapter were designed to examine the hydrodynamics for cases in which choking was not predicted by equation (4-3). The rationale for this is that choking flows are dominated by plunging flows, which were examined in the previous chapter.

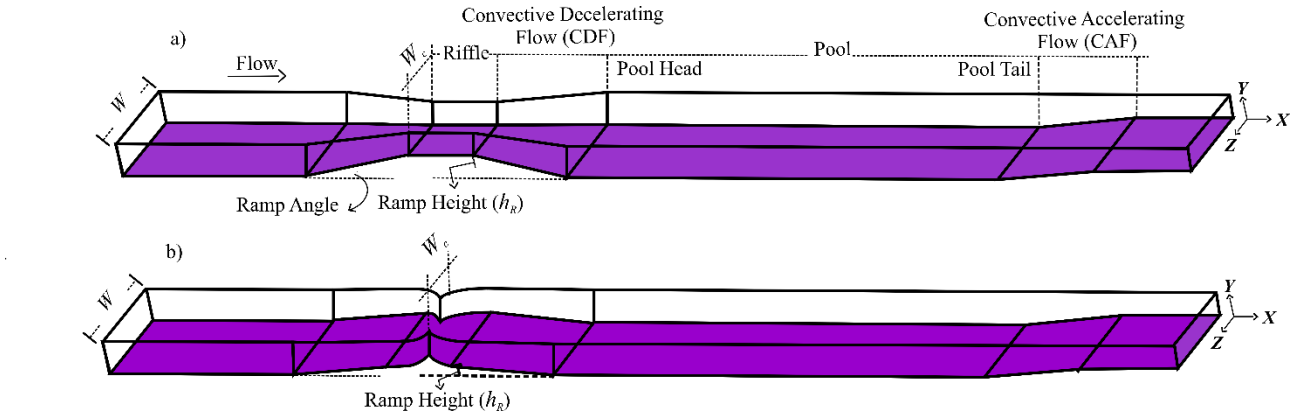

Figure 4-1- Simplified geometry of a pool-riffle unit with in-phase constriction as used in the current study, a) linear constriction, b) concave curve constriction

Table 4-1- Simulation parameters

Case name	Riffle height [m]	W [m]	constriction [%]	Constriction type	Fr at riffle
R50W60[a]	0.050	0.6	0	-	0.6
R40W30	0.040	0.3	0	-	0.5
R40W60	0.040	0.6	0	-	0.5
R40W90	0.040	0.9	0	-	0.5
R40W120	0.040	1.2	0	-	0.5
R60W30	0.065	0.3	0	-	1.0
R60W60	0.065	0.6	0	-	1.0
R60W90	0.065	0.9	0	-	1.0
R60W120	0.065	1.2	0	-	1.0
C10W15	0.000	0.15	10	Linear	0.2
C10W30	0.000	0.3	10	Linear	0.2
C10W60	0.000	0.6	10	Linear	0.2
C20W30	0.000	0.3	20	Linear	0.2
C20W60	0.000	0.6	20	Linear	0.2
C25W30L	0.000	0.3	25	Linear	0.3
C25W30C	0.000	0.3	25	Curved	0.3
R40W30C10	0.04	0.3	10	Linear	0.6
R40W60C10	0.04	0.6	10	Linear	0.6
R40W30C20	0.04	0.3	20	Linear	0.7
R40W60C20	0.04	0.6	20	Linear	0.7

R40W60C25C	0.04	0.6	25	Curved	0.8
R40W120C10	0.04	1.2	10	Linear	0.6
R40W120C20	0.04	1.2	20	Linear	0.7
R40W60C10U	0.04	0.6	10	Linear	0.5
R40W60C10D	0.04	0.6	10	Linear	0.6

Note: [a] case R50W60 is the same as case R40P240 in MacVicar and Obach (2015).

4.2.2 Numerical Method

Simulations used the commercially available ANSYS CFX Version 19.1 software. In ANSYS CFX, large eddy simulation (LES) was used to model the flow. The initial condition for the distribution of flow is considered to be uniform. The LES wall-adapting local eddy-viscosity (WALE) (Ducros et al. 1998) method was chosen, which has been widely used in similar geomorphic researches (Keylock et al., 2005, 2012). For more detailed information about the formulations and equations of LES see Rodi et al. (2013). The simulations were 3D, with a structured mesh generated using ICEM Version 19.1, and a total number of elements equal to 30×10^6. Minimum cell size in the near-wall region was 1×10^{-3} m, which was selected to satisfy the criteria suggested by Keylock et al. (2012), who recommended at least six points in the inner (near-wall) region to resolve the eddies generated in this region. Previous studies have found the inner zone to be between 10 and 20% of the flow depth (MacVicar and Obach 2015; MacVicar and Rennie 2012; Nezu and Rodi 1986), which means that there are approximately 15 points in the inner zone for the current study. Also following Keylock et al. (2012), cell sizes were 1/40 of the depth, which meets the recommendation to keep the free surface cells to less than 1/20 of the flow depth. The total time for transient modelling was 250 s, which is > 300x the largest eddy scale ($\sim h/U_o$) and easily exceeded the recommendation of 20x the eddy time scale by Keylock et al. (2012). The first 50 s were not considered because of initial condition effects, so only the results between 50 s and 250 s were recorded for analysis. On the machine we used, which has dual CPUs, each with ten cores of 2.3 GHz with CPU model Intel(R)

Xeon(R) 2650 V3, and 192 GB RAM, one complete simulation took approximately 200 hours. Post processing was completed with CFD-POST Version 19.1 and MATLAB R2017b.

4.2.3 Boundary Conditions

Using VOF, the inlet was separated into air and water zones at the experimental flow depth (h = 0.115 m). The air zone had zero velocity inlet and the constant pressure of zero. The water zone was defined as having a hydrostatic pressure distribution with a fully developed steady water velocity profile. To define the inlet velocity profile, a separate simulation was done with uniform velocity inlet (U_0 = 0.21 m/s) in a ten meter long uniform channel (i.e. without pools and riffles) with the same slope, width, flow height and simulation adjustments. The time-averaged velocity profile at the end of the plain channel was used as the inlet profile of pool-riffle simulations. The outlet was defined as having a constant hydrostatic pressure distribution for water and constant zero pressure for air. In all locations, a distance of at least 3 cm was maintained between the water surface and the top of the simulation space, which allowed the free surface to be shaped based on the hydraulic characteristics alone.

4.2.4 Validation

The experimental data for the case of R40P240 from MacVicar and Obach (2015), corresponding with case R50W60 (Table 1), was used to validate the flow behaviour, water surface elevation, and the distribution of time average streamwise flow velocity (U_x) in the numerical simulations. Time-averaged numerical results and experimental data are compared in Figure 4-2. Water surface level is similar in both numerical and experimental results, with a drop at the riffle that is consistent with what is expected from a specific energy analysis for subcritical flow (Figure 4-2a). Six time-averaged streamwise velocity profiles normalized by the inlet velocity (U_x/U_o) are shown at different points along the channel centerline between the middle of the riffle and middle of the pool (Figure 4-2b). Considering the 10% error bars,

numerical results are mostly consistent with experimental data, especially in the pool, which is a key area for assessing existing hypotheses for pool-riffle hydrodynamics. The consistency of the LES WALE model with experimental data is better than LES Smagorinsky, which is used in the previous chapter. The numerical results show higher velocity near the surface and lower near the bed, which are similar to the experiments.

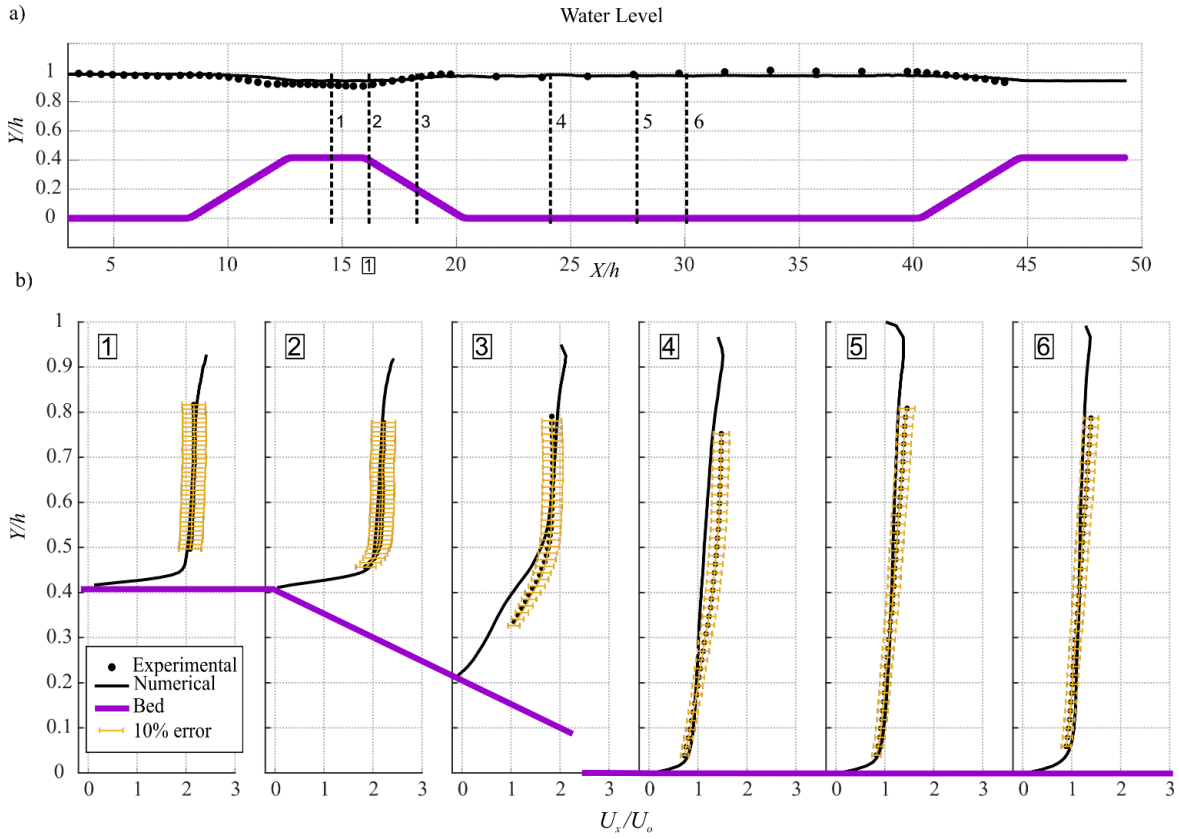

Figure 4-2- Validation of numerical results with available experimental data, a) water surface elevation at centerline, b) profiles of time-average streamwise velocity (U_x) for locations shown in a)

4.3 Results

4.3.1 The effects of total width variation on skimming flow in isolated pool-riffle units

In this part, the effects of different total channel width on the cases with skimming flows are discussed. Two sets of cases (R40 and R50 cases) were chosen to represent the skimming flow. Based on the results of the previous chapter, both cases have skimming flows, but R40 cases have weaker ramp rollers (RR) and corner eddies (CE) in compare with R50 cases.

Increasing the total width in the cases with the riffle height (h_R) equal to 40 mm, and without constriction (R40 cases), does not have any significant effects on the time average velocity and velocity fluctuations (Figure 4-3). In cases, R40W30, R40W60, and R40W120, the time average velocity peaks near the free surface and higher velocity fluctuation is near the bed. In addition, there is a region with a low velocity near the ramp, which is extended to the pool-head. Despite of lower mean velocity in that region, the velocity standard deviation (U_{stdv}) shows higher fluctuations. These are the characteristics of 'skimming flow', and as it is shown in Figure 4-3, total channel width does not change the overall flow pattern in R40 cases. However, the contour of U_{stdv} shows a more extended region of high fluctuations in the case with moderate width (R40W60).

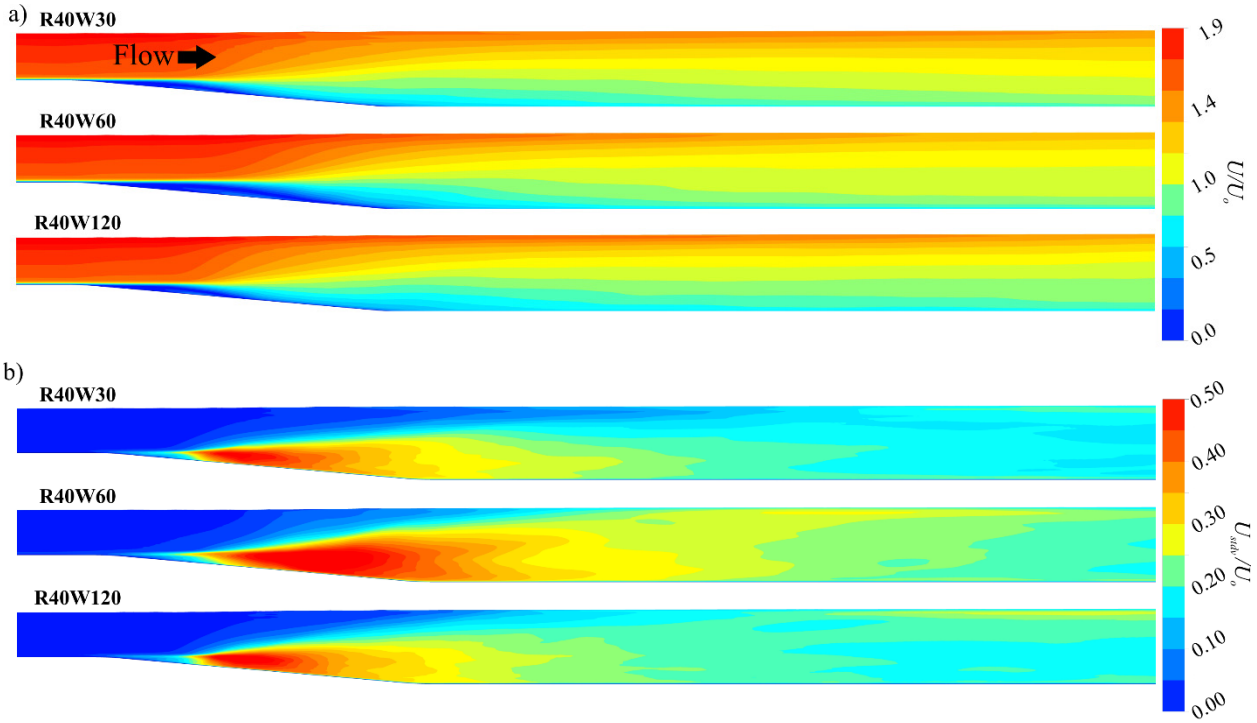

Figure 4-3- a) time-average velocity magnitude (*U*) in the *X-Y* plane at channel centerline, b) total velocity standard deviation (U_{stdv}) in the *X-Y* plane at the channel centreline in cases R40W30, R40W60, and R40W120.

The pool-head is the region where the larges turbulent structures are generated in R40 cases. As it is shown in Figure 4-4, two types of generative (RR, and CE), and one type of dissipative (AT) flow structures can be seen. The dominant vortical structures are RR. The size and strength of RR are slightly different in various widths, but they are mostly on the same scale, and they are much stronger than CE. The near bed AT, which are the residual legs of RR, have similar strength in these cases, and channel width does not have a significant effect on them. Increasing the width makes the CE to become stronger because they have more space to spread laterally. In addition, CE and the residuals of them, which are stretched and travelled to reach the free surface, stay longer in the domain before they get dissipated.

The magnitude of instantaneous shear stress is higher in the pool-head, where most of the turbulent structures are being generated. The instantaneous bed shear stress contours show that the turbulent structures, while travelling downstream, exert high shear stress pulsation to the bed; the magnitude of these pulsations can exceed the mean shear stress in the riffle crest.

As illustrated in Figure 4-5, the contours of Q-criterion show that the most of incoming turbulent strictures into the pools are RR while mean velocity contours show that velocities are lower in those regions that are occupied by turbulent structures. The contours of Q-criterion for the case R40W30 shows that RR are weaker than those for wider channels, suggesting that they are suppressed by the presence of the side walls. In wider channels, RR form at larger scales and occupy more portion of the flow depth, particularly in the centre of the channel.

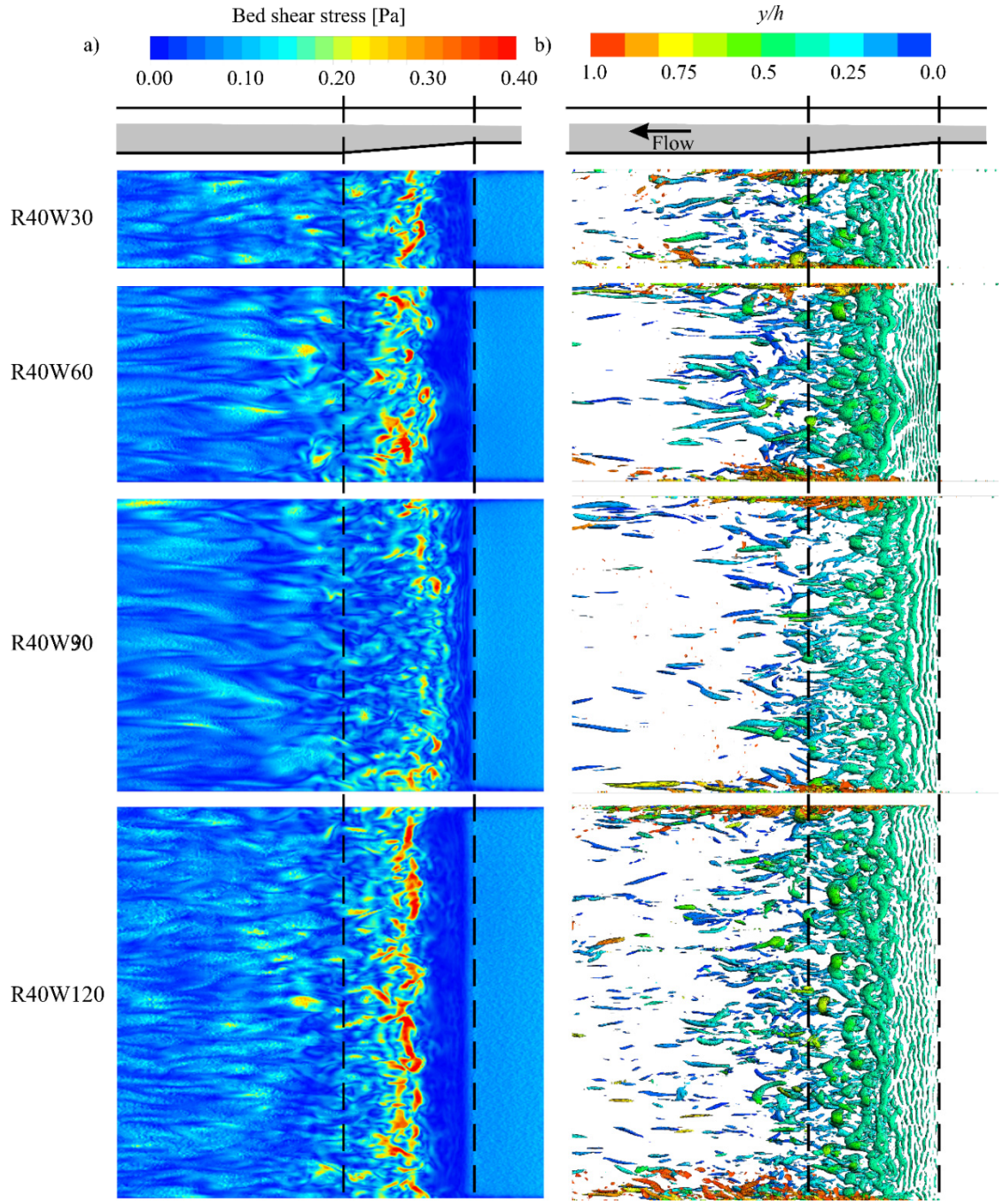

Figure 4-4- Instantaneous flow structure and hydrodynamics for cases R40W30, R40W60, R40W90, and R40W120, showing: a) contour of bed shear stress magnitude, and b) Iso-surface of Q=10 s^-2 showing flow structures.

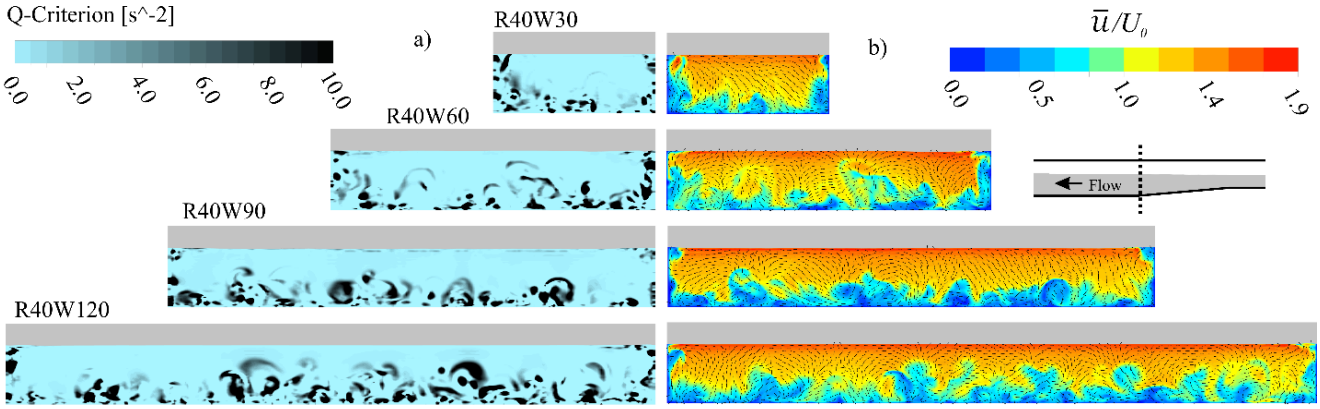

Figure 4-5- Instantaneous flow structure and velocity magnitude for cases R40W30, R40W60, R40W90, and R40W120, showing: a) contour of Q criterion b) contour and vector of velocity magnitude, in a cross-section right after the ramp at pool-head

Bed shear stress pulsations tend to peak over the ramp as flow depth increases in CDF and then decrease gradually in the pool by distancing from CDF. As it can be seen in Figure 4-6, the diagrams of 95% confidence range of bed shear stress in R40 cases show that the shear stress pulsations are lower in the riffle crest, and it peaks around the middle of the ramp. Moreover, the shear stress pulsation gradually decreases by moving downstream. The mean shear stress in the pools are lower than the mean and lower bound of shear stress in the riffles, but the higher bound of shear stress in the pools exceed the higher bound of shear stress in the riffles. All these R40 cases have similar shear stress pattern, mean, and fluctuation; and wider width does not have a significant effect on them.

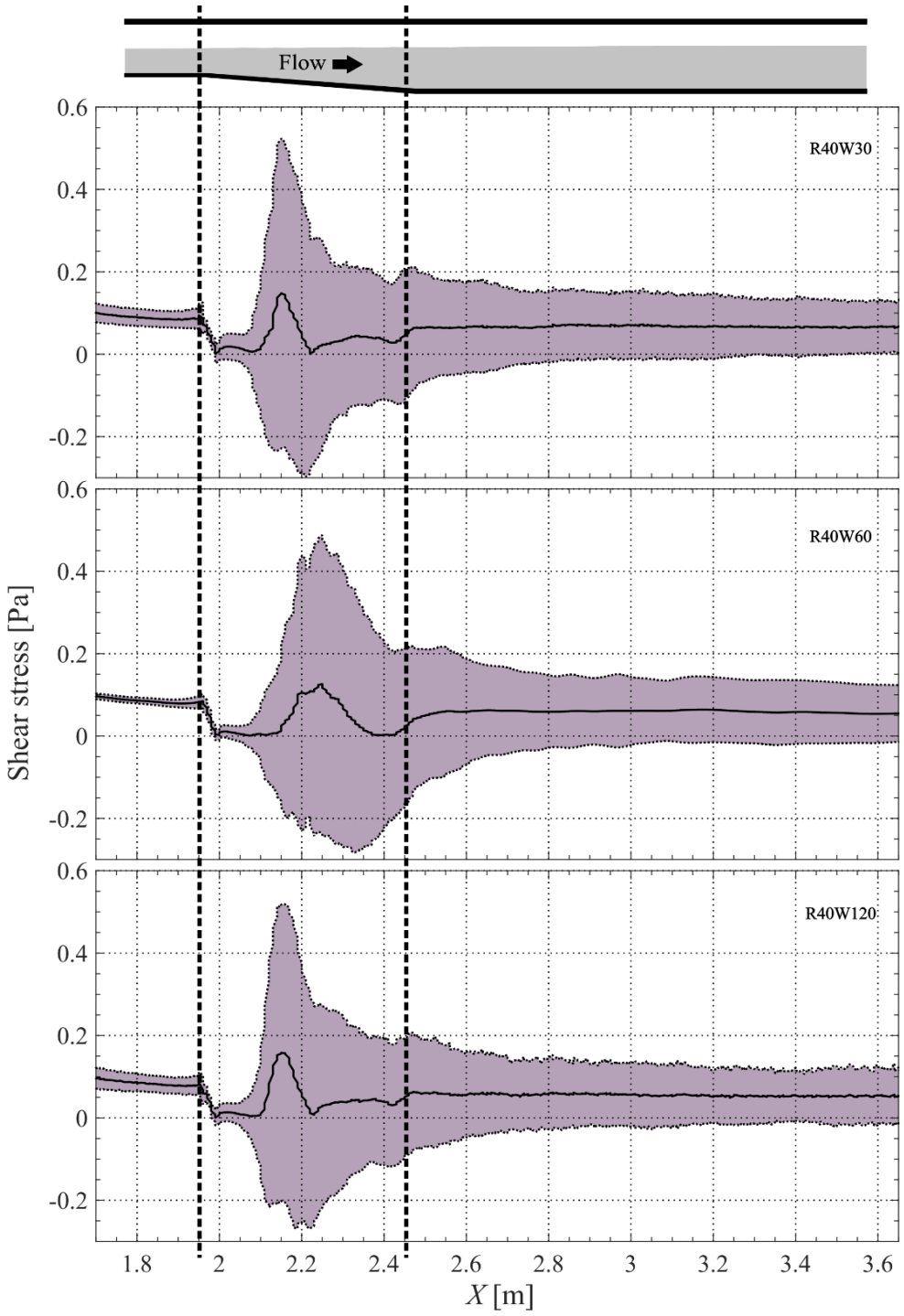

Figure 4-6 Time-average (black line) and 95% confidence range (dashed line) of bed shear stress at centreline for cases R40W30, R40W60, and R40W120.

By increasing the riffle height (h_R=50 mm) the flow pattern and distribution of turbulence are changed. As it is illustrated in Figure 4-7, the contours of time average velocity at the centreline of the channels show that the distribution of velocity at the middle of the pool, which is at the right end of these contours, changes by changing the width. The narrower R50 case, which is R50W15, has high velocity near the surface. The next case, which is R50W30, shows vertically extended core of high velocity in depth at the middle of the pool. Case R50W60 shows a typical skimming flow pattern. The widest R40, which is R50W90, has a region of low velocity near the free surface at the middle of the pool. While, the flow type can still be classified as 'skimming' given that the highest velocity at the centre of the pool is located at the first 30% of the depth from the free surface, but the appearance of this dip in velocity near the water surface indicates that the flow may be close to switching to a rifting or plunging type profile.

Increasing the channel width in R50 cases increases the velocity fluctuations and turbulence. As it is illustrated in Figure 4-7, the contours of U_{stdv} show that the velocity fluctuations are stronger and extended further downstream by increasing the width from W=15 cm to 60 cm. In case R50W90 a very thin layer of high-velocity fluctuation is shaped near the free surface, and it is extended from slightly before the riffle crest to the middle of the pool. This region of high-velocity fluctuation made the high-velocity flow to dip a little at the pool head, but the mean flow is recovered to the pattern of skimming flow as it reaches to the middle of the pool. Also, this thin layer of locally high turbulence is seen in other R50 cases as well, but they are less stronger than the one in case R50W90.

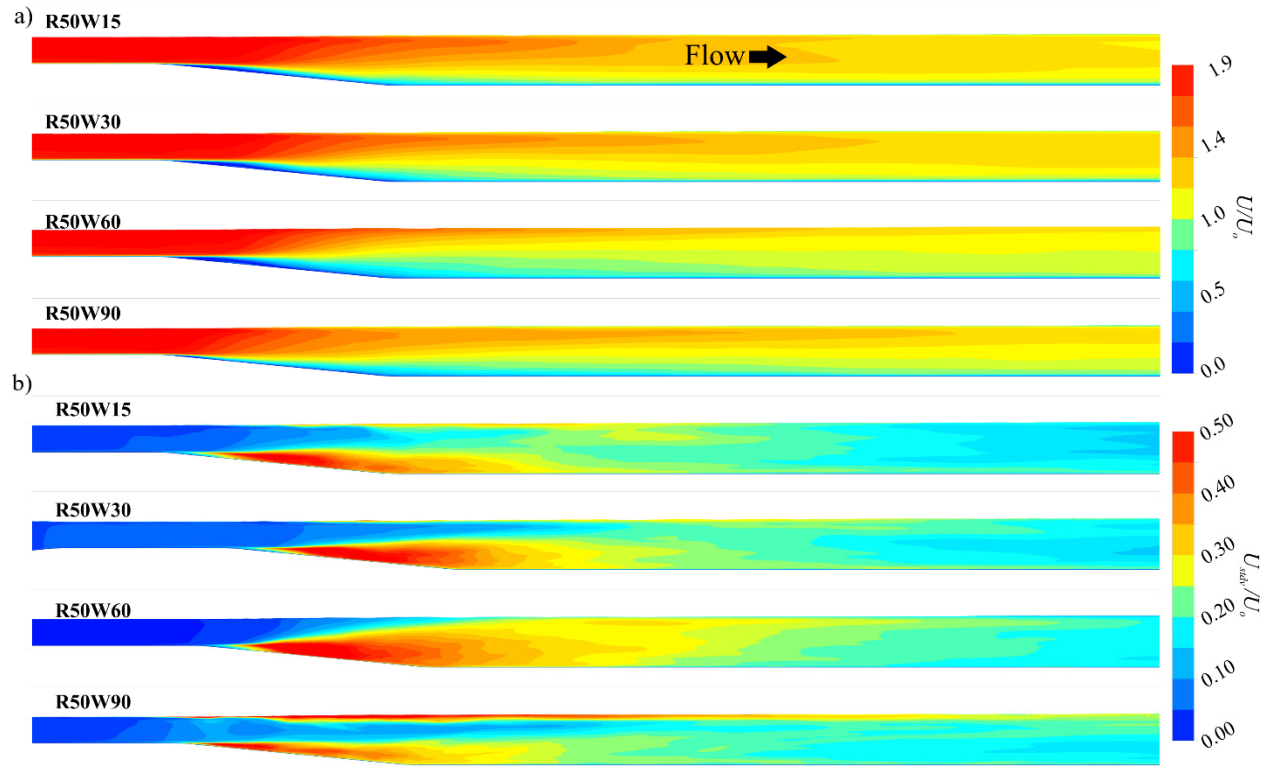

Figure 4-7- a) time-average velocity magnitude (*U*) in the *X-Y* plane at channel centerline, b) total velocity standard deviation (U_{stdv}) in the *X-Y* plane at the channel centreline of cases R50W15, R50W30, R50W60, and R50W90.

In R50 cases, the flow becomes more turbulent by increasing the total channel width. The iso-surfaces of Q-criterion in Figure 4-8 show that by increasing the total channel width, the RR become stronger, therefore, their residuals in the form AT can travel further downstream and stay longer in the domain. Because of higher h_R in R50 cases relative the R40 cases shown in Fig 1-4, both RR and CE are stronger. Moreover, increasing the width allows the CE to spread more laterally. The contours of instantaneous bed shear stress in R50 cases show that in wider channels there are more spots with excessive high shear stress in the pools in compare with the narrower ones and R40 cases. Small vortex cores identified with

the Q-criterion are also visible close to the water surface in the widest case where a velocity dip and increased near surface turbulence was observed in Figure 1-7.

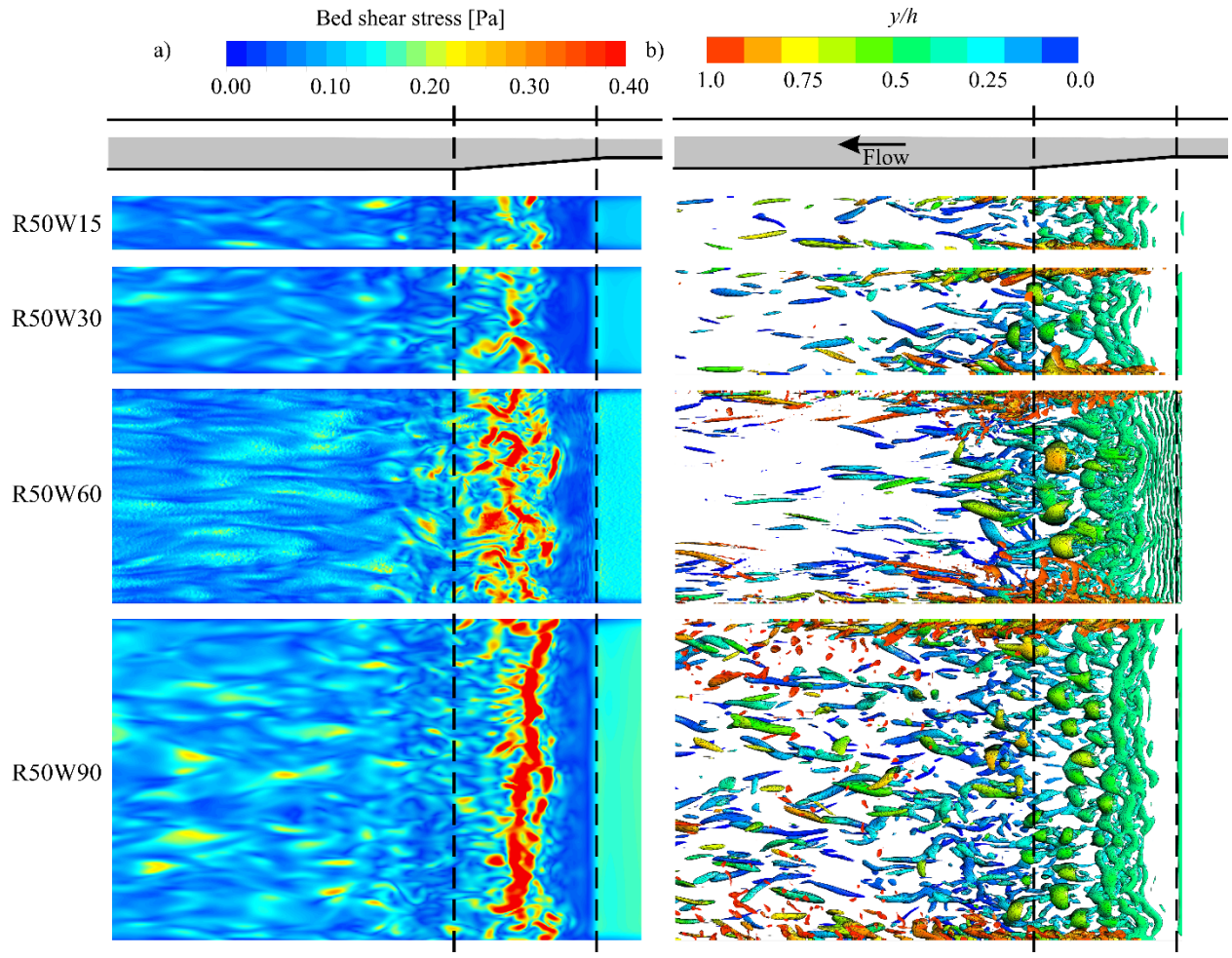

Figure 4-8- Instantaneous flow structure and hydrodynamics for cases R50W15, R50W30, R50W60, and R50W90, showing: a) contour of bed shear stress magnitude, and b) Iso-surface of Q=10 s^-2 showing flow structures.

In wider channels, RR are stronger in the middle of the channel where they are less affected by the presence of the side walls. The contours of Q-criterion at the spanwise cross section right at the pool head (Figure 4-9) show that in the narrowest channel (R50W15), the RR and CE have similar strength. In

wider channels, CE are present and can expand laterally, but they have less impact on the RR that are far away from the sides; therefore, RR have larger scales at the middle of the channel in wider channels. By increasing the width of the channel, even a part of CE can reach the free surface, and they can be transported toward the middle of the channel by the secondary flows.

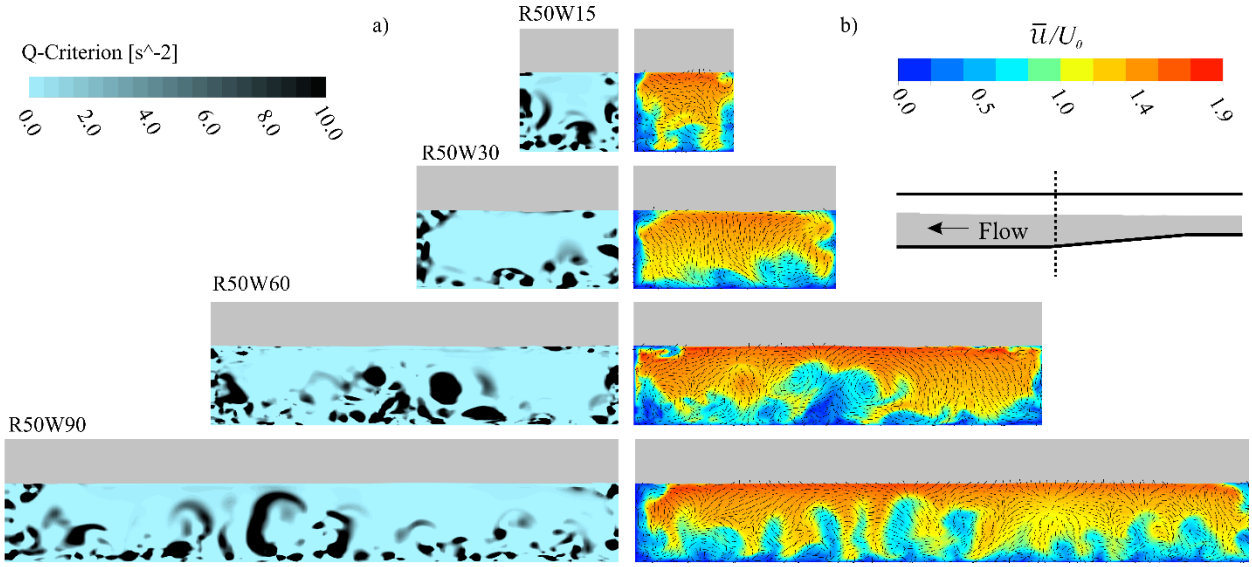

Figure 4-9 Instantaneous flow structure and velocity magnitude for cases R50W15, R50W30, R50W60, and R50W90, showing: a) contour of Q criterion b) contour and vector of velocity magnitude, in a cross-section right after the ramp at pool-head

The average bed shear stress does not change significantly by increasing the total width of the channel. The contours of average bed shear stress in Figure 4-10 show that the average bed shear stress in cases R50W15, R50W30, and R50W60, have similar pattern and magnitude, and all of them are higher than the one in case R50W90, which corresponds with the case where a slight dip in the mean velocity is noted at the water surface and a much smaller zone of high turbulence near the bed is observed (Figure 1-7). As shown in Figure 4-10, the mean shear stress is highest on the ramp in the region where the largest RR are being generated. The contours of the standard deviation of bed shear stress show that by increasing the

total width of the channel, the pulsation in bed shear stress increases as well. Moreover, more travelling length is required for the effect of these pulsations on the bed shear stress to drop off. Even though case R50W90 has lower mean and slightly lower standard deviation of shear stress, the region with relatively high pulsations extends further downstream than for the narrower channels as expected from the previous study on the effect of channel width (MacVicar and Obach, 2015).

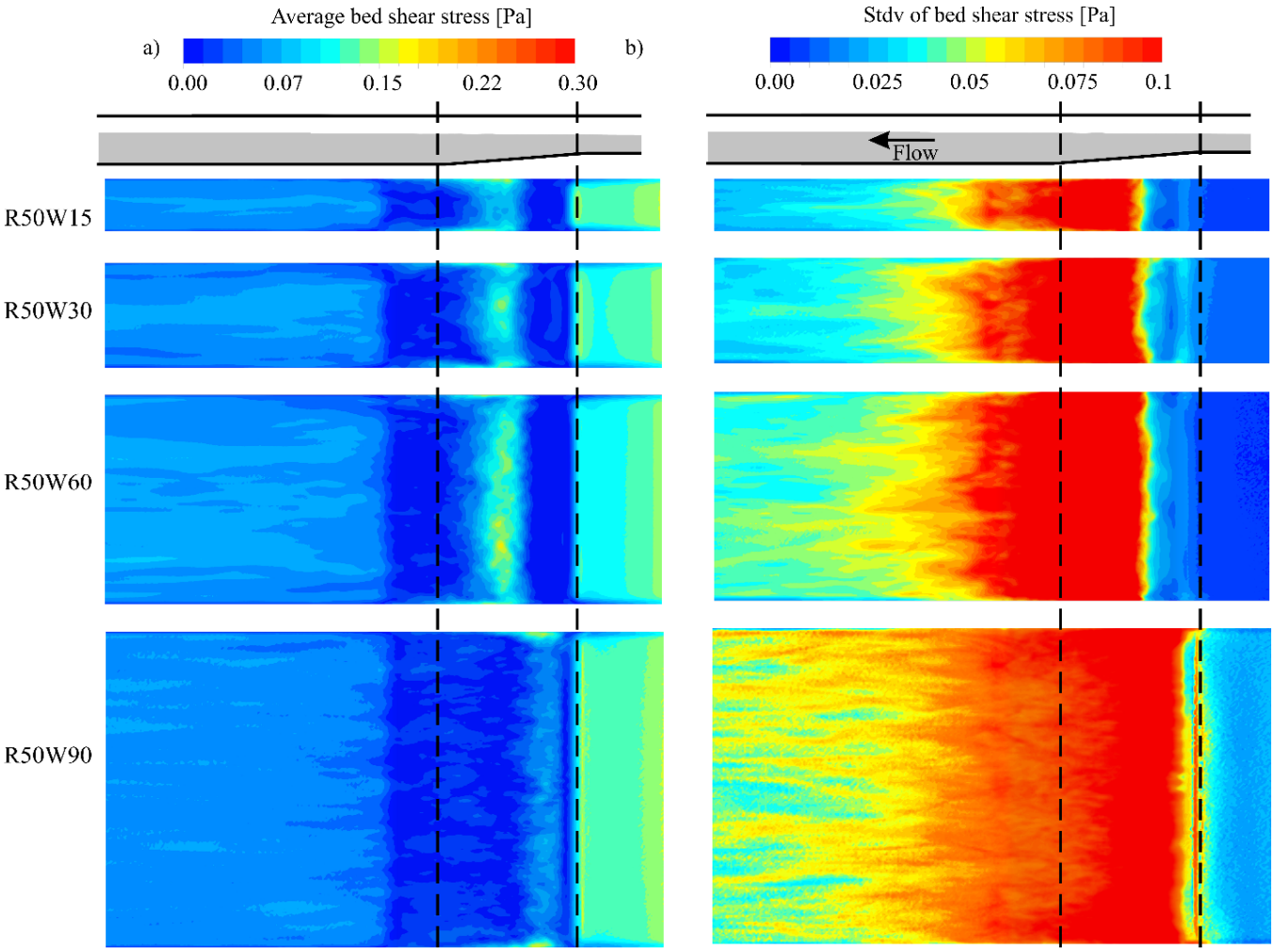

Figure 4-10- a) The contours of average bed shear stress, and b) the contours of bed shear stress standard deviation in cases R50W15, R50W30, R50W60, and R50W90.

4.3.2 The effects of total width variation on plunging flow in isolated pool-riffle units

The cases with h_R=60 mm are all characterized by plunging flow and high turbulence both near the bed and the water surface (Figure 4-11). The contours of the time average velocity in Figure 4-11a show that, in wider channels with this riffle height, the incoming main flow to the pool plunges more deeply, and the region with high-velocity core travels closer to the bed. The contours of velocity fluctuations in Figure 4-11 show that in wider channels, turbulence is produced more intensively in pool-head and turbulence intensities remain high for a longer distance downstream. The turbulence that is generated near the free-surface due to the surface undulation hydraulic jump appears to get stronger in wider channels, and high turbulence zones near the bed and the water surface tend to merge.

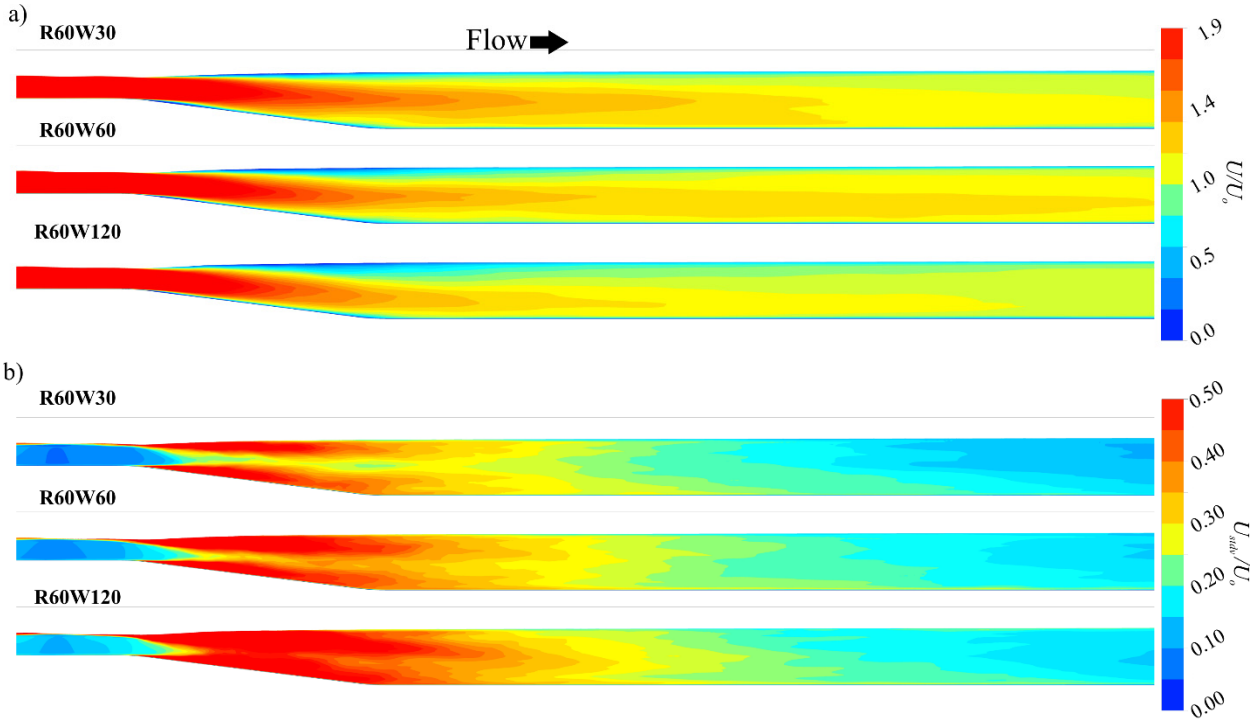

Figure 4-11 a) time-average velocity magnitude (U) in the X-Y plane at channel centerline, b) total velocity standard deviation (U_{stdv}) in the X-Y plane at the channel centreline of cases R60W30, R60W60, and R60W120.

The flow structures at pool-head in R60 cases (Figure 4-12) show both strong RR and surface turbulence (ST) in all cases. Large vortical structures detected with the Q-criterion near the water surface tend to obscure the near bed vortices in these tests (Figure 4-12 a). Moreover, in wider channel, these two types of flow structures shape more strongly. The contours of instantaneous bed shear stress in Figure 4-12 show that in wider channels there are more spots of local high bed shear stress with higher magnitudes in compare with the ones in narrower channels. Also, they stay longer in the domain by travelling downstream.

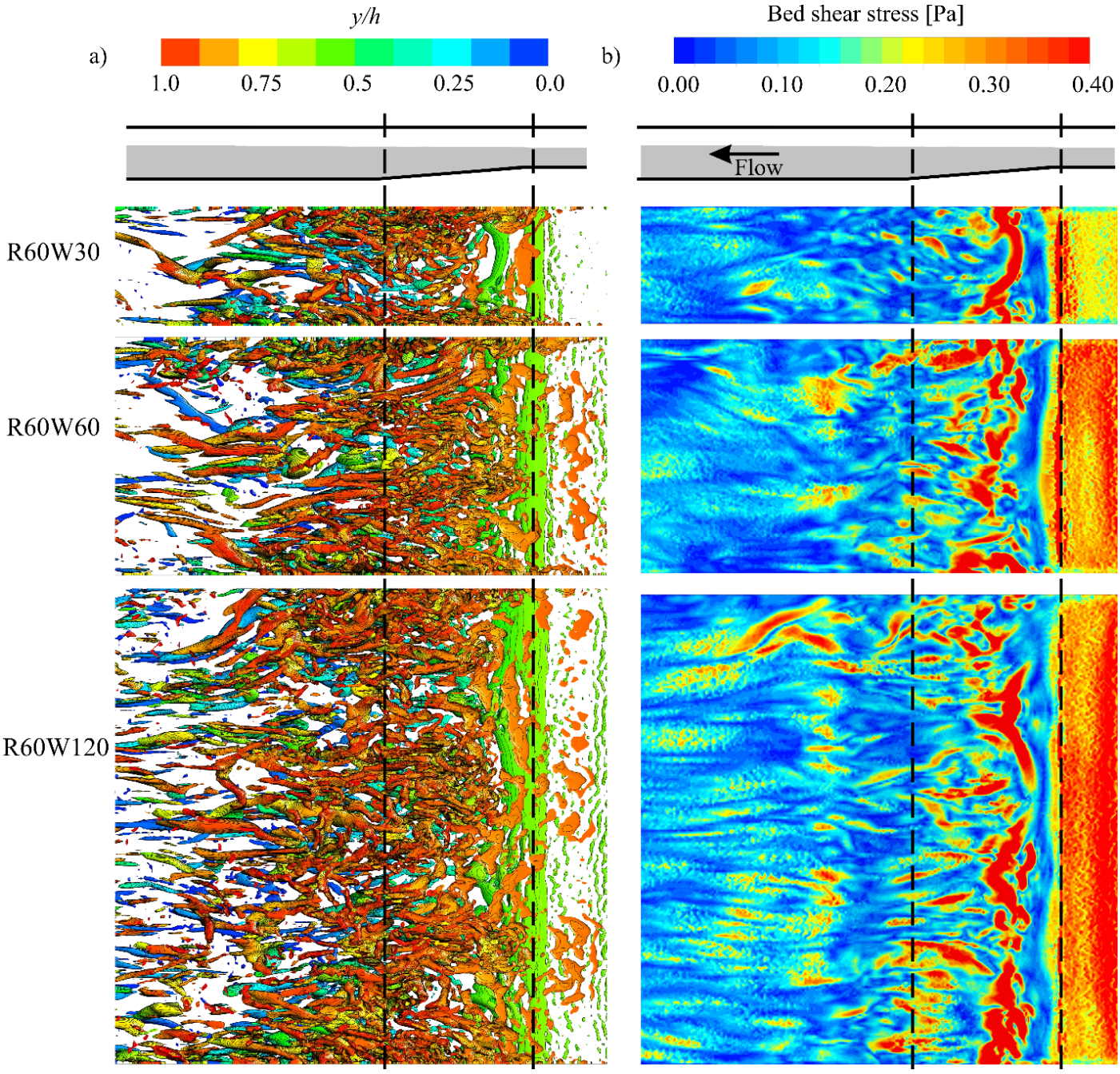

Figure 4-12 Instantaneous flow structure and hydrodynamics for cases R60W30, R60W60, and R60W120, showing: a) Iso-surface of Q=10 s^-2 showing flow structures, and b) contour of bed shear stress magnitude.

The contours of Q-criterion at the pool-head show that in R60 cases strong turbulent structures are present in all areas of the flow (Figure 4-12). All the three types of flow structures (RR, CE, and ST) are visible and strongly interacting. In all cases, ST have occupied the whole width near the free surface, and CE have occupied the sides. In the narrowest channel (R40W30), the mean flow is concentrated mostly at the centre of the cross-section and slightly near the corners between ST and CE. In the case with a midsize width (R60W60), RR are stronger than the ones in R60W30. In the widest channel (R60W120), the RR are strong enough to expand and reach the free surface, and some areas of low turbulence exist between the sidewalls and channel centerline. by resisting the flow, they can separate the mean flow into two substreams.

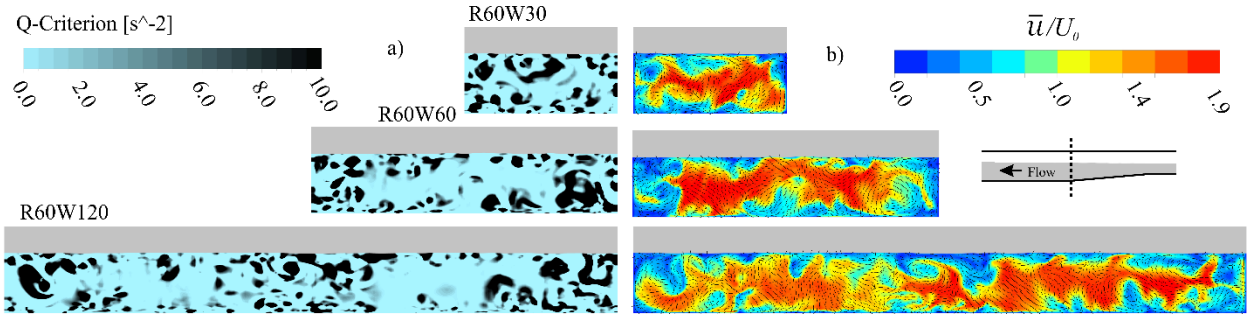

Figure 4-13 Instantaneous flow structure and velocity magnitude for cases R50W15, R50W30, R50W60, and R50W90, showing: a) contour of Q criterion b) contour and vector of velocity magnitude, in a cross-section right after the ramp at pool-head

Both the mean and standard deviation of bed shear stress are higher in wider channels for the cases with a 60 mm high riffle (Figure 4-12). The contour of mean bed shear stress in case R60W120 shows that the mean and standard deviation of bed shear stress peaks at the middle of those two substreams. Moreover, the regions with high mean and standard deviation of shear stress are extended more in the downstream. By comparing the bed shear stresses in R60 cases to the ones in R40 and R50 cases, it can be said that the

plunging flow exerts more stresses and pulsations to the bed and they are more sensitive to the channel width.

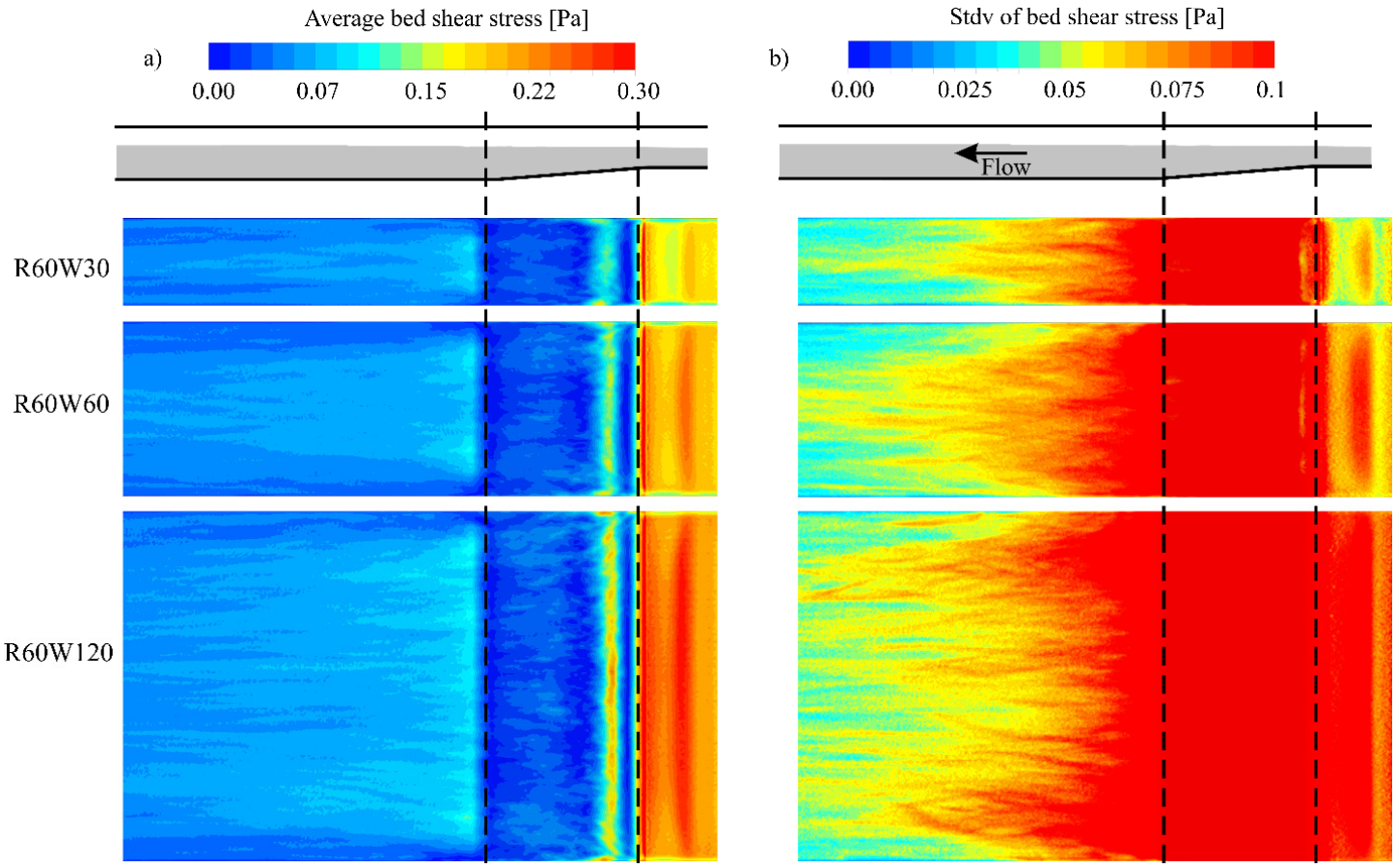

Figure 4-14 a) The contours of average bed shear stress, and b) the contours of bed shear stress standard deviation in cases R60W30, R60W60, and R60W120.

4.3.3 The effects of width constriction on vortical structures

In this section, the effects of constriction geometry in a straight and flat channel on open channel flow hydraulics is investigated. Four different geometries, with different constriction percentage ($\frac{W-W_C}{W} \times 100$) are considered. Cases C10W30, and C20W30, have 10% and 20% constriction, respectively, with linear, smooth, and gradual narrowing section from W to W_C, and a section with 40 cm length with constant W_C,

and then a linear, smooth, and gradual widening to the normal width (W). Cases C20W30C and C25W30C, have a sharp constriction with concave rather than linear sidewalls for the narrowing and widening sections. The motivation for this particular geometry comes from a constriction in Black Canyon, BC, Canada (Venditti et al. 2014) and the desire to more fully understand the hydrodynamics for this site, which includes plunging despite a relatively low Froude number in the constriction. Case C20W30S has a rectangular constriction with 20% ratio while Case C25W30L has a triangular constriction. In all cases the Froude number at the constriction, based on a 1D analysis, is between 0.2 and 0.3 (Table 4-1).

The constrictions with sharp edges or geometries that shape stronger spanwise velocity produce more turbulence and exert higher magnitude fluctuations in bed shear stress. The iso-surfaces of Q-criterion in Figure 4-15 show that the constrictions produce strong vortical structures in the CDF zone (widening section). In case C10W30 a series of vortices are shaped near the bed at the downstream of the constricted section, which we refer to these vortices as bed rollers (BR) herein, and they are stronger in case C20W30, which has higher constriction ratio. The case C20W30C has the same constriction ratio as C20W30, but with concaved curves profile in the narrowing and widening sections. The vortical structures, in this case, are stronger than previous cases. Groups of horseshoe vortices (HV) are shaped at the upstream of in CAF zone, and they are being stretched and transported to the constricted section. HV cause excessive bed shear stress at the upstream of the constriction. They interact with BR and make them weaker as they pass the constriction. The ST near the walls and downstream of the constriction are stronger and propagated more widely than previous cases. The vortical structures, in this case, stay longer in the domain before they get entirely dissipated. The case C20W30S has a rectangular constriction section that results in stronger HV that originate farther upstream from the constriction. These HV result in high bed shear stresses in and upstream of the constricted section. For the case C25W30C, which has a

25% constriction with concave curve narrowing and widening sections, the ST, HV, and BR are stronger than the ones in other cases. These strong vortical structures appear to exert higher shear stress on the bed. Case C25W30L has the same constriction ratio as case C25W30L, but the vortical structures are weaker.

BR are shaped closer to the constriction in more constricted channels, and they are weaker in cases that have strong ST and HV. The instantaneous longitudinal contours and vectors of velocity magnitude along the centerline of the channel (Figure 4-16) show that BR shape farther downstream of the constriction in cases C10W30 and C20W30, and they are stretched and elevated to the middle of the flow depth as they travel downstream. For the shorter constriction, the near-bed turbulence is stronger upstream while the near-surface turbulence develops later and is weaker along the centerline.. They are weaker than BR, and they do not grow and last longer. In case C20W30S the long HV are mixed with BR and start to elevate from the bed at the middle of the constriction. The ST, in this case, are decidedly weaker than bed turbulences, which is in contrast with case C25W30C. Bed turbulences are reduced to a thin layer near the bed that do not grow or elevate to enter the main flow. In contrast with other cases, in case C25W30C, the core of high velocity is located near the bed. In comparison with C25W30C, the ST in case C25W30L, appear later at the plane along the centerline. In addition, BR are stronger than previous cases but not strong enough to occupy the bottom half of the flow depth. In all cases, the generated turbulence are stretched in the form of AT as they leave their genesis and travel downstream.

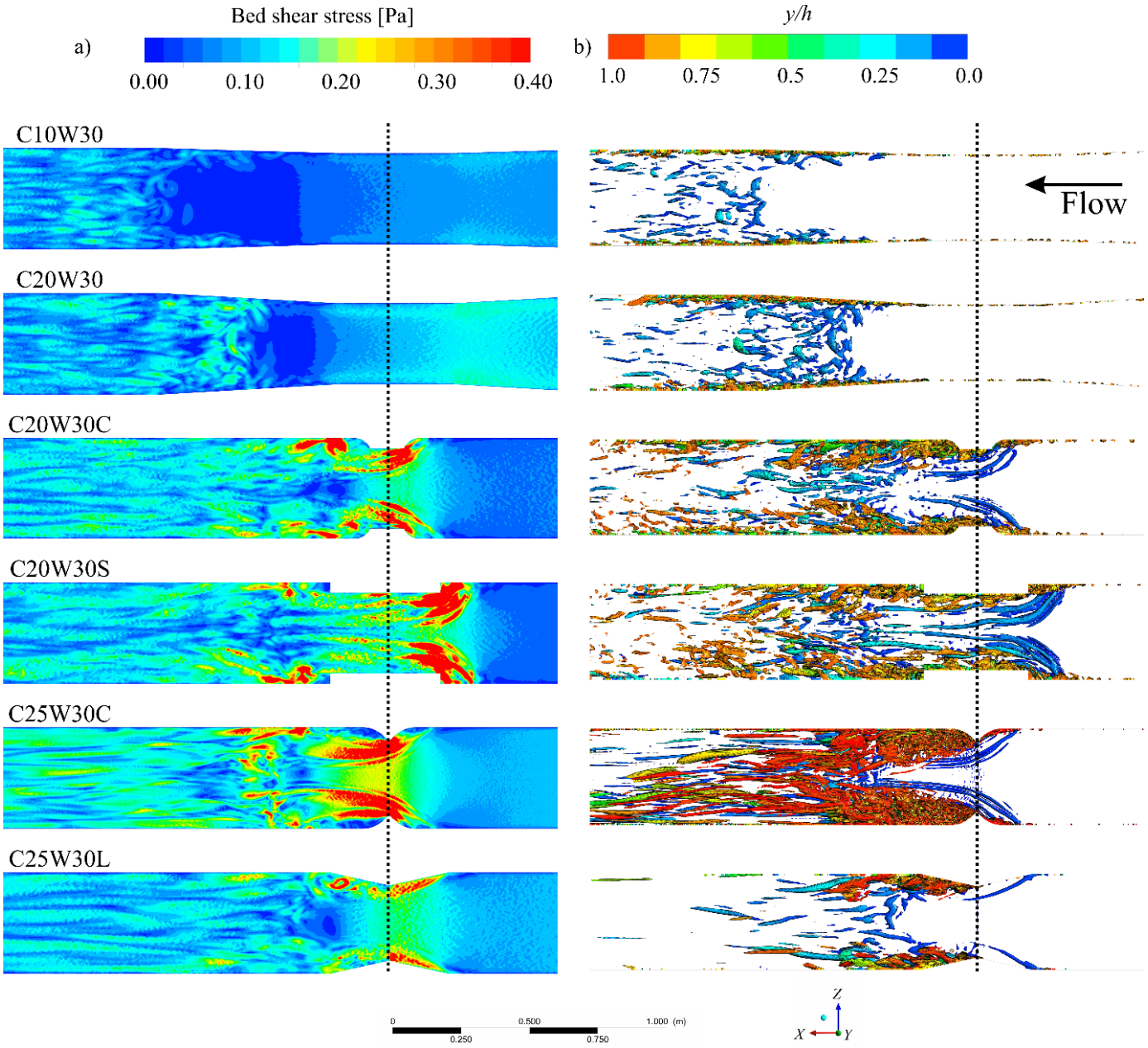

Figure 4-15 Instantaneous flow structure and hydrodynamics for cases C10W30, C20W30, C20W30C, C20W30S, C25W30C, and, C25W30L showing: a) contour of bed shear stress magnitude, and b) Iso-surface of Q=10 s^-2 showing flow structures.

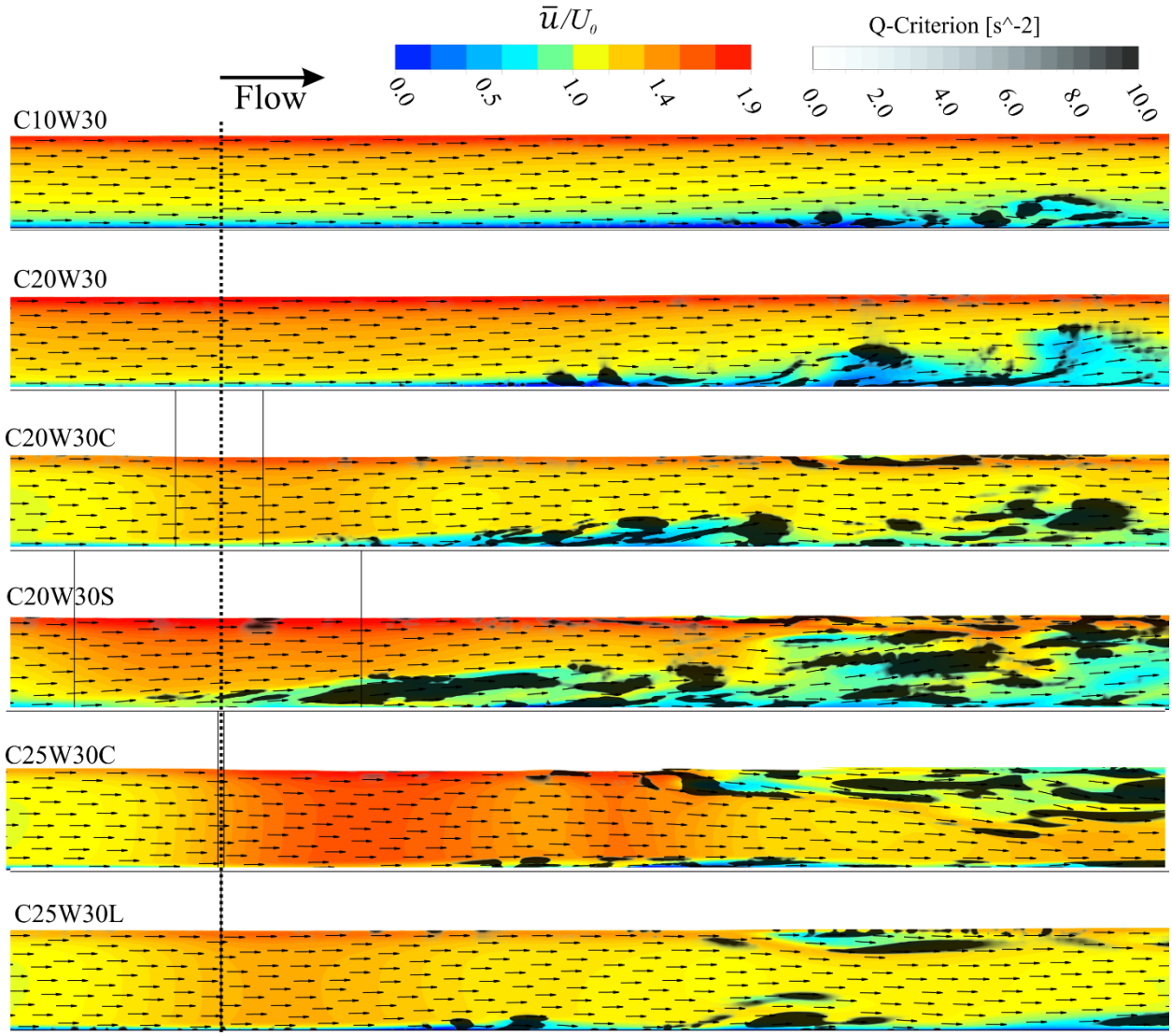

Figure 4-16 Instantaneous velocity magnitude ($\bar{u}$) and vector, and shade of Q-criterion in the X-Y plane at channel centerline in cases C10W30, C20W30, C20W30C, C20W30S, C25W30C, and C25W30L; the centre of constrictions are marked with dash line.

The cases without strong turbulence near the water surfact show no deflection and plunging of the main flow after the constriction. The case C25W30C, which has the convex narrowing and widening sections and intense surface turbulence has the highest vertical flow deflection of plunging flow. Cases C10W30

and C20W30 show mean flow acceleration in the narrowed section but no velocity dip and the average mean flow is recovered quickly after the constriction. Where there is a more abrupt change in cases C20W30C, C20W30S, and C25W30L, some acceleration is noted, and there is a minor of velocity dip, but the highest velocities remain near the water surface, and they remain categorized as skimming flow.

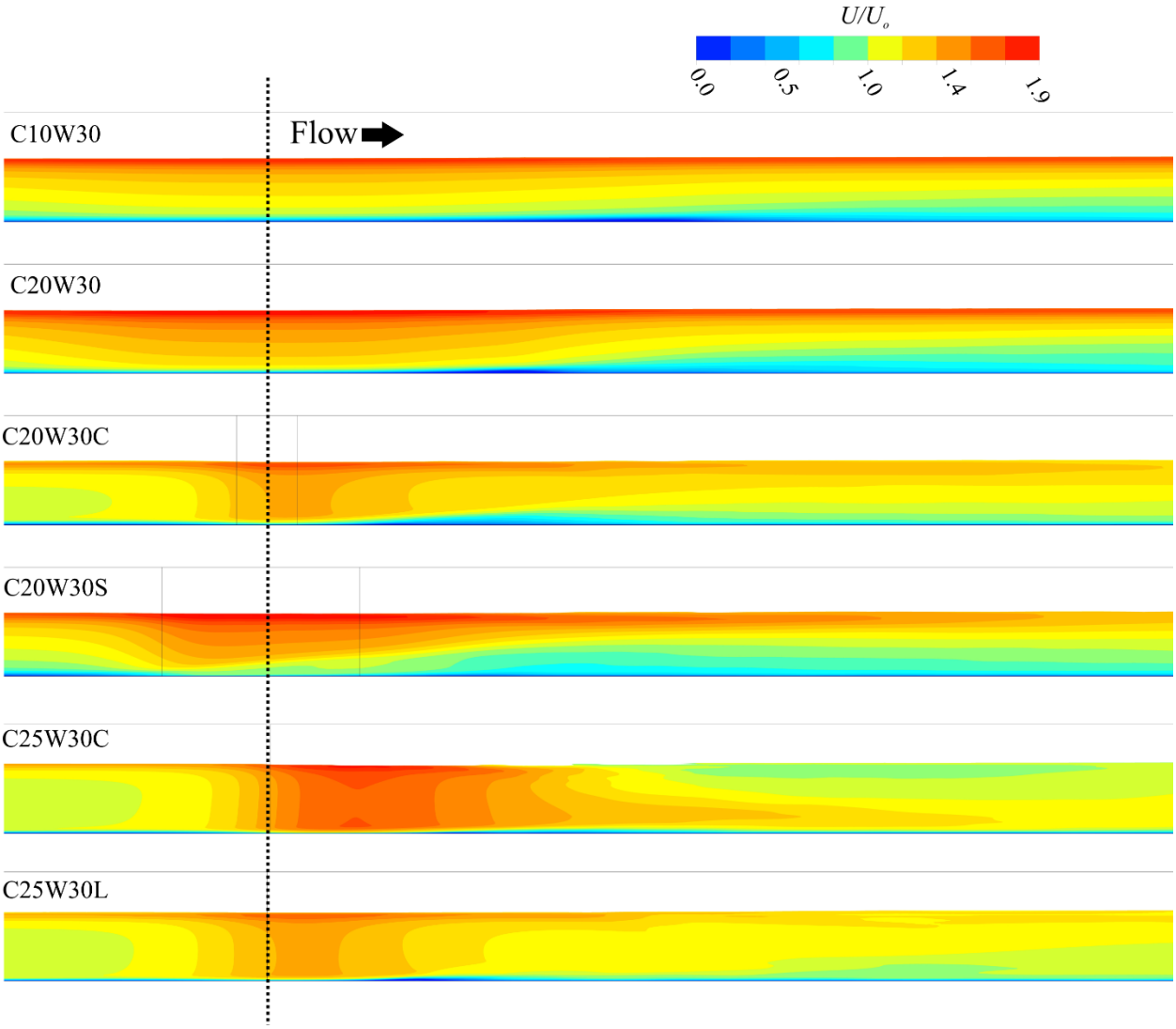

Figure 4-17 time-average velocity magnitude (*U*) in the *X-Y* plane at channel centerline in cases C10W30, C20W30, C20W30C, C20W30S, C25W30C, and C25W30L, the centre of constrictions are marked with dash line

Constrictions do not increase the mean and instantaneous bed shear stresses in all regions. The contours of mean and standard deviation of bed shear stress in Figure 4-18 for cases C10W30 and C20W30 show that there is a region in the widening section downstream of the constriction that is characterized by low mean and standard deviation of bed shear stress. The mean shear stress in this region is even lower than the one in the upstream before the constriction. This region is smaller in the cases with higher constriction percentage and sharper edges. The contour of mean and standard deviation of shear stress for the abrupt constrictions (C20W30C, C20W30S, and C25W30L) show high mean and fluctuating shear stresses upstream of the constrictions in CAF. Shear stress fluctuation is relatively lower for case C25W30L, which is characterized by more gradual triangular constrictions. In the abrupt constriction cases, the bed downstream of the constriction tends to be characterized by a low mean but high fluctuations of bed shear stress. In case C25W30C, the downstream and middle of the constriction have the highest excessive mean and standard deviation of shear stress among all cases.

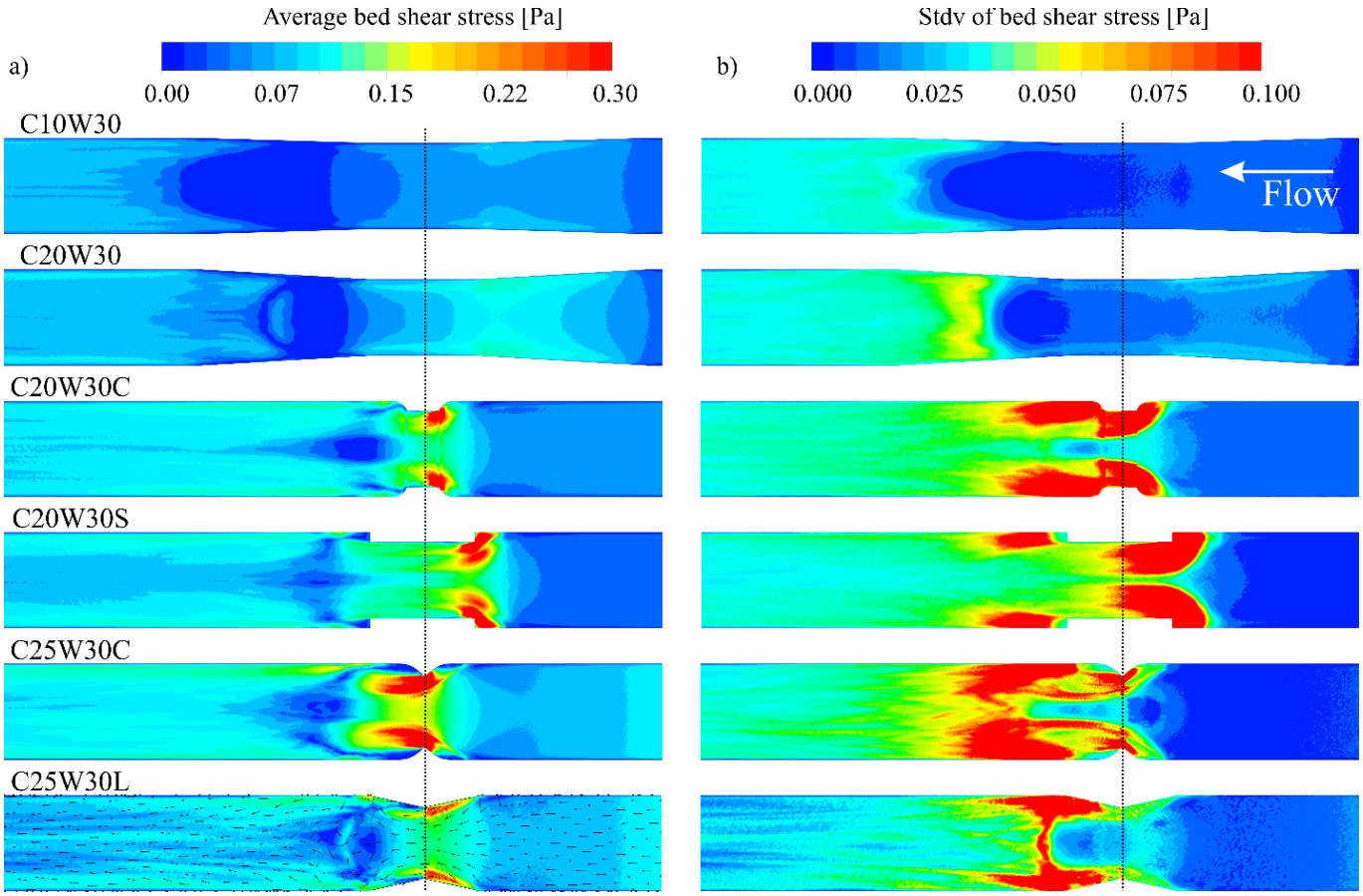

Figure 4-18 a) The contours of average bed shear stress, and b) the contours of bed shear stress standard deviation in cases C10W30, C20W30, C20W30C, C20W30S, C25W30C, and C25W30L.

4.3.4 Effects of constriction on skimming flow in pool-riffle units

In this sections, the combined effects of width constriction with pool-riffle units on the flow pattern and formation of vortical structures are investigated. The constriction is placed at the riffle, which means that the variation of bed and side walls are in phase (Table 4-1). In all cases except R40W60C25, the narrowing section starts at the upsloping ramp at the upstream of the riffle, the uniform part of the constricted region has the same length as the length of the riffle crest. The type of narrowing is thus comparable to the cases C10W30 and C20W30 from the previous section. The widening part of

constriction ends at the end of the downsloping ramp at the pool-head. The exception to the type of narrowing investigated is case R40W60C25C where a convex narrowing and widening planform was added to compare with case C25W30C from the previous section. The sharp edges of the constriction are at the middle of the riffle crest.

The results show that in all cases a constriction and a greater degree of constriction will create a greater dip in the highest velocity below the water surface. In comparison, a velocity dip was not observed for cases with comparable riffle height in the absence of a constriction (for e.g. in Figure 4-3) nor with comparable constrictions in the absence of a riffle (for e.g. in Figure 4-18). The contours of average velocity at the plane along the centerline of the channel show that cases R40W30C10, R40W60C10, R40W120C10, and R40W120C20 have a small degree of velocity dip, though still categorized as 'skimming flow' herein, while The inversion of velocity is higher in cases R40W30C20, R40W60C25C and R40W60C20, and the flow types are categorized as 'rifting flow.' The shape of the sharper edges

Similar to other cases where velocity inversions were observed, the contours of velocity standard deviation in Figure 4-19b show that the cases with greater degree of velocity dip have higher turbulence near the surface. For example, comparing the cases with 20% constriction ratio, the narrower cases (R40W30C20 and R40W30C10) have higher velocity fluctuations in the center plane. In case R40W120C20, no surface turbulence have appeared in the centerline plane, and the velocity remains highest near the water surface. The turbulence near the bed, which are mostly generated in the zone of flow expansion are stronger in wider channels and need more length to be recovered towards uniform flow values.

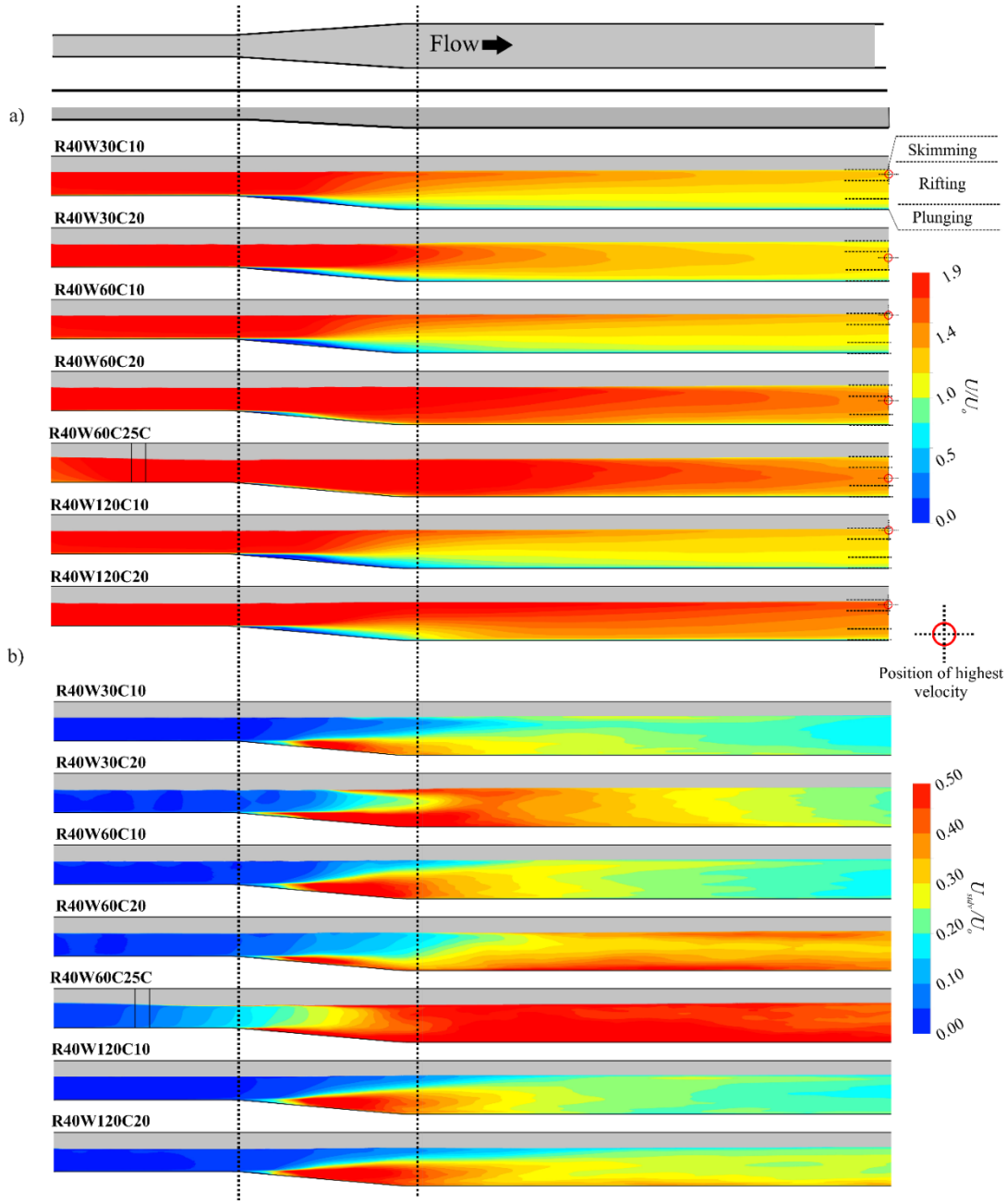

Figure 4-19 a) time-average velocity magnitude (*U*) in the *X-Y* plane at channel centerline, and the position of highest velocity at the middle of the pool, b) total velocity standard deviation (U_{stdv}) in the *X-Y* plane at the channel centreline for case R40W30C10, R40W30C20, R40W60C10, R40W60C20, R40W60C25C, R40W120C10, and R40W120C20.

Looking at the whole domain, turbulent structures in the cases with constrictions and pools are much stronger than the previously examined configurations with this riffle height (40 mm). For visualization of the most powerful structures, the threshold for Q-criterion was therefore chosen to be double that of the previous cases (Q=20 s^-2) (Figure 4-20). For cases with the same channel widths (e.g. R40W30C10 and R40W30C20), the case with the greater degree of constriction (i.e. the C20 cases) were always characterized by stronger surface (ST) and near bed turbulence (RR). They also generally persisted farther in the domain before dissipating. Among the cases with the same constriction ratio, the case with wider width has stronger vortical structures. In cases R40W30C20 and R40W60C10, the one with a narrower width and higher constriction ratio has stronger vortical structures.

The results from these simulations were also interesting for the interpretation of pool and riffle dynamics because of examples of instantaneous and mean lateral asymmetry. In cases R40W60C20 and R40W60C25C, for example, the vortical structures in one side of the channel are stronger than the other side in these instantaneous plots, which is expected given the turbulent nature of the flow. However, the mean and standard deviations of bed shear stress were also found to be asymmetric.

Moreover, these cases have the highest bed shear stress among other cases. RR in the cases with asymmetric flow structures (R40W60C20 and R40W60C25C), (Figure 4-19), are not as strong as the ones in other cases in the centerline plane. In case R40W30C10, ST appears later in centerline plane, than the ones in R40W30C20. Case R40W120C20 has stronger CE and weaker RR than the ones in case R40W120C10. HV are not strong enough to pass the thresholding of Q-criterion, but the trace of them can be seen in the instantaneous bed shear stress in cases R40W120C10 and R40W10C20.

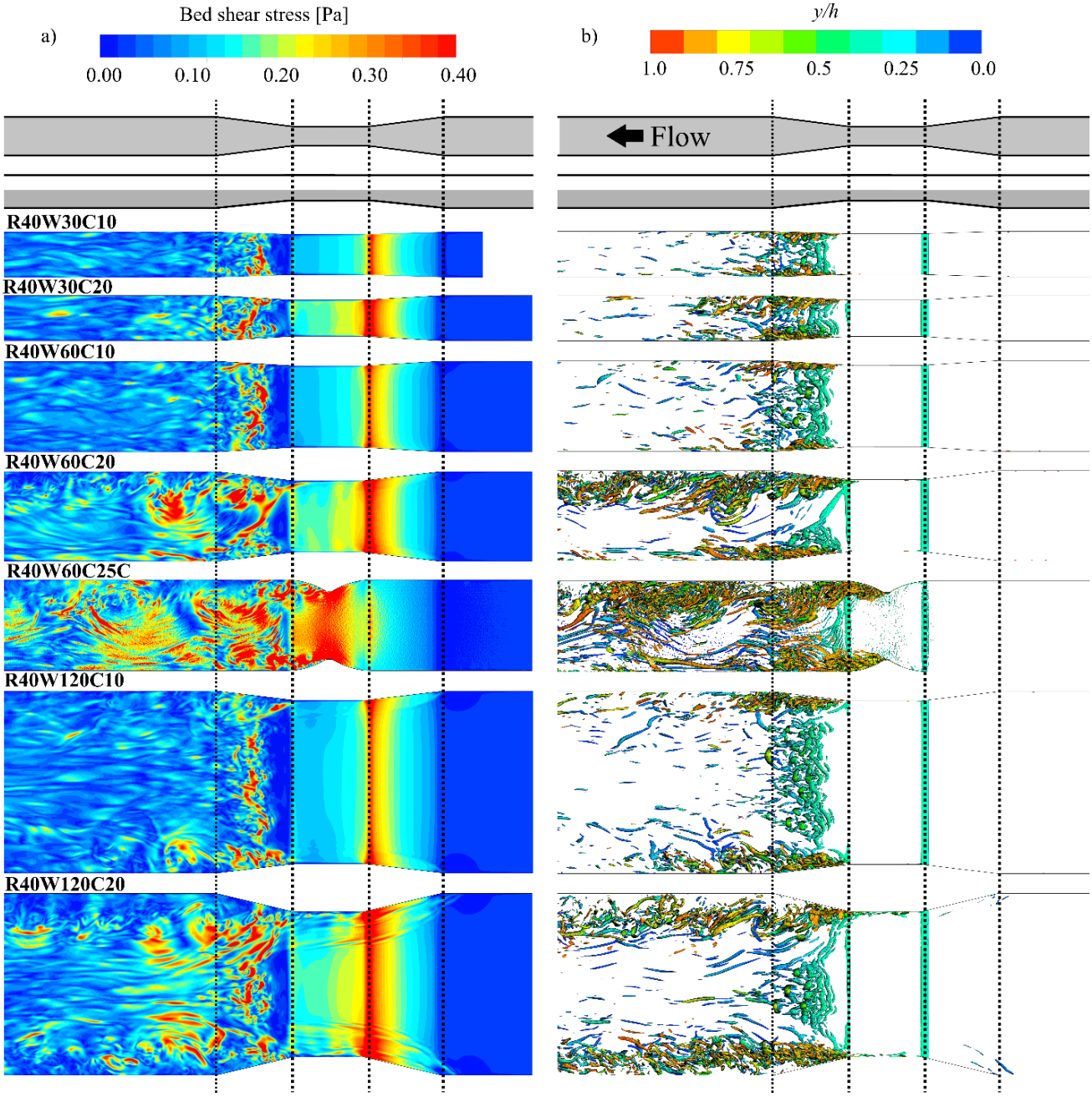

Figure 4-20- Instantaneous flow structure and hydrodynamics for cases R40W30C10, R40W30C20, R40W60C10, R40W60C20, R40W60C25C, R40W120C10, and R40W120C20 showing: a) contour of bed shear stress magnitude and b) Iso-surface of Q=20 s^-2 showing flow structures.

The contours of mean and standard deviation of bed shear stress in R40 cases with constrictions show that the cases with narrower constrictions have more pulsations in bed shear stress. The mean shear stress distribution in cases R40W30C10, R40W30C20, R40W60C10, and R40W120C10, have similar magnitude and pattern. The distribution of mean shear stress on the riffle crest in the cases with 20% constriction show slightly higher magnitude than the one in cases with 10% constriction. The mean and standard deviation of shear stress in case R40W60C25C have the highest magnitude among other cases. In case R40W60C20, the region with excessive shear stress pulsation and mean is extended further downstream than those in cases R40W30C10, R40W30C20, R40W60C10, and R40W120C10. Cases R40W30 and R40W120C20, are the only cases with traces of excessive bed shear stress pulsation in the upstream ramps (CAF) and riffle crests.

The diagrams of 95% confidence range of bed shear stress at centerline, in Figure 4-22, show that the mean shear stress in the riffle crest in case R40W60C10 has ~10% higher value than the one in case R40W60. Moreover, in case R40W60C10 the mean shear stress in the downstream ramp of the riffle is slightly higher than the one in case R40W60. The mean shear stress at the middle of the pool in the case R40W30 is the lowest, and the one in R40W30C25C is the highest. In all cases, the upper bound of shear stress in the pools are higher than the mean shear stress in the riffle crests. Case R40W60C20 has the same maximum value of shear stress as case R40W60C10 in downsloping ramp; however, the magnitude of shear stresses in the pool are much higher than those in the case with lower constriction ratio (R40W60C10). Both the mean and standard deviation of bed shear stress are extensively higher in case R40W60C25C than the ones in other cases.

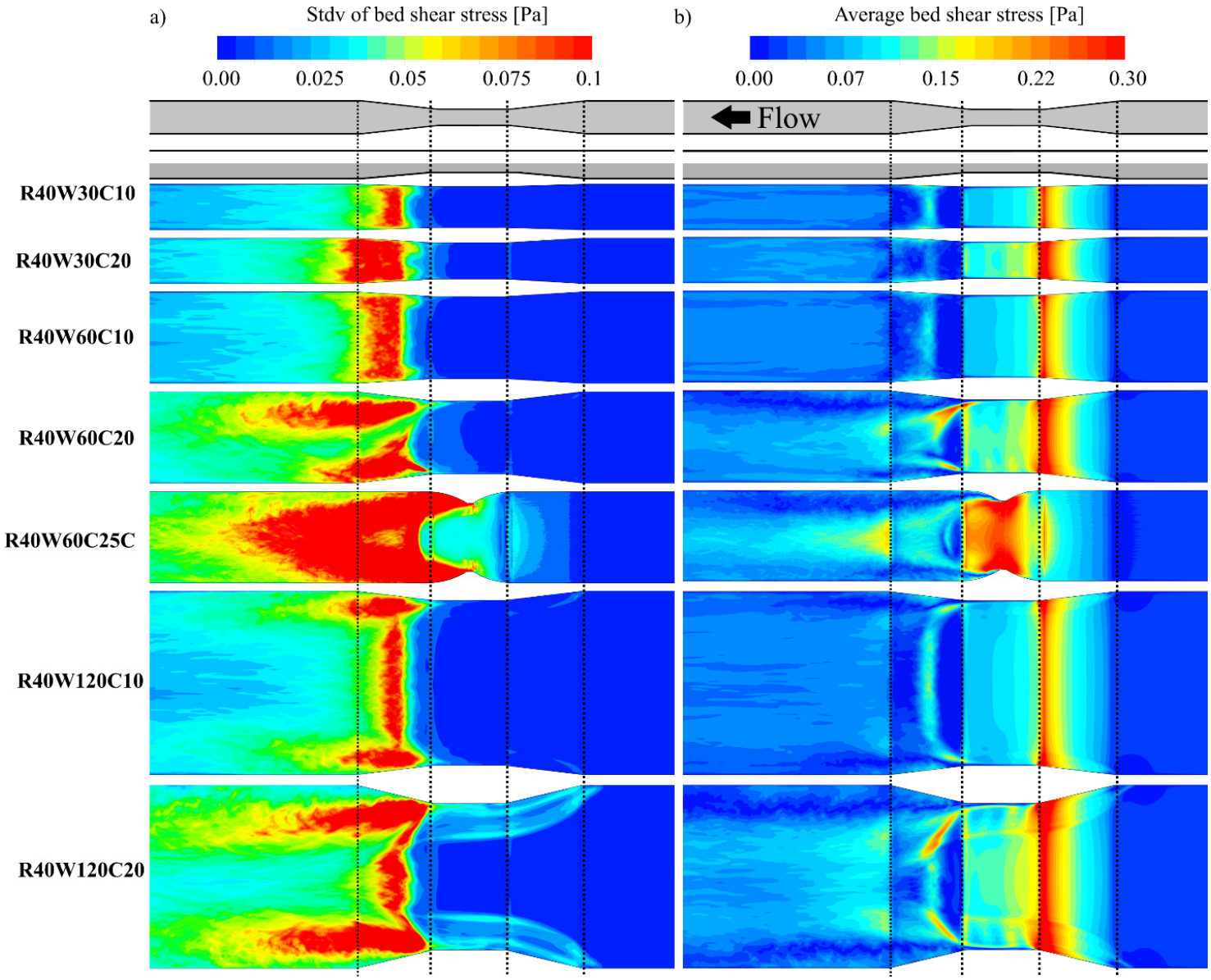

Figure 4-21 a) the contours of bed shear stress standard deviation, and b) The contours of average bed shear stress, in cases R40W30C10, R40W30C20, R40W60C10, R40W60C20, R40W60C25C, R40W120C10, and R40W120C20.

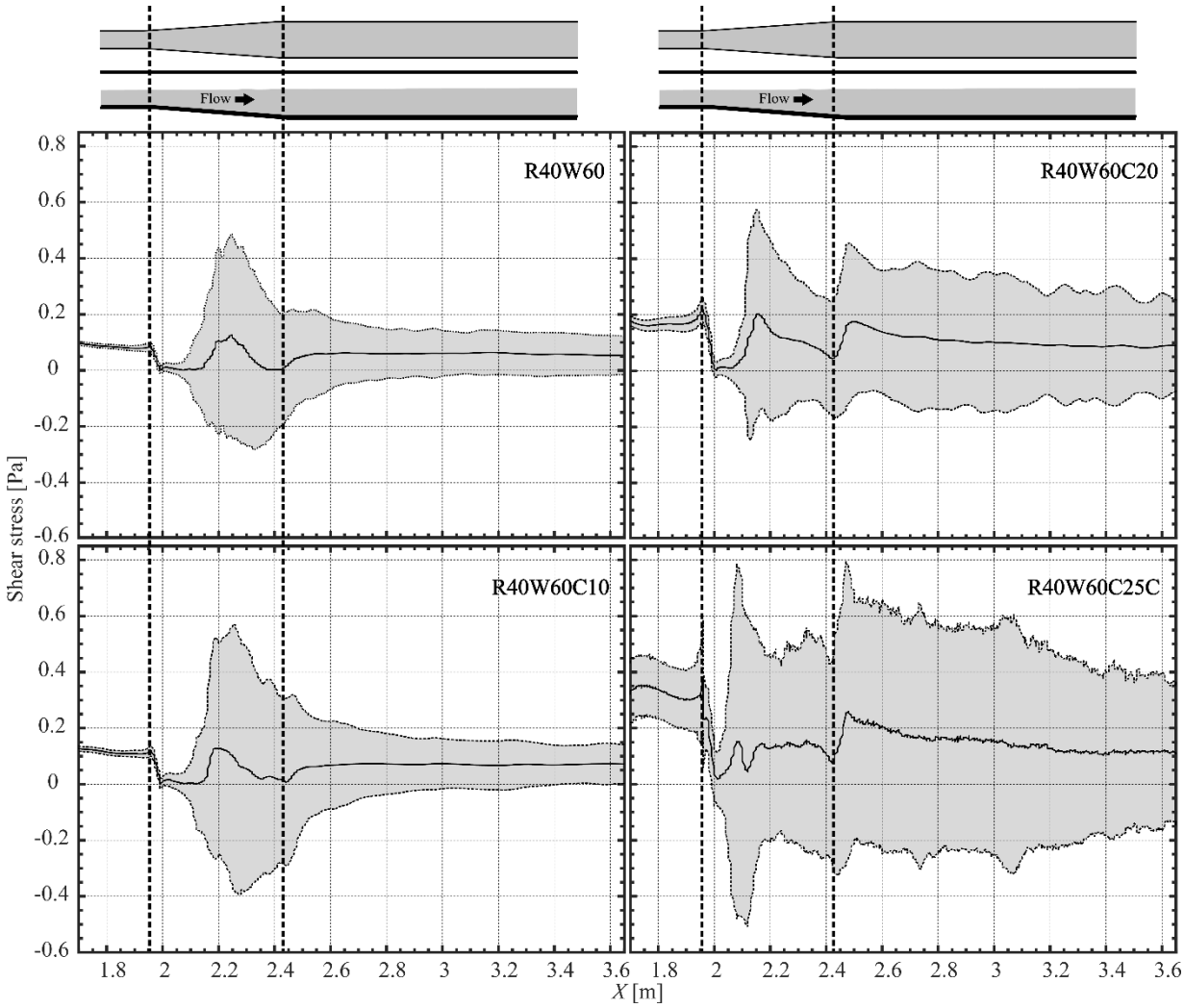

Figure 4-22 Time-average (black line) and 95% confidence range (dashed line) of bed shear stress at centreline for cases R40W60, R40W60C10, R40W60C20 and R40W60C25C.

4.3.5 The effects of constriction location on bed shear stress

Two cases were designed to investigate the effects of constriction location on the flow pattern and bed shear stress. The constriction ratio is 10%, with the same geometry of constriction in case R40W60C10. As it is illustrated in Figure 4-23, case R40W60C10U has a narrowing section at the upstream of the riffle, the uniform constricted part is at the upsloping ramp, and the widening part is at the riffle crest.

Case R40W60C10D has the narrowing part at the riffle crest, the uniform constricted part is at the downsloping ramp, and the widening part is at the pool head. RR in case R40W60C10U is stronger than other cases illustrated in Figure 4-23. CE are stronger in case R40W60C10 than other cases. Case R40W60C10D has the weakest RR among other cases.

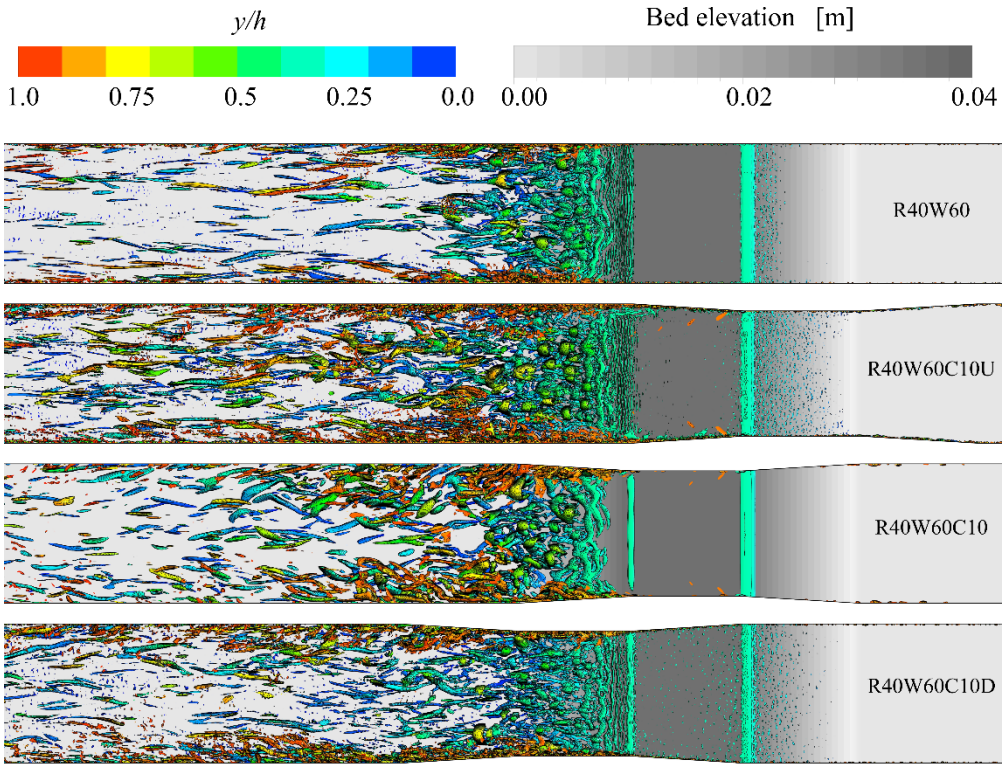

Figure 4-23 Instantaneous flow structure for cases R40W60, R40W60C10U, R40W60C10, and R40W60C10D showing Iso-surface of Q=5 s^-2, and the contour of bed elevation.

The diagrams of 95% confidence range of bed shear stress, in Figure 4-24, show that the case with widening part at the riffle crest has the lowest mean shear stress at the riffle crest. The case with narrowing part at the riffle crest has the highest mean shear stress and fluctuation in the riffle crest, even

more than the ones in case R40W60C10, where the narrowest part is in the riffle crest. Case R40W60C10D has the lowest upper bound of shear stress in the downsloping ramp and the pool.

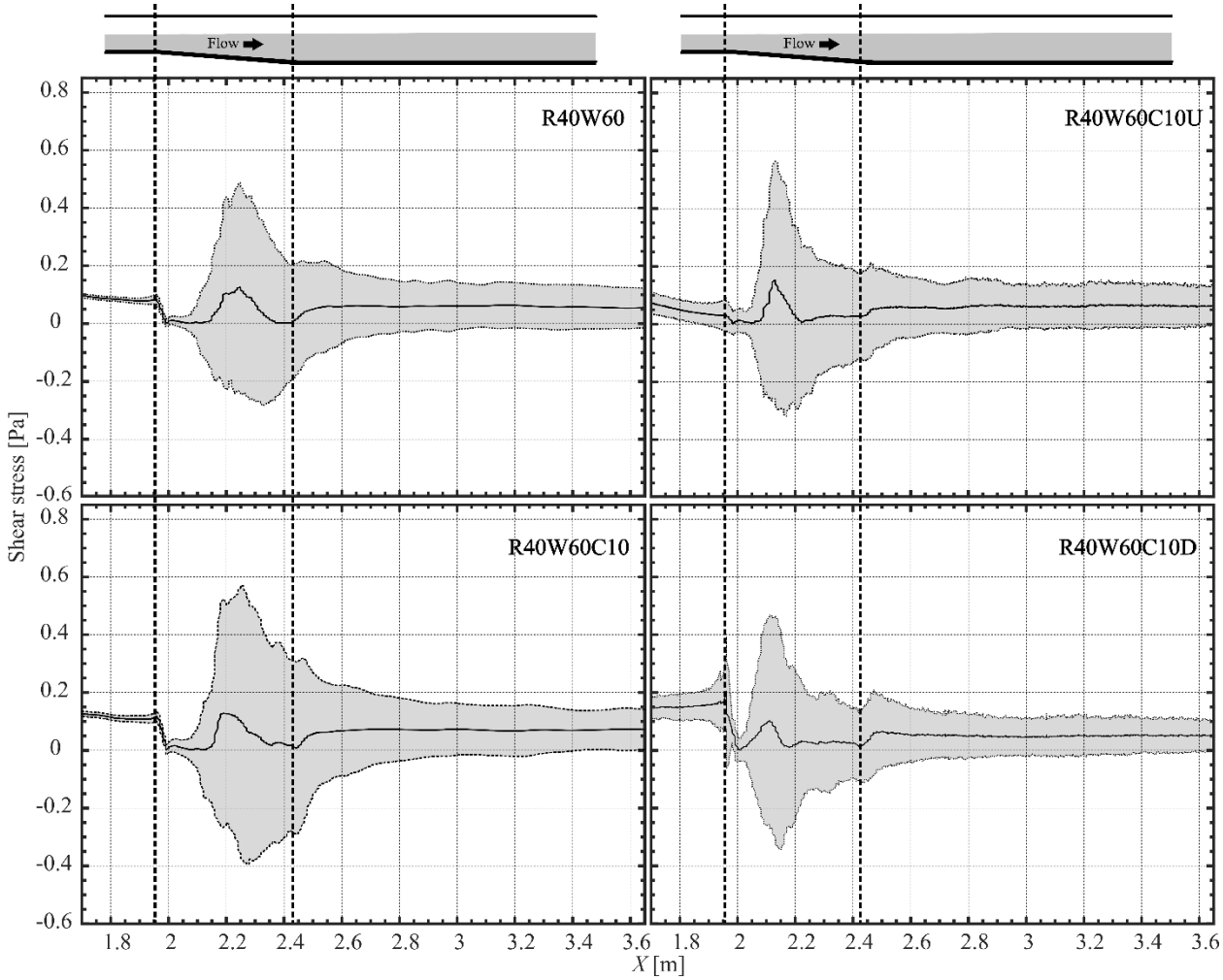

Figure 4-24 Time-average (black line) and 95% confidence range (dashed line) of bed shear stress at centreline for cases R40W60, R40W60C10U, R40W60C10, and R40W60C10D.

4.4 Discussion

In the previous chapter, the formation mechanism of skimming, rifting, and plunging flow; and bifurcation in mean flow are discussed by introducing the vortex-resistance hypothesis. We showed that the reason for scouring and high shear stress in the stable pools is not only the high velocity near the bed, which previously named as velocity reversal (Keller, 1971). This chapter for designing new models aims to investigate the effects of constriction on flow pattern and maintenance of pool-riffle units, which previously described as flow convergence hypothesis (MacWilliams et al. 2006).

MacVicar & Best, (2013) used the concept of recovery from perturbation to describe the effects of geometry induced flow behaviour. They mentioned two stages for recovery from perturbation. The first stage that is called “spreading” refers to production, propagation, and transport of turbulence, which is induced by morphological changes, and streamwise adverse pressure gradient (positive). After the completion of “spreading” phase, the “relaxation” phase is initiated. “Relaxation” refers to the phase that there are no significant irregularities in the morphology and the flow tries to recover to the normal state, which it had before the emergence of perturbation. In the “relaxation” phase, the vortical structures get stretched, break into smaller scales and finally dissipated by viscous forces, while they are travelling downstream. The concept of “spreading and relaxation,” and the length that the flow should travel to reach the normal state (recovery length), is used in this section to qualitatively describe the hydrodynamic response of the channel to the total and local variation of the width.

The most of perturbation generations, in spreading phase, happen in CDF zone, which is located at the widening section and downsloping ramp at the pool-head. The widening section and downsloping ramp are in phase in the cases that are described previously in this chapter. Four generative vortical structures (RR, BR, CE, and ST) produce perturbation in CDF.

In the cases without local width variation (no spanwise constriction and expansion), and with skimming flows (R40 and R50 cases) the strength of RR and CE, which are related to their sizes, are mostly controlled by the height of the riffle (h_R). This claim is shown in the previous chapter and comparing the hydrodynamics in R40 and R50 cases. These two major vortical structures (RR and CE) appear to influence each other's strength such that in narrower channels, these two types of vortices are forming very closely to each other and do not have enough space to shape and grow fully. In wider channels, RR in the centre of the channel, far away from CE, have more space and grow to bigger sizes. Meanwhile, CE have more space as well and they are also stronger in wider channels. Stronger RR and CE mean that the "spreading" phase results in larger and more powerful eddies that require a longer streamwise distance to dissipate. The differences in turbulent eddies with respect to channel width thus help explain the longer recovery length for wider channels. The contours of the standard deviation of shear stress in the previous section show that longer recovery lengths extend the excessive pulsation in shear stress to farther downstream. This pattern of hydrodynamic response to morphological irregularities can be found in the cases with plunging flows (R60 cases) as well. The resistance of stronger RR at the middle of the width in wider channels acts as a wall and divides the channel into two substreams; therefore, with more walls and CE, there are more sources of turbulence in CDF.

In the cases with just a constriction (i.e. without a riffle), the perturbation generations in "spreading" phase commence before the constriction (in CAF). The illustration of vortical structures for these cases in the previous section shows that there are three major generative vortical structures in those cases. BR and CE at the downstream of the constriction (CDF zone), and HV at the upstream (CAF zone). HV are reported by various researchers that have studied the vortical structures around obstacles in shallow streams (Beheshti et al. 2017; Celik et al. 2014; Ettema et al. 2017; Kumar et al. 2012; Zeng and Constantinescu 2017). They reported that HV are the result of the combination of downward flow at the upstream face of the obstacle that induces vortices at the front of the obstacle that is then stretched around

the base of the object by the main flow. BR have similar formation mechanism as RR in pool-riffle units both cases are forced by an adverse pressure gradient and result in mean flow moving away from the bed and creating a region of relatively high strain at the middle of the profile that can generate new turbulence(Krogstad and Skåre 1995). The formation of CE are due to the irregularity in the sidewalls and the impact of secondary flow to the walls. If the constriction has sharper edges or a geometry that shape more powerful spanwise component of velocity, the CE become stronger. In sharp edge constrictions, CE are stronger near the surface, because the logarithmic profile of incoming flow has higher velocity near the surface than near the bed. Therefore, CE near the surface in the form of ST have larger sizes than the ones near the bed. Stronger CE, BR, and HV need more recovery length in "relaxation" phase.

By adding the constriction to pool-riffle units, the constriction induced vortical structures both amplify and suppress some vortical structures found in the straight pool-riffle units. BR combine and amplify the RR, but they are not strong enough to cancel out the impact of CE and HV. HV, which are generated in CAF zone at the upstream, amplify CE, confine the generation space of RR and decrease the impact of RR on suppressing the CE. The CE, which are induced by the constriction, amplify the CE in the pool. The strong CE, at the downstream of the riffle, can get transported to the free surface by the secondary flow. The combination of secondary flow and transported CE can make boiling structures on the free surface. These ST guide the mean flow to plunge into the pool. The secondary effect of plunging flow suppress the formation of RR and amplify the secondary flow and CE; therefore, as positive feedback, the CE become stronger until the system reaches to an equilibrium balance of forces and momentums. Due to the resistance of CE and powerful plunging flow, bifurcation can happen to the mean flow and deflect it to one side. The deflected mean flow amplify the vortical structures of one side; therefore, the "relaxation" phase will be delayed, and the flow needs a more prolonged recovery length to reach the normal state.

4.4.1 Plunging flow in Black Canyon

The Black Canyon, BC, Canada has a similar geometry to the R40 cases of this study with a constriction (Figure 4-25). Both have similar Froude number in the pools (~0.2), similar W/h ($2.3 < W/h < 17.3$), and no critical flow condition or choking flow in the entire domain. Venditti et al., (2014) found plunging flow and boiling structures in the pool section of the Black Canyon. They postulated that the reason for plunging flow formation is the reduction in near bed dynamic pressure due to the upwelling flows. This phenomenon can be interpreted differently by the results of this chapter and the vortex resistance hypothesis. As noted before, the Froude number is not near 1, and the constriction does not make a choking flow; therefore, the plunging flow and boiling structures are not thought to be related to a surface undulation hydraulic jump. Based on the results from the current study, the surface boiling structures and turbulence (ST) appear to be similar to turbulent structures observed in cases with 20-25 % constrictions of the channel in phase with a riffle (R40W30C20, R40W60C20, and R40W60C25C). Based on this comparison, there should be strong CE near the walls in CDF zone of Black Canyon due to the constriction and downsloping ramp. The observed boiling structures near the free surface might be the result of the interaction of the secondary flow and CE. Moreover, these surface boiling structures in the form of ST likely help to guide the main flow to plunge into the pool.

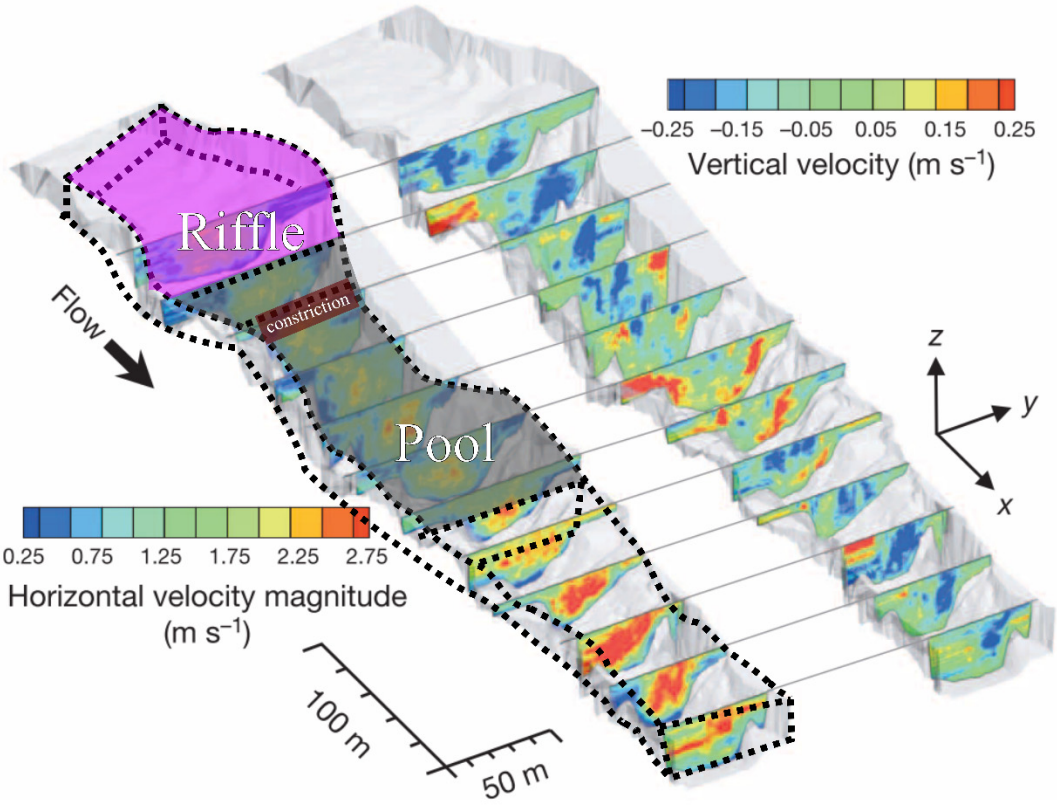

Figure 4-25 the distribution of horizontal and vertical velocity in black canyon reported by Venditti et al., (2014), the lines for showing the pool, riffle and constriction are added by the author of the present thesis.

4.4.2 Meandering initiations from straight channels

The initiation of meandering from a straight channel is an interesting question for researchers in this field. To answer this question, many reasons are mentioned in previous studies, such as a) For the initiation of meandering, there is a need for regular scour and deposition, which can be induced by convergence and divergence of the mean flow (Keller, 1972); b) a secondary flow induced by wall turbulence can shape a meandering thalweg (Einstein and Shen 1964); c) the link between secondary flow, helical flow, and pool-riffle units initiate the meandering (Thompson, 1986); and d) the recent studies postulated that the

existence of small random perturbation and propagation of instabilities make irregularities in the morphology and then results in the initiation of meandering (Hooke 2013; Seminara 2006).

The results of this study can show that another source of perturbation in the initiation and development of meandering can be those vortical structures that are discussed in the previous section. Moreover, the bifurcation of mean flow, which are seen in the cases with plunging flow (e.g. R65W60 from chapter 3 and R40W60C20), can be another source of instability, the formation of meandering thalweg, irregular deposition of sediment, and formation of strong secondary and helical flows (Figure 4-26).

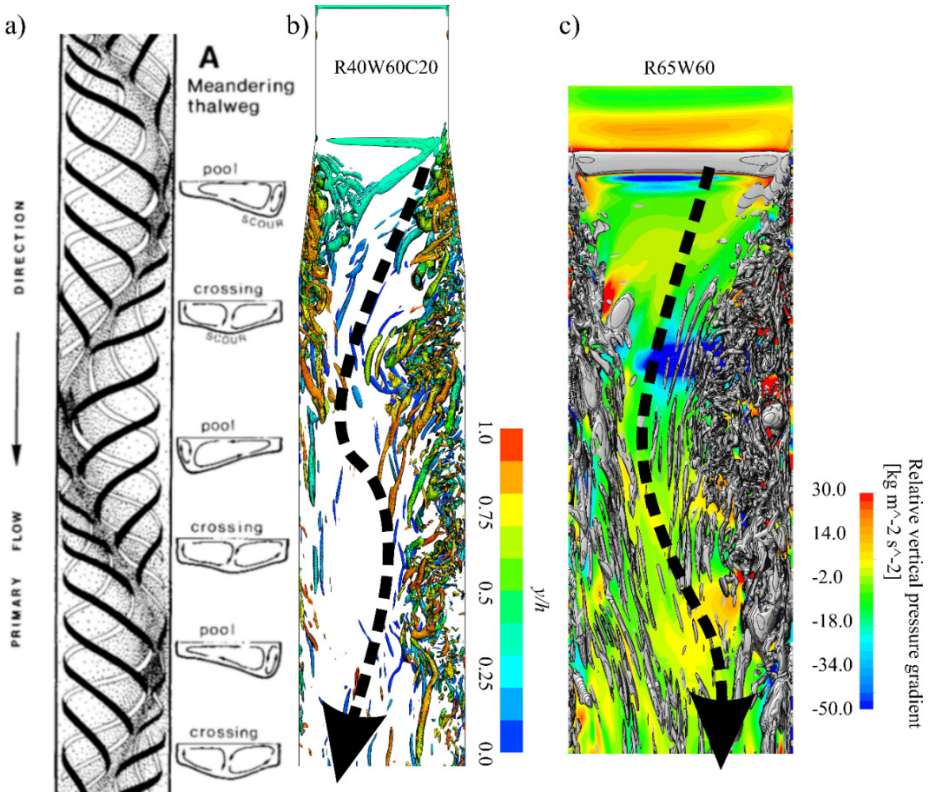

Figure 4-26 a) Schematic illustration of helical flow in a straight channel extracted from (Thompson, 1986)**, b) vortical structures in CDF zone of case R40W60C20 with schematic pattern of meandering flow, c) the contour of relative pressure gradient and vortical structures in CDF zone of case R65W60 from chapter 3, with schematic pattern of meandering flow.**

4.4.3 A suggestion for designing self-maintaining pool-riffle units

Based on the results in the previous section, it can be seen that the constrictions provide a low shear stress zone with low standard deviation in their widening section (Figure 4-18), and high shear stress with high standard deviation at the downstream. One of the challenges of restoration projects is to design stable riffles in combination with pools that are 'self-scouring' in that they maintain their relatively higher depth during floods. Placing the widening part of the constriction on the riffle crest can reduce the mean and fluctuation of shear stress in the riffles (Figure 4-24); therefore, the riffle becomes more stable. The BR at the downstream of the constriction can amplify the RR and exert stronger shear stress pulsation to the pool bed; therefore, excessive sediments cannot deposit in the pools. The locally low shear stress on the riffles can act as a trap point to deposit the incoming sediments on the riffle, however, if they pass the riffle, high shear stress pulsations in the pools can wash them away and keep the pools clean.

4.5 Conclusion

The results of this chapter show that:

1. As has been found in other studies, the hydrodynamics of straight pool-riffle units are dominated by the generation and dissipation of turbulent structures generated in the region of an adverse pressure gradient (also called convectively decelerating flow or CDF).
2. The interplay between turbulent structures generated in near the bed (called 'ramp' or 'bed' rollers herein) with those generated near the side wall (called 'corner eddies' herein) help explain the variety of hydrodynamics found in pool-riffle units.
3. Generation of turbulence near the bed is associated with higher mean velocities near the water surface ('skimming'), while stronger turbulence generated near the side walls of the channel at the water surface will result in the peak velocity dipping below the surface or even plunging to the bed of the channels through the pool. Conceptually the turbulence can be thought of as helping to steer the main flow through the concept of vortex resistance
4. Not all of the strongest vortical structures are generated in CDF; horseshoe vortices are formed upstream of constrictions in the region of a favourable pressure gradient (convectively accelerating flow or CAF).
5. Wider widths provide more space for vortical structures in the CDF zone to form and grow.
6. Wider channels produce more turbulence and bed shear stress pulsation.
7. The plunging flow is not just the result of a hydraulic jump; the vortical structures that are generated in constrictions can guide the flow to plunge as well.

8. In addition to the lateral bifurcation of the distribution in mean flow that can occur where a submerged hydraulic jump is induced downstream of the riffle crest, turbulence feedback mechanisms can induce it in subcritical flows where a constriction is present in the riffle.

Chapter 5: Effect of turbulent structures on sediment entrainment in isolated pool-riffle units

5.1 Introduction

The self-maintenance of pool-riffle units is one of the biggest challenges facing river restoration and rehabilitation processes. There are controversial views on maintenance mechanism of the pool-riffle units. For instance, Keller & Florsheim (1993) suggested that there is a need for scouring in the pools to prevent them from filling. The authors assumed that scouring was caused by high velocity flows near the bed due to a phenomenon that they referred to as 'velocity reversal.' MacWilliams et al. (2006) suggested a competing hypothesis known as flow convergence. They attributed scouring and routing of incoming sediment to upstream constriction-induced jet-like flow in the pools. Sear (1996) suggested that sediment transport does not require shear stress nor velocity reversal, which means that neither contributes to scouring and filling mechanisms in pool-riffle units. Instead, he suggested that the riffle bed becomes tightly packed and interlocked during low flow stages due to high turbulence and in situ vibrations of particles. The interlocked riffle bed remains stable during high flow stages with less

turbulence. This results in the pool material becoming mobile and flushed out due to rapidly rising shear stress.

The conflict in these views is probably due to the lack of comprehensive characterization of the interaction between sediments, hydrodynamic and turbulence in pool-riffle units, especially the influence of turbulence on sediment entrainment. Raudkivi, (1963) showed that sediment motion is related to the turbulence induced pulsation, as well as mean shear stress. Sumer et al., (2003) showed that a 20% increase in the turbulence results in an increase the sediment transport by a factor of six for the same value of the Shields parameter. Diplas et al., (2008) argued that the impulse (product of force and duration) is the most relevant parameter for initiating the dislodgement. Their work showed that to initiate the dislodgement; there is a need for higher forces if the application duration is shorter. The study was based on modelling the electromagnetic lift and drag forces on a metal sphere.

The response of sediment to turbulence and hydrodynamic is dependent on various parameters and conditions which are not easily analyzed. Experimental methods have many limitations in acquiring instantaneous hydrodynamic and turbulence data. Without empirical equations or simplification of the force balance (lift is notoriously difficult to parameterize(Schmeeckle 2014)), there is no efficient numerical method available for simulating sediment transport. Due to these limitations in both numerical and experimental methods in sediment-related studies, a combined method can help researchers better understand this complex phenomenon.

In this chapter, a pool-riffle case with skimming flow is modelled both experimentally and numerically to link the numerical results of hydrodynamic and turbulence to the results of experimental sediment entrainment tests. Skimming flow is of particular interest because it results in low mean shear at the channel bed but high turbulence with generative structures including ramp rollers and corner vortices. Given the relatively large size and strength of these structures, the overall aim was to assess whether they

had any role in moving, shaking, or sorting the bed particles by size. The specific objectives are to investigate:

1. the effect of bed roughness on vortical structures and flow pattern,
2. the sediment entrainment in different parts of pool-riffle units,
3. the entrainment of particles based on their size in different parts of pool-riffle units,

The results of this chapter can help researchers and engineers to understand the mechanisms underlying self-maintenance of pool-riffle units better. It thus contributes towards developing a systematic design methodology for self-maintaining pool riffle-units.

5.2 Methods

5.2.1 Model Geometry

Both experimental and numerical models utilize the same geometry. They both use a simplified straight geometry of pool and riffle units in a 0.6 m wide channel with bed roughness of 4 mm and slope of 0.0015 m/m. As shown in Figure 5-1, the simulated and actual flumes are 18 m long with the following sections:

- 7 m long uniform upstream
- 1.03 m long upsloping ramp
- flat uniform shallow 'riffle' of 0.61 m with height (h_R) of 0.08 m
- 1.03 m long downsloping ramp
- flat uniform deep 'pool' of 4.56 m
- final upsloping ramp and short uniform shallow section used to define the downstream boundary of the model

Hydraulic conditions in the flume were designed based on multiple criteria including the normal depth of flow, specific energy of the flow, measurement considerations, and particle mobility. The average inlet velocity (U_o), the flow depth in the pool (h) and the Froude number in the pool were 0.472 m/s, 0.312 m, and 0.27, respectively. This flow height was chosen to form a normal flow on the rough bed. (Figure 5-1). The Manning roughness for the 4 mm rough bed was set as n= 0.024 based on the suggestions of Phillips & Tadayon, (2006). Using the Shields diagram (Shields 1936) and implementing the flow height and slope of this model, 4 mm particles are very close to the entrainment threshold in a straight and flat channel. Therefore, larger particles should be below the threshold and not move under uniform flow conditions. For reference, X, Y, and Z represent the streamwise, vertical, and spanwise directions, respectively. Because the Froude number at the riffle crest is 0.5, based on one-dimensional energy conservation equation in open channel flows, and the results of chapter 3, the expected flow pattern is 'skimming.'

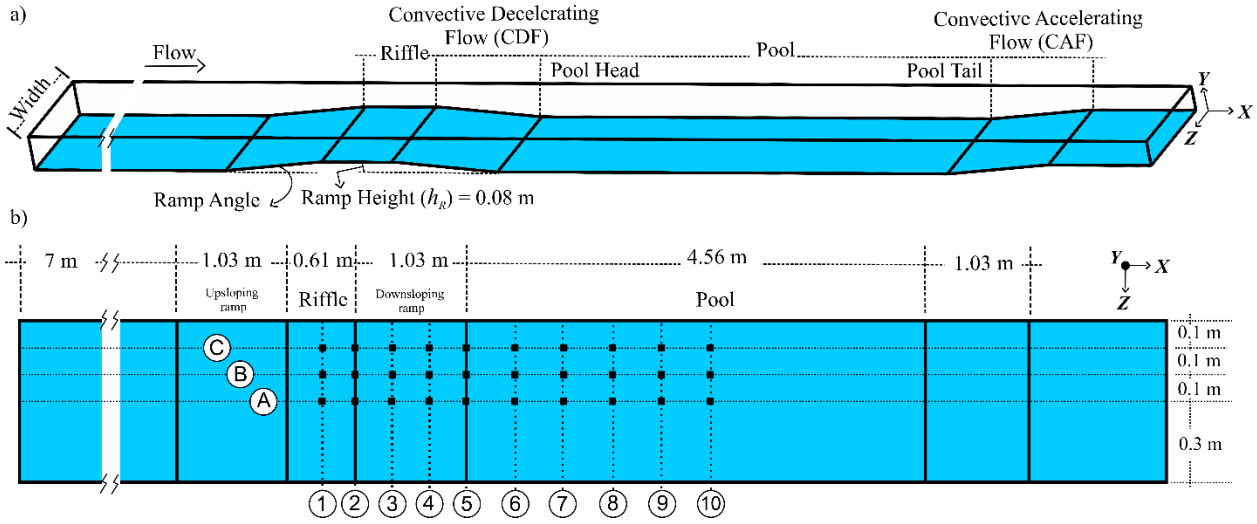

Figure 5-1 The geometry of pool-riffle unit for both numerical and experimental parts, a) perspective view and b) plan view of the channel, and measurement locations.

5.2.2 Experimental Method

The experimental part of this chapter was completed in the flume (Rocky) in the Fluid Mechanics Laboratory at the University of Waterloo. This flume is 18 m long, 1.2 m wide, and 0.6 m deep. Rocky is a tilting flume, with the slope adjustable by hydraulic jacks and held in place at the upstream pivot point and 4 additional supports along the flume. Water is pumped from a sub-floor reservoir to a head tank at a central location in the laboratory, which then gravity feeds the head tank for the flume. A butterfly valve is used to control the discharge in the flume. The large size of the head tank, baffles, and floating styrofoam boards help to dissipate the kinetic energy of flow, break-up the large vortices, and reduce the surface fluctuations in the flow as it exits the head tank. A set of stacked small pipes (40 mm diameter) placed at the outlet of the head tank further reduce fluctuations in the inlet flow. The flume outlet is controlled by a variable height gate. A basin at the end of the flume traps any transported sediments and guides the flow to the returning channel that routes the flow to the sub-floor reservoir.

5.2.2.1 Experiment setup

The riffles were made of ¾ inch PVC sheets and glued to the flume bed. For making the rough bed, series of roughness mats were made by gluing 4 mm gravels to sheets of canvas fabric by extra strength PL glue and painting with water-resistant paint for better fixing of gravels and more adhesion. The whole bed of the flume and riffles were covered with these roughness mats (Figure 5-2a). Due to the limitations in supplying enough discharge for the flume, the flume was narrowed down using false walls made of stainless steel, which are fixed in place using silicone glue and bagged sands for the support. For supporting the false walls and controlling the leakage underneath of the walls, the back of the walls was filled with water with the same height as the main flow (Figure 5-2e). As it can be seen in Figure 5-2f, for reducing the effect of local pocket geometry on sediment entrainment, the gap between gravels were filled

with silicone in a 3cm ×3cm square at the test points that are shown in Figure 5-1. 0.5-mm sand was sprinkled on the wet silicone to keep the surface rough. These spots are referred to test pads herein.

Velocity profiles were measured with a Vectrino II profiler manufactured by Nortek Solutions (Craig et al. 2011). The Vectrino uses a bistatic acoustic Doppler velocimetry method with one central emitter and four receivers (Figure 5-2f) to measure velocity in streamwise, vertical and lateral velocities over a 3 cm profile of velocity in a series of spatial bins as small as 1 mm in height at a frequency of up to 100 Hz. The sampling bins are located from 4 cm to 7 cm below the central emitter, though bins near the limits of this range are known to suffer from low signal to noise ratios (MacVicar et al., 2014). Vectrino II also shows higher velocity near the upper bound and lower velocity near the lower bound of its profiling range. For the current experiment, the Vectrino II was used at frequency of 50 Hz, and bin size of 1mm. The acquired velocity profiles were despiked and organized by the open source MATLAB algorithms called "multi-instrument turbulence toolbox (MITT)" developed by MacVicar et al., (2014).

5.2.2.2 Experiment procedure

A qualitative scoring method based on visual inspection was designed to evaluate particle entrainment. Evaluations started after carefully placing a test particle in the middle of the test pad using a bolt grabber. The bolt grabber is a long thin device with a catch and release mechanism designed for retrieving bolts from hard to reach locations in machinery or beneath grates. In the flume it allowed us to place the particle from a slightly downstream angle to minimize the disturbance to the flow. For each test, particle entrainment was classified after waiting for 120 s, which ensured that the particles experienced approximately 200 cycles of flow sweeps and bursts ($\sim h/U_o$) (Nezu and Rodi 1986). The scores, which are listed in Table 5-1, are varied from one (no movement) to five (shooting). Five different particle sizes (4, 5, 6, 7, and 8 mm), which are colour coded using fluorescent paints (Figure 5-2g), and at least four different particles for each size, and three trials for each particle was done and scored. To make

sure that the particles were placed at the test pads on their most stable side, the particles were resting on a flat surface before grabbing and moving to the test pads. Particles were placed at different flow attack angles for different trials.

Table 5-1 entrainment score

Score	Description
1	No movement or vibration
2	The particle vibrates or moves but stays in the test pad
3	The particle moves out of the test pad but still touches the pad border
4	The particle moves out of the test pad completely
5	The flow shoots the particle rapidly

Four profiles of velocity were measured for 120 s duration at A1, A3, A6, and A8 locations. The velocity profile of the first 10 cm of the flow depth, from free surface, was not measurable because there is a need for at least 6 cm water height above the centre of the probe for preventing the air bubbles to get trapped under the probe, and Vectrino II can only measure the velocity between 4 cm and 7 cm under the centre of the probe.

Figure 5-2 experiment apparatuses, a) The flume bed and riffles are covered with roughness mats, b) the probe holder trolley for Vectrino II, c, and d) placing a particle on the test pad using a bolt grabber, e) looking upstream of the flume that is narrowed by false walls, f) the Vectrino II probe measuring velocity profile, g) different sizes of painted particles

5.2.3 Numerical method

Simulations used the commercially available ANSYS CFX Version 19.1 software. In ANSYS CFX, large eddy simulation (LES) was used to model the flow. The initial condition for the distribution of flow is considered to be uniform. The LES wall-adapting local eddy-viscosity (WALE) (Ducros et al. 1998) method was chosen, which has been widely used in similar geomorphic researches (Keylock et al., 2005, 2012). For more detailed information about the formulations and equations of LES see Rodi et al. (2013). The simulations were 3D, with a structured mesh generated using ICEM Version 19.1, and a total number of elements equal to 45×10^6. A coarser mesh size was selected for the first 5 m of the uniform section at the upstream. Minimum cell size in the near-wall region was 1.5×10^{-3} m, which was selected to satisfy the criteria suggested by Keylock et al. (2012), who recommended at least six points in the inner (near-wall) region to resolve the eddies generated in this region. Previous studies have found the inner zone to be between 10 and 20% of the flow depth (MacVicar & Obach, 2015; MacVicar & Rennie, 2012; Nezu & Rodi, 1986), which means that there are approximately 20 points in the inner zone for the current study. Also following Keylock et al. (2012), cell sizes were 1/50 of the depth, which meets the recommendation to keep the free surface cells to less than 1/20 of the flow depth. The total time for transient modelling was 250 s, which is > 400x the largest eddy scale ($\sim h/U_o$) and easily exceeded the recommendation of 20x the eddy time scale by Keylock et al. (2012). The first 50 s were not considered because of initial condition effects, so only the results between 50 s and 250 s were recorded for analysis. On the machine we used, which has dual CPUs, each with ten cores of 2.3 GHz with CPU model Intel(R) Xeon(R) 2650 V3, and 192 GB RAM, the simulation took approximately 240 hours. Post processing was completed with CFD-POST Version 19.1 and MATLAB R2017b.

5.2.4 Boundary Conditions

The side walls and bed are defined as no-slip smooth walls and rough wall (4 mm roughness), respectively. Using VOF, the inlet was separated into air and water zones at the experimental flow depth (h = 0.312 m). The air zone had zero velocity inlet and the constant pressure of zero. The water zone was defined as having a hydrostatic pressure distribution with uniform water velocity profile (U_o= 0.472 m/s). The outlet was defined as having a constant hydrostatic pressure distribution for water and constant zero pressure for air. In all locations, a distance of at least 5 cm was maintained between the water surface and the top of the simulation space, which allowed the free surface to be shaped based on the hydraulic characteristics alone.

5.2.5 Validation

The time average, organized and despiked profile of velocity magnitude at A1, A3, A6, and A8 locations, which are measured in the flume, was used to validate the flow behaviour, water surface elevation, and the distribution of time average flow velocity magnitude (U) in the numerical simulations. Time-averaged numerical results and experimental data are compared in Figure 5-3. Water surface level is similar in both numerical and experimental results, with a drop at the riffle that is consistent with what is expected from a specific energy analysis for subcritical flow (Figure 5-3a). Four time-averaged velocity magnitude profiles normalized by the inlet velocity (U/U_o) are shown at different points along the channel centerline between the middle of the riffle and middle of the pool (Figure 5-3b). Considering the 10% error bars, numerical results are mostly consistent with experimental data, especially in the middle of the flow depth. The near bed parts of the experimentally acquired velocity profiles are not matched with numerical results. This divergence can have several potential sources:

- The cells near the edges of measuring range in Vectrino II have very low signal to noise ratio, which causes uncertainty in results;

- Vectrino II shows higher velocity near the upper bound and lower velocity near the lower bound of its profiling range. It can be seen in the different parts of the profile shown in Figure 5-3
- the probe holder is very bulky (Figure 5-2b), and for reaching the points near the bed, most of the probe holder, lateral brace for fixing the probe, and clamps should dip into the water, which disturb and reshape the flow.

Still, the numerical results show higher velocity near the surface and lower near the bed, which are similar to the experiments.

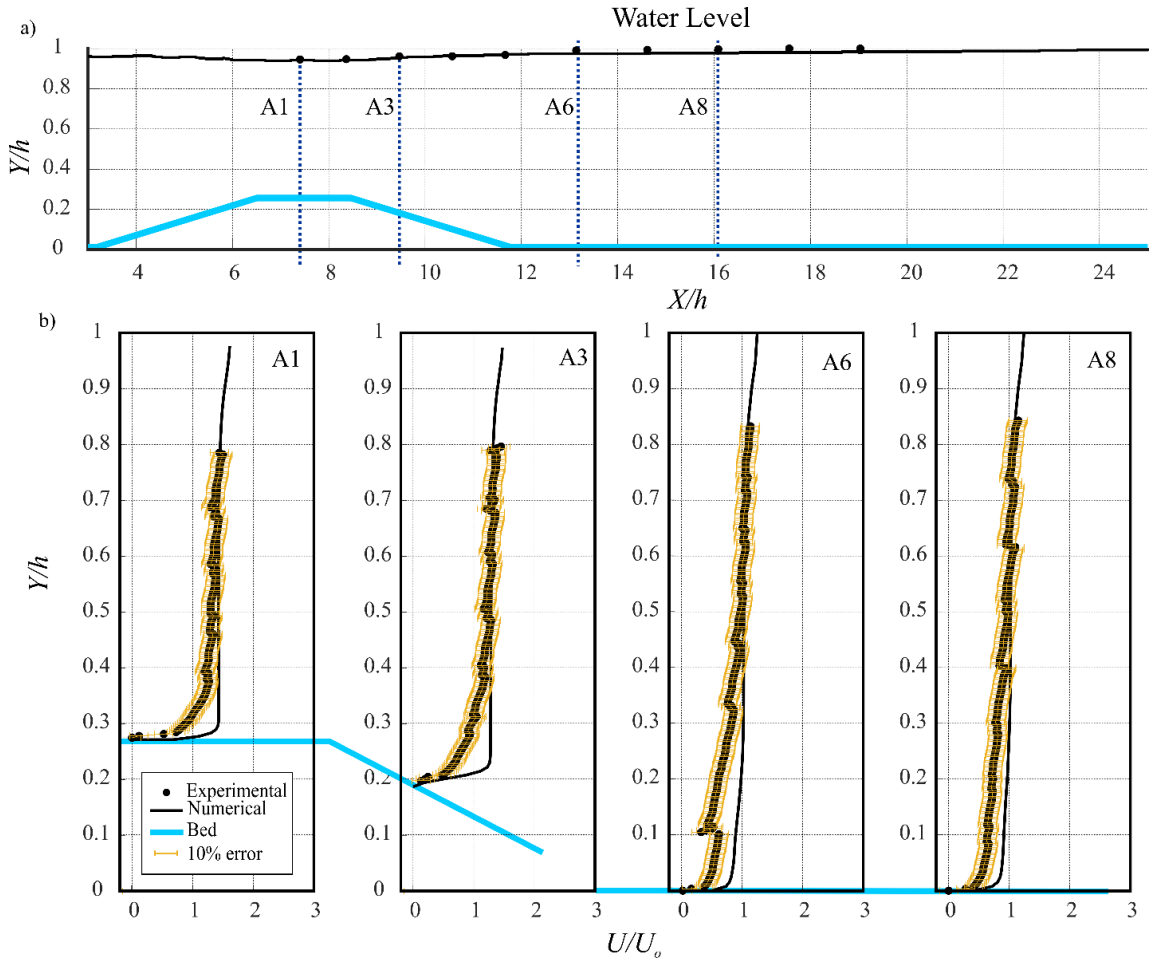

Figure 5-3 Validation of numerical results with experimental data, a) water surface elevation at centerline, b) profiles of time-average velocity magnitude (*U*) for locations shown in a)

5.3 Results

5.3.1 Hydrodynamics and vortical structures

The results of this part are extracted from the numerical model. Convective decelerating flow zone (CDF) at the downsloping ramp is the genesis of most of the strong vortical structures. The iso-surface of Q-criterion in Figure 5-4a shows that ramp rollers (RR), which are generative vortical structures, are shaping in CDF zone and as they travel downstream they get stretched in the form of axial tails (AT), which are dissipative. Small-scale turbulent structures are seen all over the bed even on the riffle crest; these structures are called bed turbulences (BT), herein. These structures are remarkably smaller than RR, corner eddies (CE), and AT. CE are generated in CDF zone are getting stronger till they reach the end of downsloping. They become slightly weaker by entering the pool, but they keep their strength while they are travelling down the pool. The contour of Q-criterion in the near-bed plane (Figure 5-4b), which is 1 cm offset from the bed, show that AT travel very close to the bed and they become weaker as they travel downstream. BT are not seen in that bed offset plane. The contour of instantaneous bed shear stress in Figure 5-4c shows that there is a region with low shear stress on the downsloping ramp before the formation of RR. This figure shows low shear stress at the intersection of the downsloping ramp and the pool bed. The spots with locally excessive shear stress become thinner and more stretched in farther downstream in the pool. The contour of instantaneous pressure deviation from the time average pressure at the bed shows locally high and low pressure deviation regions right downstream and upstream of the location where RR are shaping, respectively (Figure 5-4). Sporadic spots of varying pressure are seen in the pool, and they are becoming weaker by distancing the CDF zone.

Shear stress in CDF zone (downsloping ramp) has a lower mean but higher standard deviation than the ones in the pool. As shown in Figure 5-5a, the mean shear stress decreases in the pool by distancing from the CDF zone. The mean shear stress decreases spanwise by becoming closer to the sidewalls, which is in

contrast with the shear tress pulsation that peaks near to the walls at pool head (Figure 5-5 a and b). The bed at the riffle crest has the highest mean and lowest standard deviation of shear stress in the whole domain. Over the downsloping ramp, a region at the middle of the width, close to the pool-head has the highest mean shear stress in CDF zone. Moreover, a region right at the centre of the downsloping ramp has the highest shear stress standard deviation in CDF zone (Figure 5-5 a and b). Pressure standard deviation peaks at the region that has the highest shear stress standard deviation (Figure 5-5c). The contour of pressure standard deviation shows excessive pressure fluctuations near the wall at the downsloping ramp, close to the riffle crest. In addition, the pressure pulsation on the bed increases along the pool downstream. The contour of time average and standard deviation of velocity magnitude show higher velocity near the surface and higher pulsation near the bed (Figure 5-5 d and e).

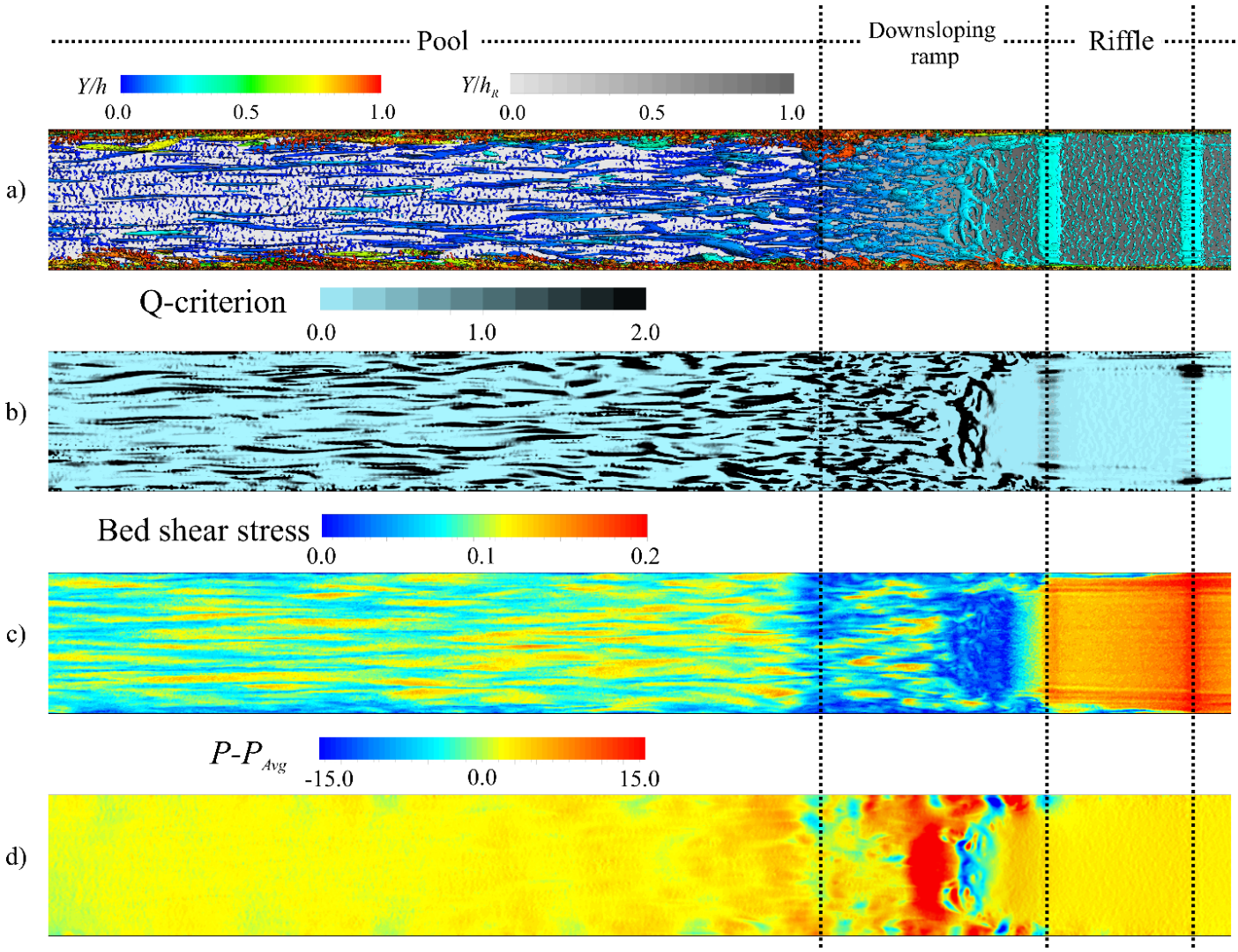

Figure 5-4 Instantaneous flow structure and hydrodynamics for the numerical case, showing: a) Iso-surface of Q=2 s^-2 with shade of normalized *Y* on the contour of bed elevation, b) contour of Q on a plane with 1 cm vertically offset from the bed, c) contour of bed shear stress magnitude, and d) contour of instantaneous pressure deviation from the time average pressure at the bed.

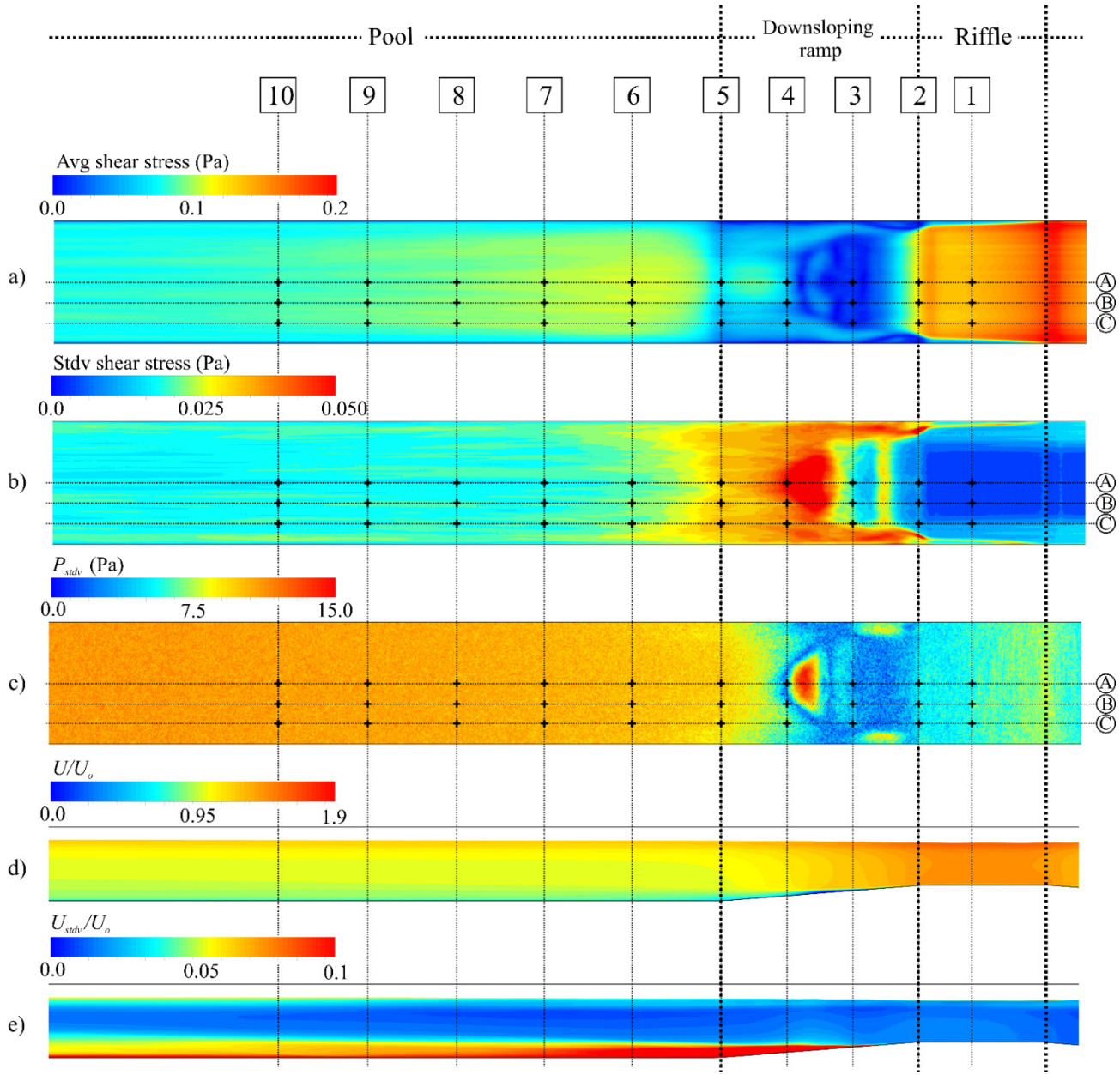

Figure 5-5 Results from numerical simulation showing, a) contour of time average bed shear stress, b) contour of standard deviation of bed shear stress, c) contour of pressure standard deviation at bed, d) contour of time average velocity magnitude at the plane along the centerline, and, e) contour of time velocity magnitude standard deviation at the plane along the centerline.

5.3.2 Sediment entrainment

The shear stress diagrams in this part are extracted from the numerical model. The entrainment scores are acquired by experiments in the flume. The entrainment score (ES) in the riffle is always higher than other locations for all particle sizes. Also, ES is lower at the middle of the pool for larger particles. The diagram of shear stress in line A (Figure 5-6) shows that the riffle crest has the highest mean bed shear stress with the lowest fluctuation at the downstream edge. On the downsloping ramp shear stress patterns are complex as the mean, and standard deviation of shear stress drops at A3, the mean stays relatively constant while the standard deviation increases at location A4 and then the mean increases while the standard deviation increases at A5, which is the bottom of the ramp. In the flat section of the pool, the standard deviation of shear stress decreases gradually downstream while the mean shear stress increases at A6 (local maximum in mean shear stress) then decreases gradually. As shown in Figure 5-6, the entrainment of 4 mm particles has the highest score at riffle (ES=5), slightly decreases at the head of the ramp (location A3), then maximizes at A4 (ES=5), drop to its lowest value (ES= 4.3) at the entrance of the pool (A5), then gradually increases in the pool to reach (ES=4.7) at A6. By moving downstream, after A6, the mean ES does not change significantly.

Particles 5 - 6 mm in diameter have similar entrainment patterns to the 4 mm particles. The diagram of ES for 5-, 6-, and 7-mm particles show the highest value at the riffle, the lowest value at the pool head (location A5), local maximum at A6 or A7, and then declining in the downstream. Between these three particle sizes, 7-mm particles have the lowest ES, and 5-mm particles have the highest ES at the middle of the pool (A10). 8-mm particles have the lowest ES among all particle sizes in the downsloping ramp and the pool head (Figure 5-6).

The mean shear stress along the line B is lower than the one in line A in the pool. However, line B has more excessive shear stress fluctuation than the one in line A in the pool (Figure 5-7). In line B, the point

with maximum mean shear stress in the pool is located at the upstream of location B6. ES for 4-, 5-, 6-,7-mm particles are low at the pool head (B5). 5- and 6-mm particles have a general declining ES trend in the pool. ES in 7-mm particles have a local peak at B7 and then declining. 7 mm particles have lower ES in the downsloping ramp at line B than the one in 6-, 5-, and 4-mm particles (Figure 5-7).

Over the downsloping ramp, line C has slightly lower mean and standard deviation of shear stress as line B (Figure 5-8). However, they both have similar shear stress standard deviations in the pool. 8-mm particles have strictly decreasing ES trend from the riffle crest to the middle of the pool. Location A4, B4, and C4 have lower mean but higher standard deviation of shear stress than locations A6, B6, and C6 (Figure 5-6Figure 5-7Figure 5-8). In addition, these two locations have approximately similar higher bound of shear stress. ES for these two locations are approximately similar for 4- and 5-mm particles. 8-mm particles in all three lines and, 7- and 6-mm particles in line B and C have lower ES in location A6 than in location A4.

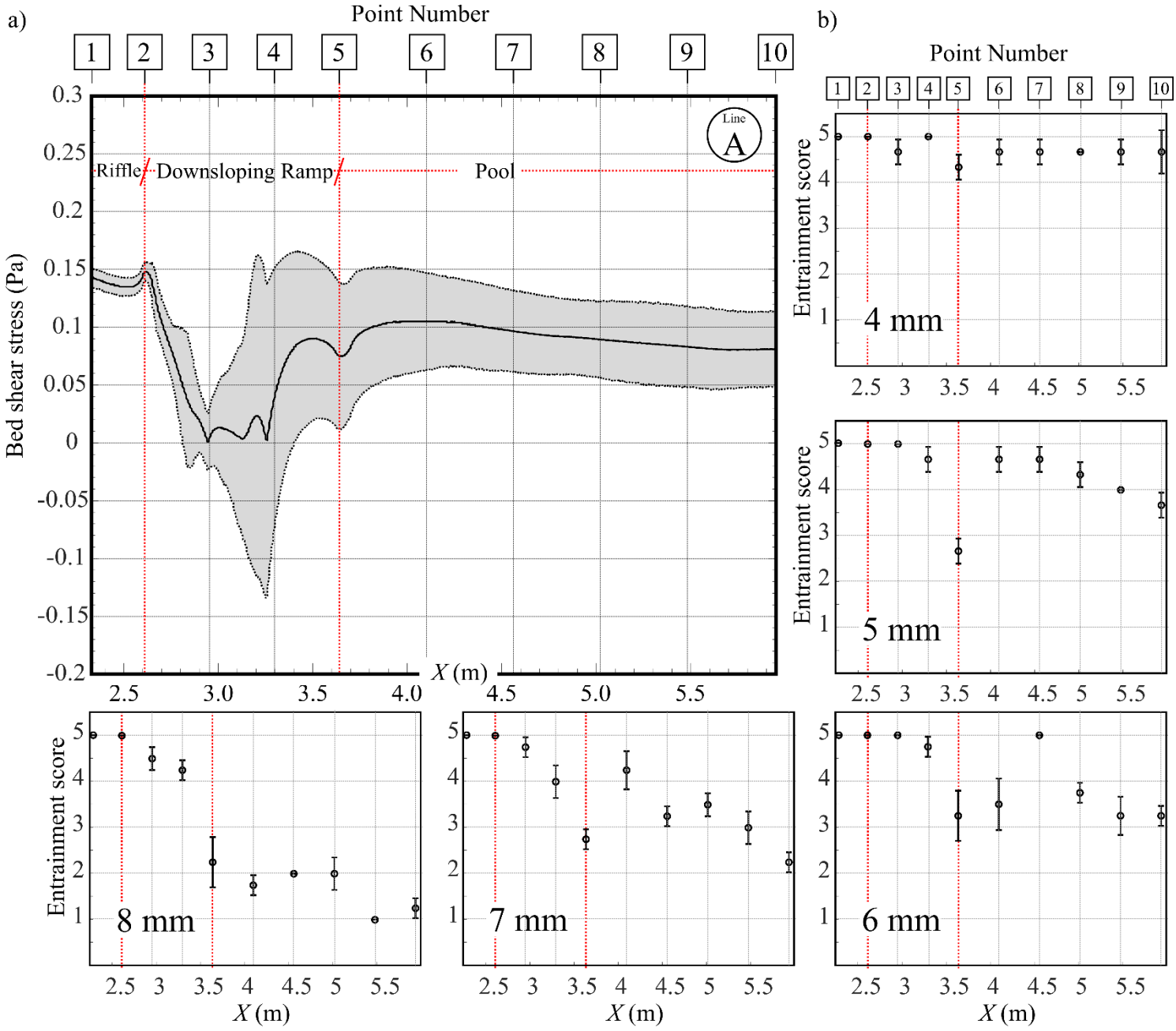

Figure 5-6 a) Time-average (black line) and 95% confidence range (dashed line) of bed shear stress at line A extracted from numerical model, and b) entrainment scores with error bar for 4-, 5-, 6-, 7-, and 8-mm particles.

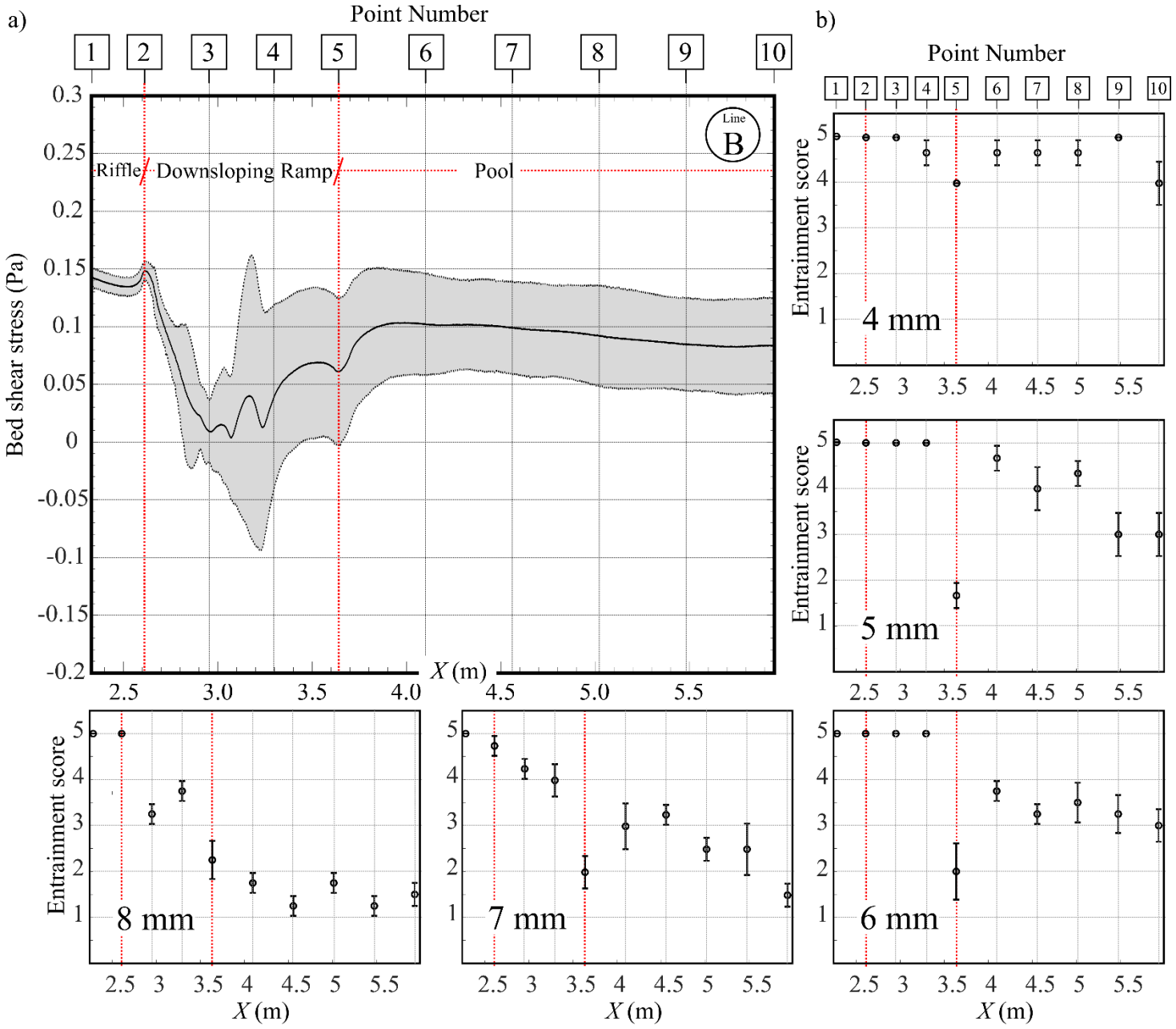

Figure 5-7 a) Time-average (black line) and 95% confidence range (dashed line) of bed shear stress at line B extracted from numerical model, and b) entrainment scores with error bar for 4-, 5-, 6-, 7-, and 8-mm particles.

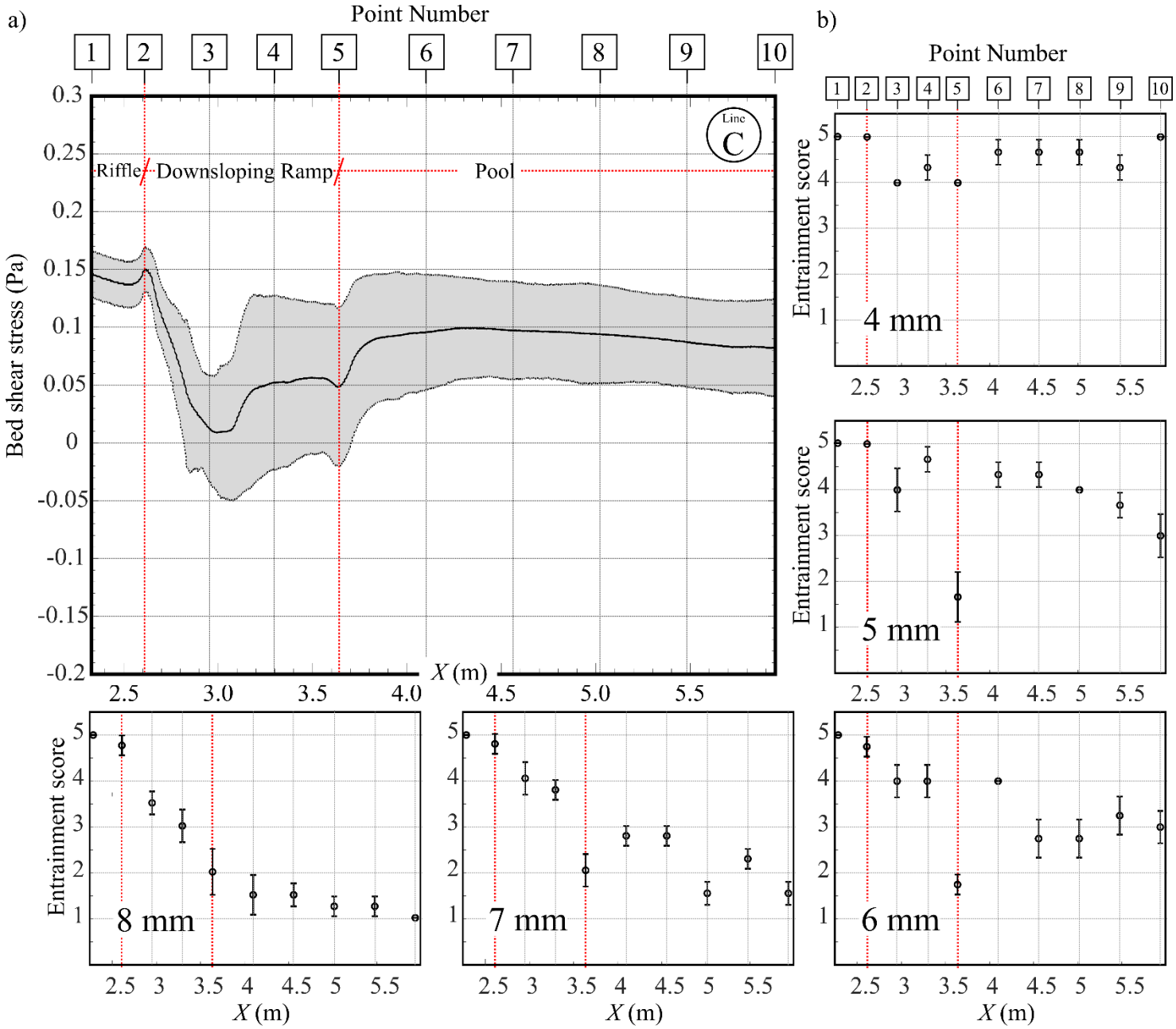

Figure 5-8 a) Time-average (black line) and 95% confidence range (dashed line) of bed shear stress at line C extracted from numerical model, and b) entrainment scores with error bars for 4-, 5-, 6-, 7-, and 8-mm particles.

5.4 Discussion

Based on Shields thresholding for moving of sediments, in this case, 4-mm particles are very close to the entrainment threshold, and they should barely move in the pool, and larger particles should not move at all. The results herein showed that this thresholding does not anticipate the mobility of sediments precisely in such cases with high pulsation and variable shear stress distribution. This finding is thus in general agreement with recent studies on the relevance of turbulent structures for sediment transport (Celik et al. 2013; Diplas et al. 2008; Lamb et al. 2015; Sumer et al. 2003). The particle entrainment generally has a positive relation with shear stress, which means that in the regions with both higher mean and standard deviation of shear stress, entrainment is higher. However, pulsation can amplify the effect of mean shear stress. The entrance of the pool near the end of downsloping ramp mostly has the lowest sediment entrainment score which can act as a trap point to deposit the particles in that region and prevent them from entering the pool. The downsloping ramp, generally, have lower mean shear stress and higher pulsation than upstream part of the pool. By comparing the results of A4, B4, and C4 locations, which are the points right upstream of the pool entrance on downsloping ramp, with A6, B6, and C6 locations, which are the points right downstream of the pool entrance in the pool, it can be said that smaller particles (4-, 5-, and 6-mm particles) in the regions with lower mean shear stress can have similar entrainment if the pulsation be higher. Pulsation, which is referred to shear standard deviation herein, has less effect on the entrainment of larger particles.

The results can be used to develop a conceptual model of sediment sorting by size in a riffle-pool unit due to differential entrainment and deposition. All particles are assumed to move intermittent saltation, rest, and entrainment cycles rather than suspension. We consider the effects of pocket geometry, covering effects, and interlocking as an increase in the threshold of entrainment score. By considering these effects, we assume that ES< 3 means deposition with no movement afterwards. Based on our observations, the

bed median size articles (4 mm), travel down the ramp, enter the pool, travel down the pool, pass the middle of the pool, and may deposit at the far end downstream of the pool. In contrast, a fraction of the 5-mm particles will pass the ramp but are likely to get trapped at the end of the ramp. If they pass that trap point, they pass the pool head and deposit at the middle of the pool near the wall and further downstream at the centerline as well. In a downstream direction, they will deposit before 4-mm particles. 6- and 7-mm particles have a similar scenario as 5-mm particles, but the size gradation means that the larger particles will deposit before the smaller sized particles deposit later. They both deposit much earlier than 5-mm particles near the sidewalls and centerline. In contrast with the smaller particles, the 8-mm particles will leave the riffle crest but start to deposit on the ramp, particularly near the channel walls, and there is a low possibility for them to enter the pool. In this scenario, the larger particles form a coarse deposit on the downstream face of the riffle and cannot reach the pool or be transported through the channel.

By looking at this assumptive scenario of incoming sediment, the downstream fining process, which is reported previously by many researchers (Hoey & Ferguson, 1997; Milan, 2013; Seal & Paola, 1995; Sear, 1996; Thompson, 2013), can be seen. The generated turbulence at CDF, travelling near the bed, plays a crucial role in the downstream fining process. This process is due to the gradually decreasing of bed mean and standard deviation shear stress because of gradually dissipation of vortical structures that are formed in CDF. In this scenario, the riffle and downsloping part of the riffle become armoured by large particles, which can trap more smaller particles at the riffle and prevent them from entering the pool. Armoured riffles are reported in the field and experimental studies previously (Madej et al., 2009; Sear, 1996; Thompson, 2006; Yager & Schott, 2013). The pool head stays clean, because the small particles that are entered the pool are washed away from the upstream part of the pool, and they respectively deposit by their size in the downstream. This sediment routing mechanism herein describes the self-maintaining mechanism of pool-riffle units that is induced by turbulence.

5.5 Conclusion

Based on the linking of numerical and experimental results, we can conclude that:

1. Turbulence plays a key role in sediment routing.
2. Pulsation in shear stress amplify the effect of mean shear stress in moving the particles.
3. The zone with local low shear stress at the end of the downsloping ramp, trap the particles before entering the pool.
4. Large particles are trapped in the riffle, and there is a low chance for them to enter the pool.
5. The turbulence that is generated in the region with convective declarative flow keep the pool head clean from the deposition of incoming particles that are passed the riffle.
6. Particles that pass the riffle deposit respectively in the pool by their size, in a way that larger particles deposit earlier than smaller ones.
7. The downstream fining is due to the gradually dissipation and decay of vortical structures that are generated in the CDF zone.

Chapter 6: Conclusions and future work

6.1 Summary of Thesis Contributions

A summary of the contributions of this thesis and their possible impacts are presented in this chapter. The chapter also lists the important directions of future work. The central problem addressed in this thesis is the characterization of the effects of macromorphological variations in natural and restored streams on flow pattern and turbulent structures. The focus of the thesis is on pools and riffles, i.e., deeper and shallower part of the bed. More specifically, the work presented in this thesis thoroughly studies the effects of

(a) riffle height,

(b) riffle width,

(c) width constriction, and

(d) response of sediment to turbulence

on hydrodynamics and sediment entrainment in pools and riffles.

An approach that combines hydraulic and geomorphological techniques utilizing both experimental and computational fluid dynamic methodologies was employed in this thesis to provide a more comprehensive and accurate analysis of sediment routing and flow patterns in pools and riffles. The direct implication of this analysis is to enable practical design and study practices that can be incorporated in

pool-riffle maintenance and shaping. Eventually, this will lead to better rehabilitation and maintenance strategies for natural or restored streams.

The reliance on a more holistic approach in this thesis combining both numerical simulations and experimentation helped in settling a long-standing critical debate on the reason behind the formation and maintenance mechanisms for pool-riffle units. The results in this thesis showed that scouring can be attributed to either higher near bed velocity (plunging flow) or turbulence near the pool bed (skimming flow). The consolidation of both perspectives by providing the hydrodynamic conditions where both or either can be observed in the field should help to resolve some longstanding debates in the field.

6.1.1 Contribution 1: Proposing and validating the vortex-resistance hypothesis

The thesis proposed and evaluated the 'vortex-resistance hypotheses'. The main claim is that vortices exert resistance to the flow by increasing the mixing effects and changing the pressure domain. The significance of this hypothesis is that it links the role that turbulence structures play in formation of flow patterns. Moreover, it provides a unified framework for explaining the effects of different geometrical parameters on the flow pattern.

6.1.2 Contribution 2: Study of the influence of the riffle height on the characteristics of the vortical structures

The effects that the riffle height have on flow turbulent structures were carefully investigated in this thesis. This was further linked to the flow pattern relying on the vortex-resistance hypothesis, which provided a plausible interpretation for forming plunging, rifting, and skimming flow patterns in pools. Through numerical simulations, the following findings were identified:

- Surface turbulence, ramp rollers, corner eddies, and axial tails are shaped in the convective decelerating flow zone;

- In skimming flow, ramp and corner eddies are dominant near the bed and responsible for high bed shear stress;
- Riffles with Froude number close to one can result into surface undulation hydraulic jump, which steers the flow to plunge into the pool near the bed;
- If ramp rollers are strong enough, they push the flow to skim the free-surface and increase near bed turbulence;
- Strong plunging flow can cause axial bifurcation, where one side of the channel experiences higher velocities and shear stresses while the opposite side is dominated by flow recirculations.

6.1.3 Contribution 3: Study of the influence of the channel width variation on the characteristics of the vortical structures

Relying on advanced numerical approaches that model transient and turbulent flow, the influence of variability in channel width on the characteristics of vortical structures has been investigated in detail. Among the most relevant findings, the analysis revealed the following:

- Strong vortical structures can be generated in areas other than CDF. For instance, the horseshoe vortices are formed upstream of constrictions in the region of a favourable pressure gradient, such as convectively accelerating flow;
- Wider channels produce more turbulence and bed shear stress pulsation;
- Plunging flow cannot be only attributed to a hydraulic jump. The thesis also identified that vortical structures generated in constrictions can lead the flow to plunge as well; and
- Turbulence feedback mechanisms can induce lateral bifurcation in subcritical flows where a constriction is present in the riffle.

6.1.4 Contribution 4: Study of the influence of vorticial structures on sediment entrainment

Pool-riffle case with skimming flow is modelled both experimentally and numerically to link the numerical results of hydrodynamic and turbulence to the results of experimental sediment entrainment tests. Skimming flow is of interest because it results in low mean shear at the channel bed but high turbulence with generative structures including ramp rollers and corner vortices. Given the relatively large size and strength of these structures, the overall aim was to assess whether they had any role in moving, shaking, or sorting the bed particles by size.

We can conclude that:

1. Pulsation in shear stress amplify the effect of mean shear stress in moving the particles;
2. The zone with local low shear stress at the end of the downsloping ramp, trap the particles before entering the pool;
3. Large particles are trapped in the riffle, and there is a low chance for them to enter the pool;
4. The turbulence that is generated in the region with convective declarative flow keep the pool head clean from deposition of incoming particles that are passed the riffle;
5. Particles that pass the riffle, deposit respectively in the pool by their size, in a way that larger particles deposit earlier than smaller ones; and
6. The downstream fining is due to the gradually dissipation and decay of vortical structures that are generated in the CDF zone.

The results of this chapter can help researchers and engineers to understand the mechanisms underlying self-maintenance of pool-riffle units better. It thus contributes towards developing a systematic design methodology for self-maintaining pool riffle-units.

6.2 Future research

1) The geometry, which is used in this study, is a simplified geometry of pool rifle units. Including more various geometry factors can make the results more applicable in designing and developing projects. There are various controversial views that link the formation and maintenance of pool-riffle units to development of meandering and bends; therefore, considering the effect of channel bend and interaction of curvature-induced vortices with pool-riffle vortical structures can more clarify the evolution mechanism of streams.

2) Hyporheic flow, defined as the intragranular flow in the shallow subsurface below a riverbed, is another interesting topics with direct relevance for the function and habitat utility of pool-riffles. The effect of different types of flow that are found in this study (plunging, rifting, and skimming) should be investigated for their interactions with hyporheic flows in riffles and beneath the pools.

3) Modelling sediment transport with more realistic conditions in pool-riffle units (e.g. fully mobile bed and various conditions of sediment feeding) can lead to a more complete understanding of the formation and maintenance mechanisms of pool-riffle units.

References

De Almeida, Gustavo Adolfo Mazza and José F. Rodríguez. (2012). "Spontaneous Formation and Degradation of Pool-Riffle Morphology and Sediment Sorting Using a Simple Fractional Transport Model." Geophys. Res. Lett. 39(6):L06407.

De Almeida, Gustavo Adolfo Mazza, José F. Rodríguez. (2011). "Understanding Pool-Riffle Dynamics through Continuous Morphological Simulations." Water Resour. Res. 47(1):1–15.

Ancey, C., a. C. Davison, T. Böhm, M. Jodeau, and P. Frey. (2008). "Entrainment and Motion of Coarse Particles in a Shallow Water Stream down a Steep Slope." J. Fluid Mech. 595:83–114.

Beheshti, Ali-Asghar A. A., Behzad Ataie-Ashtiani, and Hamed Dashtpeyma. (2017). "Numerical Simulations of Turbulent Flow around Side-by-Side Circular Piles with Different Spacing Ratios." Int. J. River Basin Manag. 15(2):227–38.

Bernhardt, E. S., M. A. Palmer, J. D. Allan, G. Alexander, K. Barnas, S. Brooks, J. Carr, S. Clayton, C. Dahm, D. Galat, S. Gloss, P. Goodwin, D. Hart, B. Hassett, R. Jenkinson, S. Katz, G. M. Kondolf, P. S. Lake, R. Lave, J. L. Meyer, T. K. O. Donnell, L. Pagano, B. Powell, and E. Sudduth. (2005). "Synthesizing U.S. River Restoration Efforts." Science 308(5722):636–37.

Bernhardt, Emily S. and Margaret A. Palmer. (2007). "Restoring Streams in an Urbanizing World." Freshw. Biol. 52(4):738–51.

Boussinesq, J. (1877). "Théorie de l'écoulement Tourbillant." Mem. Présentés Par Divers Savants Acad. Sci. Inst. Fr 23(46–50):5–6.

Bradbrook, K. F., S. N. Lane, K. S. Richards, P. M. Biron, and A. G. Roy. (2000). "Large Eddy Simulation of Periodic Flow Characteristics at River Channel Confluences." J. Hydraul. Res. 38(3):207–15.

Buffington, John M. (1999). "The Legend of A. F. Shields." J. Hydraul. Eng. 125(4):376–87.

Buffington, John M., Thomas E. Lisle, Richard D. Woodsmith, and Sue Hilton. (2002). "Controls on the Size and Occurrence of Pools in Coarse-Grained Forest Rivers." River Res. Appl. 18(6):507–31.

Buffington, John M. and David R. Montgomery. (1997). "A Systematic Analysis of Eight Decades of Incipient Motion Studies, with Special Reference to Gravel-Bedded Rivers." Water Resour. Res. 33(8):1993–2029.

Caamaño, D., P. Goodwin, and J. M. Buffington. (2012). "Flow Structure through Pool-Riffle Sequences and a Conceptual Model for Their Sustainability in Gravel-Bed Rivers." River Res. Appl. 28(3):377–89.

Caamaño, Diego, Peter Goodwin, John M. Buffington, Jim C. Liou, and Steve Daley-Laursen.

(2009). “Unifying Criterion for the Velocity Reversal Hypothesis in Gravel-Bed Rivers.” J. Hydraul. Eng. 135(1):66–70.

Carling, P. A. (1991). “An Appraisal of the Velocity-reversal Hypothesis for Stable Pool-riffle Sequences in the River Severn, England.” Earth Surf. Process. Landforms 16(1):19–31.

Celik, Ahmet O., P. Diplas, and C. L. Dancey. (2014). “Instantaneous Pressure Measurements on a Spherical Grain under Threshold Flow Conditions.” J. Fluid Mech 741:60–97.

Celik, Ahmet Ozan, Panayiotis Diplas, and Clint L. Dancey. (2013). “Instantaneous Turbulent Forces and Impulse on a Rough Bed: Implications for Initiation of Bed Material Movement.” Water Resour. Res. 49(4):2213–27.

Clifford, N. J. J. (1993). “Differential Bed Sedimentology and the Maintenance of Riffle-Pool Sequences.” Catena 20(5):447–68.

Clifford, N. J. and K. Richards. (1992). “The Reversal Hypothesis and the Maintenance of Riffle-Pool Sequences: A Review and Field Appraisal.” Lowl. Floodplain Rivers 43–70.

Clifford, Nicholas J. NJ. (1993). “Formation of Riffle—pool Sequences: Field Evidence for an Autogenetic Process.” Sediment. Geol. 85(1–4):39–51.

Coleman, S. E. and V. I. Nikora. (2008). “A Unifying Framework for Particle Entrainment.” Water Resour. Res. 44(4):1–10.

Craig, Robert G. A., Chris Loadman, Bernard Clement, Peter J. Rusello, and Eric Siegel. (2011). “Characterization and Testing of a New Bistatic Profiling Acoustic Doppler Velocimeter: The Vectrino-II.” Pp. 246–52 in 2011 IEEE/OES/CWTM 10th Working Conference on Current, Waves and Turbulence Measurement, CWTM 2011. IEEE.

Dietrich, William E., J. Dungan Smith, and Thomas Dunne. (1979). “Flow and Sediment Transport in a Sand Bedded Meander.” J. Geol. 87(3):305–15.

Diplas, Panayiotis, Clint L. Dancey, Ahmet O. Celik, Manousos Valyrakis, Krista Greer, and Tanju Akar. (2008). “The Role of Impulse on the Initiation of Particle Movement under Turbulent Flow Conditions.” Science 322(5902):717–20.

Dolling, R. K. (1968). “Occurrence of Pools and Riffles: An Element in the Quasi-Equilibrium State of River Channels.” Ontario Geogr. 2:03–Nov.

Dubief, Yves and Franck Delcayre. (2000). “On Coherent-Vortex Identification in Turbulence.” J. Turbul. 1(January):1–22.

Ducros, F., F. Nicoud, and T. Poinsot. (1998). “Wall-Adapting Local Eddy-Viscosity Models for Simulations in Complex Geometries.” Conf. Numer. Methods Fluid Dyn. 1–7.

Einstein, H. A. and H. W. Shen. (1964). “A Study on Meandering in Straight Alluvial Channels.” J. Geophys. Res. 69(24):5239–47.

Ettema, Robert, George Constantinescu, and Bruce W. Melville. (2017). “Flow-Field Complexity and Design Estimation of Pier-Scour Depth: Sixty Years since Laursen and Toch.” J. Hydraul. Eng. 143(9):03117006.

Gorman, O. T. and James R. Karr. (1978). “Habitat Structure and Stream Fish Communities.” Ecology 59(3):507–15.

Guillén Ludeña, S., Z. Cheng, G. Constantinescu, and M. J. Franca. (2017). “Hydrodynamics of Mountain-River Confluences and Its Relationship to Sediment Transport.” J. Geophys. Res. Earth Surf. 122(4):901–24.

Halwas, Karen L. and Michael Church. (2002). “Channel Units in Small, High Gradient Streams on Vancouver Island, British Columbia.” Geomorphology 43(3–4):243–56.

Hardy, R. J., S. N. Lane, M. R. Lawless, J. L. Best, L. Elliott, and D. B. Ingham. (2005). “Development and Testing of a Numerical Code for Treatment of Complex River Channel Topography in Three-Dimensional CFD Models with Structured Grids.” J. Hydraul. Res. 43(5):468–80.

Heritage, G. L. and D. J. Milan. (2004). “A Conceptual Model of the Role of Excess Energy in the Maintenance of a Riffle-Pool Sequence.” Catena 58(3):235–57.

Hirt, C. .. and B. .. Nichols. (1981). “Volume of Fluid (VOF) Method for the Dynamics of Free Boundaries.” J. Comput. Phys. 39(1):201–25.

Hoey, Trevor B. and Robert I. Ferguson. (1997). “Controls of Strength and Rate of Downstream Fining above a River Base Level.” Water Resour. Res. 33(11):2601–8.

Hooke, J. M. M. (2013). River Meandering. Elsevier Ltd.

Hunt, Brendan, Jeremy G. Venditti, and Eva Kwoll. (2018). “Experiments on the Morphological Controls of Velocity Inversions in Bedrock Canyons.” Earth Surf. Process. Landforms 43(3):654–68.

Jackson, J. R., G. B. Pasternack, and J. M. Wheaton. (2015). “Virtual Manipulation of Topography to Test Potential Pool–riffle Maintenance Mechanisms.” Geomorphology 228:617–27.

Keller, E. A. (1972). “Development of Alluvial Stream Channels: A Five-Stage Model.” Bull. Geol. Soc. Am. 83(5):1531–36.

Keller, E. A. (1975). “Channelization: A Search for a Better Way.” Geology 3(5):246–48.

Keller, E. A. EA and WN N. Melhorn. (1978). “Rhythmic Spacing and Origin of Pools and Riffles.” Geol. Soc. Am. … 89(80):723–30.

Keller, E. A. and J. L. Florsheim. (1993). “Velocity-Reversal Hypothesis: A Model Approach.” Earth Surf. Process. Landforms 18(8):733–40.

Keller, Edward A. EA A. (1971). “Areal Sorting of Bed-Load Material: The Hypothesis of Velocity Reversal.” Geol. Soc. Am. Bull. 82(3):753–56.

Keylock, C. J., R. J. Hardy, D. R. Parsons, R. I. Ferguson, S. N. Lane, and K. S. Richards. (2005). “The Theoretical Foundations and Potential for Large-Eddy Simulation (LES) in Fluvial Geomorphic and Sedimentological Research.” Earth-Science Rev. 71(3–4):271–304.

Keylock, C. J., G. Constantinescu, and R. J. Hardy. (2012). “The Application of Computational Fluid Dynamics to Natural River Channels: Eddy Resolving versus Mean Flow Approaches.” Geomorphology 179:1–20.

Keylock, Christopher J., Kyoungsik S. Chang, and George S. Constantinescu. (2016). “Large Eddy Simulation of the Velocity-Intermittency Structure for Flow over a Field of Symmetric Dunes.” J. Fluid Mech. 805:656–85.

Kieffer, S. W. (1985). “The 1983 Hydraulic Jump in Crystal Rapid: Implications for River-Running and Geomorphic Evolution in the Grand Canyon.” J. Geol. 93(4):385–406.

Kieffer, Susan Werner. (1989). “Geologic Nozzles.” Rev. Geophys. 27(1):3–38.

Kline, S. J., W. C. Reynolds, F. A. Schraub, and P. W. Runstadler. (1967). “The Structure of Turbulent Boundary Layers.” J. Fluid Mech. 30(04):741.

Koken, Mete, George Constantinescu, and Koen Blanckaert. (2013). “Hydrodynamic Processes, Sediment Erosion Mechanisms, and Reynolds-Number-Induced Scale Effects in an Open Channel Bend of Strong Curvature with Flat Bathymetry.” J. Geophys. Res. Earth Surf. 118(4):2308–24.

Krogstad, Per-Åge and Per Egil Skåre. (1995). “Influence of a Strong Adverse Pressure Gradient on the Turbulent Structure in a Boundary Layer.” Phys. Fluids 7(8):2014–24.

Kumar, Ashish, Umesh C. Kothyari, and Kittur G. Ranga Raju. (2012). “Flow Structure and Scour around Circular Compound Bridge Piers - A Review.” J. Hydro-Environment Res. 6(4):251–65.

Lamb, Michael P., Noah J. Finnegan, Joel S. Scheingross, and Leonard S. Sklar. (2015). “New Insights into the Mechanics of Fluvial Bedrock Erosion through Flume Experiments and Theory.” Geomorphology 244:33–55.

Launder, B. E. and D. B. Spalding. (1974). “The Numerical Computation of Turbulent Flows.” Comput. Methods Appl. Mech. Eng. 3(2):269–89.

Leopold, L. B., M. G. Wolman, and G. M. Wolman. (1960). “Rivee Meanders.” Bull. Geol. Soc. Am. 71(3):769–94.

Lisle, TE and S. Hilton. (1992). “The Volume of Fine Sediment in Pools: An Index of the Supply of Mobile Sediment in Stram Channels.” Water Resour. Bull. 28(2):371–83.

Lisle, Thomas. (1979a). “A Sorting Mechanism for a Riffle-Pool Sequence.” Bull. Geol. Soc. Am. 90(7 PART II):1142–57.

Lisle, Thomas. (1979b). “Geological Society of America Bulletin A Sorting Mechanism for a Riffle-Pool Sequence A Sorting Mechanism for a Riffle-Pool Sequence.” Geol. Soc. Am. Bull. 90(7):616.

Lisle, Thomas E. (1982). “Effects of Aggredation and Degredation on Riffle-Pool Morphology in Natural Gravel Channels, Northwest California.” Water Resour. Res. 18(6):1643–51.

Lisle, Thomas E., Hiroshi Ikeda, and Fujiko Iseya. (1991). “Formation of Stationary Alternate

Bars in a Steep Channel with Mixed-size Sediment: A Flume Experiment." Earth Surf. Process. Landforms 16(5):463–69.

Lohse, Detlef and Siegfried Grossmann. (2002). Theories of Turbulence. edited by M. Oberlack and F. H. Busse. Vienna: Springer Vienna.

Lotsari, E., M. Vaaja, C. Flener, H. Kaartinen, A. Kukko, E. Kasvi, H. Hyypp??, J. Hyypp??, and P. Alho. (2014). "Annual Bank and Point Bar Morphodynamics of a Meandering River Determined by High-Accuracy Multitemporal Laser Scanning and Flow Data." Water Resour. Res. 50(7):5532–59.

MacVicar, B. J. and J. L. Best. (2013). "A Flume Experiment on the Effect of Channel Width on the Perturbation and Recovery of Flow in Straight Pools and Riffles with Smooth Boundaries." J. Geophys. Res. Earth Surf. 118(3):1850–63.

MacVicar, B. J. and L. Obach. (2015). "Shear Stress and Hydrodynamic Recovery over Bedforms of Different Lengths in a Straight Channel." J. Hydraul. Eng. 141(11):04015025.

MacVicar, B. J., Lana Obach, and James L. Best. (2013). "Large-Scale Coherent Flow Structures in Alluvial Pools." Pp. 243–59 in *Coherent Flow Structures at Earth's Surface*. Chichester, UK: John Wiley & Sons, Ltd.

MacVicar, B. J. and Colin D. Rennie. (2012). "Flow and Turbulence Redistribution in a Straight Artificial Pool." Water Resour. Res. 48(2):W02503.

MacVicar, B. J. and A. G. Roy. (2007a). "Hydrodynamics of a Forced Riffle Pool in a Gravel Bed River: 1. Mean Velocity and Turbulence Intensity." Water Resour. Res. 43(12):W12401.

MacVicar, B. J. and A. G. Roy. (2007b). "Hydrodynamics of a Forced Riffle Pool in a Gravel Bed River: 2. Scale and Structure of Coherent Turbulent Events." Water Resour. Res. 43(12):W12402.

MacVicar, B. J. and A. G. Roy. (2011). "Sediment Mobility in a Forced Riffle-Pool." Geomorphology 125(3):445–56.

MacVicar, BJ, Scott Dilling, J. Lacey, and K. Hipel. (2014). "A Quality Analysis of the Vectrino II Instrument Using a New Open-Source MATLAB Toolbox and 2D ARMA Models to Detect and Replace Spikes." Pp. 1951–59 in *River Flow 2014*.

MacVicar, Bruce J., Scott Dilling, and Jay Lacey. (2014). "Multi-Instrument Turbulence Toolbox (MITT): Open-Source MATLAB Algorithms for the Analysis of High-Frequency Flow Velocity Time Series Datasets." Comput. Geosci. 73:88–98.

MacVicar, Bruce J., Colin D. Rennie, and André G. Roy. (2010). "Discussion of 'Unifying Criterion for the Velocity Reversal Hypothesis in Gravel-Bed Rivers' by D. Caamaño, P. Goodwin, J. M. Buffington, J. C. P. Liou, and S. Daley-Laursen." J. Hydraul. Eng. 136(8):550–52.

MacWilliams, M. L. (2004). "Three-Dimensional Hydrodynamic Simulation of River Channels and Floodplains." (March).

MacWilliams, M. L., Joseph M. Wheaton, Gregory B. Pasternack, Robert L. Street, and Peter K. Kitanidis. (2006). “Flow Convergence Routing Hypothesis for Pool-Riffle Maintenance in Alluvial Rivers.” Water Resour. Res. 42(10):1–21.

Madej, Mary Ann, Diane G. Sutherland, Thomas E. Lisle, and Bonnie Pryor. (2009). “Channel Responses to Varying Sediment Input: A Flume Experiment Modeled after Redwood Creek, California.” Geomorphology 103(4):507–19.

Milan, D. J. J., G. L. L. Heritage, A. R. G. R. G. Large, and M. E. E. Charlton. (2001). “Stage Dependent Variability in Tractive Force Distribution through a Riffle–pool Sequence.” Catena 44(2):85–109.

Milan, David J. (2013). “Sediment Routing Hypothesis for Pool-Riffle Maintenance.” Earth Surf. Process. Landforms 38(14):1623–41.

Miller, Jerry R. and R. Craig Kochel. (2009). “Assessment of Channel Dynamics, in-Stream Structures and Post-Project Channel Adjustments in North Carolina and Its Implications to Effective Stream Restoration.” Environ. Earth Sci. 59(8):1681–92.

Montgomery, D. R. (1995). “Pool spacing in forest channels” Water Resour Eng. 31(4):1097–1105.

Montgomery, David R., John M. Buffington, Richard D. Smith, Kevin M. Schmidt, and George Pess. (1995). “Pool Spacing in Forest Channels.” Water Resour. Res. 31(4):1097–1105.

Nelson, Jonathan M., Ronald L. Shreve, Stephen R. McLean, and Thomas G. Drake. (1995). “Role of Near-Bed Turbulence Structure in Bed Load Transport and Bed Form Mechanics.” Water Resour. Res. 31(8):2071–86.

Nelson, Peter A., Andrew K. Brew, and Jacob A. Morgan. (2015). “Morphodynamic Response of a Variable-Width Channel to Changes in Sediment Supply.” Water Resour. Res. 51(7):5717–34.

Newbury, Robert W. (2013). “Designing Fish-Passable Riffles as Gradient Controls in Canadian Streams.” Can. Water Resour. J. 38(3):232–50.

Nezu, Iehisa and Wolfgang Rodi. (1986). “Open-channel Flow Measurements with a Laser Doppler Anemometer.” J. Hydraul. Eng. 112(5):335–55.

Nowell, Arthur R. M. and Michael Church. (1979). “Turbulent Flow in a Depth-Limited Boundary Layer.” J. Geophys. Res. 84(C8):4816.

Phillips, Jeff V and Saeid Tadayon. (2006). Selection of Manning’s Roughness Coefficient for Natural and Constructed Vegetated and Non-Vegetated Channels, and Vegetation Maintenance Plan Guidelines for Vegetated Channels. Reston, Virginia: 2007: U.S. Department of the Interior- Scientic Investigations Report 2006–5108.

Raudkivi, A. J. (1963). “Study of Sediment Ripple Formation.” J. Hydraul. Div. Proc. Am. Soc. Civ. Eng. 89(HY6):15–33.

Rodi, Wolfgang, George Constantinescu, Thorsten Stoesser, George Constantinescu, and Thorsten Stoesser. (2013). Large-Eddy Simulation in Hydraulics. CRC Press.

Roy, André G., Pascale M. Biron, Thomas Buffin-Bélanger, and Mylène Levasseur. (1999). "Combined Visual and Quantitative Techniques in the Study of Natural Turbulent Flows." Water Resour. Res. 35(3):871–77.

Roy, Andre G., Thomas Buffin-Blanger, Hlne Lamarre, and Alisttair D. Kirkbride. (2004). "Size, Shape and Dynamics of Large-Scale Turbulent Flow Structures in a Gravel-Bed River." J. Fluid Mech. 500(2004):1–27.

Sawyer, April M., Gregory B. Pasternack, Hamish J. Moir, and Aaron A. Fulton. (2010). "Riffle-Pool Maintenance and Flow Convergence Routing Observed on a Large Gravel-Bed River." Geomorphology 114(3):143–60.

Schlatter, P., Q. Li, R. Örlü, F. Hussain, and D. S. Henningson. (2014). "On the Near-Wall Vortical Structures at Moderate Reynolds Numbers." Eur. J. Mech. B/Fluids 48:75–93.

Schmeeckle, Mark W. (2014). "Numerical Simulation of Turbulence and Sediment Transport of Medium Sand." J. Geophys. Res. Earth Surf. 119(6):1240–62.

Seal, Rebecca and Chris Paola. (1995). "Observations of Downstream Fining on the North Fork Toutle River Near Mount St. Helens, Washington." Water Resour. Res. 31(5):1409–19.

Sear, D. A. (1996). "Sediment Transport Processes in Pool-Riffle Sequences." Earth Surf. Process. Landforms 21(3):241–62.

Sear, D. A. DA A. and MD D. Newson. (2004). "The Hydraulic Impact and Performance of a Lowland Rehabilitation Scheme Based on Pool-Riffle Installation: The River Waveney, Scole, Suffolk, UK." River Res. Appl. 20(7):847–63.

Seminara, Giovanni. (2006). "Meanders." J. Fluid Mech. 554(1):271–97.

Shields, a. (1936). "Application of Similarity Principles and Turbulence Research to Bed-Load Movement." Mitt. Preuss. Versuchsanst. Wasserbau Schiffbau 26(5–24):47.

Smagorinsky, J. (1963). "General Circulation Experiments with the Primitive Equations: I. The Basic Experiment." Mon. Weather Rev. 91(3):99–164.

Smits, A. J. and D. H. Wood. (1985). "The Response of Turbulent Boundary Layers to Sudden Pertubations." Annu. Rev. Fluid Mech. 17(1):321–58.

Stoesser, T., C. Braun, M. García-Villalba, W. Rodi, M. Garcia-Villalba, W. Rodi, M. García-Villalba, and W. Rodi. (2008). "Turbulence Structures in Flow over Two-Dimensional Dunes." J. Hydraul. Eng. 134(1):42–55.

Stoesser, Thorsten. (2014). "Large-Eddy Simulation in Hydraulics: Quo Vadis?" J. Hydraul. Res. 52(4):441–52.

Stoesser, Thorsten, Nils Ruether, and Nils Reidar Boe Olsen. (2010). "Calculation of Primary and Secondary Flow and Boundary Shear Stresses in a Meandering Channel." Adv. Water Resour. 33(2):158–70.

Sumer, B. Mutlu, Lloyd H. C. Chua, N. S. Cheng, and Jørgen Fredsøe. (2003). "Influence of Turbulence on Bed Load Sediment Transport." J. Hydraul. Eng. 129(8):585–96.

Thompson, Alan. (1986). “Secondary Flows and the Pool-Riffle Unit: A Case Study of the Processes of Meander Development.” Earth Surf. Process. Landforms 11(6):631–41.

Thompson, D. M. (2013). “Pool-Riffle.” Pp. 364–78 in *Treatise on Geomorphology*, vol. 9. Elsevier.

Thompson, D. M. and E. E. Wohl. (2009). “The Linkage between Velocity Patterns and Sediment Entrainment in a Forced-Pool and Riffle Unit.” Earth Surf. Process. Landforms 34(2):177–92.

Thompson, D. M., E. E. Wohl, and R. D. Jarrett. (1996). “A Revised Velocity-Reversal and Sediment-Sorting Model for a High-Gradient, Pool-Riffle Stream.” Phys. Geogr. 17(2):142–56.

Thompson, Douglas M. (2001). “Random Controls on Semi-Rhythmic Spacing of Pools and Riffles in Constriction-Dominated Rivers.” Earth Surf. Process. Landforms 26(11):1195–1212.

Thompson, Douglas M. (2004). “The Influence of Pool Length on Local Turbulence Production and Energy Slope: A Flume Experiment.” Earth Surf. Process. Landforms 29(11):1341–58.

Thompson, Douglas M. (2006). “Changes in Pool Size in Response to a Reduction in Discharge: A Flume Experiment.” River Res. Appl. 22(3):343–51.

Thompson, Douglas M. DM. (2002). “Geometric Adjustment of Pools to Changes in Slope and Discharge: A Flume Experiment.” Geomorphology 46(3–4):257–65.

Thompson, Douglas M., Jonathan M. Nelson, and Ellen E. Wohl. (1998). “Interactions between Pool Geometry and Hydraulics.” Water Resour. Res. 34(12):3673–81.

Thompson, Douglas M., Ellen E. Wohl, and Robert D. Jarrett. (1999). “Velocity Reversals and Sediment Sorting in Pools and Riffles Controlled by Channel Constrictions.” Geomorphology 27(3–4):229–41.

Venditti, J. G., W. E. Dietrich, P. A. Nelson, M. A. Wydzga, J. Fadde, and L. Sklar. (2010). “Effect of Sediment Pulse Grain Size on Sediment Transport Rates and Bed Mobility in Gravel Bed Rivers.” J. Geophys. Res. Earth Surf. 115(3):1–19.

Venditti, Jeremy G., Colin D. Rennie, James Bomhof, Ryan W. Bradley, Malcolm Little, and Michael Church. (2014). “Flow in Bedrock Canyons.” Nature 513(7519):534–37.

White, Jason Q., Gregory B. Pasternack, and Hamish J. Moir. (2010). “Valley Width Variation Influences Riffle-Pool Location and Persistence on a Rapidly Incising Gravel-Bed River.” Geomorphology 121(3–4):206–21.

Wiberg, Patricia L. and J. Dungan Smith. (1987). “Calculations of the Critical Shear Stress for Motion of Uniform and Heterogeneous Sediments.” Water Resour. Res. 23(8):1471–80.

Wilcock, Peter R. and Brian W. Mcardell. (1997). “Partial Transport of a Sand / Gravel Sediment Flume.” Water Resour. Res. 33(1):235–45.

Wilcock, Peter R. and Brian W. McArdell. (1993). “Surface Based Fractional Transport Rates:

Mobilization Thresholds and Partial Transport of a Sand???Gravel Sediment." Water Resour. Res. 29(4):1297–1312.

Wilkinson, S. N., Robert J. Keller, and Ian D. Rutherfurd. (2004). "Phase-Shifts in Shear Stress as an Explanation for the Maintenance of Pool–riffle Sequences." Earth Surf. Process. … 29(6):737–53.

Wilkinson, S. N., Ian D. Rutherfurd, and Robert J. Keller. (2008). "An Experimental Test of Whether Bar Instability Contributes to the Formation, Periodicity and Maintenance of Pool-Riffle Sequences." Earth Surf. Process. Landforms 33(11):1742–56.

Wohl, Ellen, Paul L. Angermeier, Brian Bledsoe, G. Mathias Kondolf, Larry MacDonnell, David M. Merritt, Margaret A. Palmer, N. LeRoy Poff, and David Tarboton. (2005). "River Restoration." Water Resour. Res. 41(10):1–12.

Wohl, Ellen E. and Douglas M. Thompson. (2000). "Velocity Characteristics along a Small Step-Pool Channel." Earth Surf. Process. Landforms 25(4):353–67.

Wohl, Ellen and David M. Merritt. (2008). "Reach-Scale Channel Geometry of Mountain Streams." Geomorphology 93(3–4):168–85.

Wyrick, J. R. and G. B. Pasternack. (2014). "Geospatial Organization of Fluvial Landforms in a Gravel-Cobble River: Beyond the Riffle-Pool Couplet." Geomorphology 213:48–65.

Yager, E. M. and H. E. Schott. (2013). The Initiation of Sediment Motion and Formation of Armor Layers. Elsevier Ltd.

Zeng, Jie and George Constantinescu. (2017). "Flow and Coherent Structures around Circular Cylinders in Shallow Water." Phys. Fluids 29(6).